Stochastic Simulation of Carbonaceous Nanoparticle Precursor Formation in Combustion

by

Jason Yue Wai Lai

A dissertation submitted in partial fulfillment
of the requirements for the degree of
Doctor of Philosophy
(Mechanical Engineering)
in the University of Michigan
2014

Doctoral Committee:

Associate Professor Angela Violi, Chair
Professor Arvind Atreya
Professor John R Barker
Professor Andre L Boehman
Senior Research Fellow Paolo Elvati

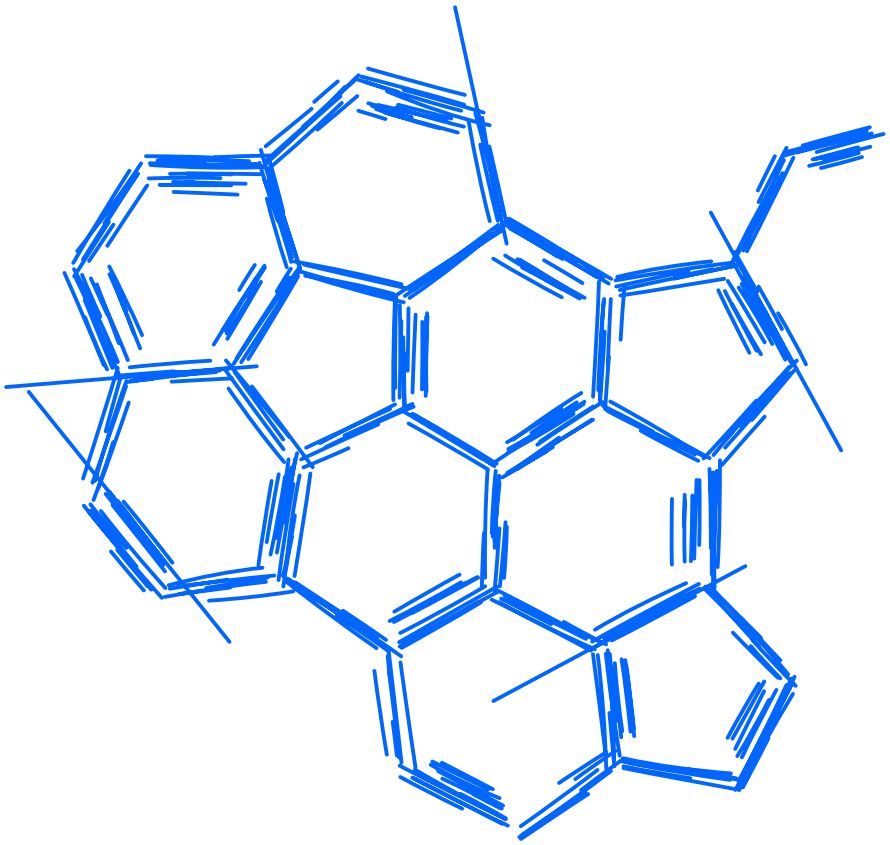

"Think of it this way.
Our aim is to make the world more beautiful
than it was when we came into it.
It can be done. You can do it."

-Kurt Vonnegut

To my family,

Mom, Dad, Patricia, Michelle,

for love and support.

ACKNOWLEDGEMENTS

This dissertation is the culmination of many long years of work and would absolutely not be possible without the support of my advisor, Professor Angela Violi, who has challenged and guided me in the exploration of my research with her considerable expertise and force of will. Nor would it possible without my close collaborator, Dr. Paolo Elvati, whose technical and research prowess has been and continues to be incredibly valuable. To say I have learned an extraordinary amount is an understatement for which I am eternally grateful.

Thank you as well to the remainder of my dissertation committee, Professors Arvind Atreya, John R. Barker, and Andre Boehman, for generously contributing their time and expertise to the completion of my work.

To all my friends in the Violi Group, especially my fellow comrades, Tyler Dillstrom, Jeff Lowe, Alex Chong, and our newest member Elizabeth "EBau" Baumeister – thank you for making the lab fun and lively. It has been an absolute pleasure working alongside all of you.

To the rest of my friends I have met in Michigan, especially Mathieu Davis, Jenna Campbell, Rebecca Tarrien, and Tomi Ogundimu, as well as the Toronto crew, Maria Wong, Greg Chung, Chloe Koo, Edith Cheng, Yoan Kagoma, Nina Coutinho, Jonathan Bright, Sasha Tailor, Sherry Yang, Jen Forsyth, and Jeff Li – all of you have supported me throughout my time at Michigan, for which I am deeply thankful. Your friendship means the world to me.

Finally, my greatest thanks go to my family, Jacob, Elaine, Patricia, and Michelle. Your love and support has been a constant throughout my entire life and especially during the all of the challenges I have faced in completing my Doctoral studies. This work is as much yours as it is my own.

TABLE OF CONTENTS

LIST OF FIGURES

Figure

LIST OF TABLES

Table

LIST OF ABBREVIATIONS

AMPI Atomistic Model for Particle Inception

CNP carbonaceous nanoparticle

HACA hydrogen abstraction, acetylene addition

kMC kinetic Monte Carlo

MD molecular dynamics

PAH polycyclic aromatic hydrocarbon

SNAPS Stochastic Nanoparticle Simulator

SPRINT social permutation invariant

ABSTRACT

Stochastic Simulation of Carbonaceous Nanoparticle Precursor Formation in Combustion

by

Jason Yue Wai Lai

Chair: Angela Violi

Combustion-generated nanoparticles (diameter less than or equal to 100 nm) are prevalent in modern society. Carbonaceous nanoparticles (CNPs) are especially important, finding applications as pigments in ink, in composite materials, or as catalysts. Despite such useful applications, CNPs have attracted the most attention as hazardous emissions from combustion sources like automotive engines, especially as aggregate particles known as soot, as their primary constituents are carcinogenic polycyclic aromatic hydrocarbons (PAHs). Critically, the formation of CNPs in combustion environments remains an area of considerable uncertainty, particularly the growth from gas phase precursors through the nucleation of solid phase particles. Towards elucidating PAH formation via chemical reactions, a significant element of the growth process, a novel simulation software was developed, named the Stochastic Nanoparticle Simulator (SNAPS), along with a corresponding PAH chemical reaction mechanism. This software was then applied to investigate the chemical and physical properties of PAHs formed in combustion.

SNAPS simulations were corroborated through comparisons with existing experi-

mental measurements in flames utilizing a variety of fuels. Furthermore, simulations provided molecular-level detail that revealed key aspects of a complex chemical growth process. Importantly, these simulations provided insights into chemical reaction and composition details beyond those typically inaccessible by experiment. For all studied flames, analysis of the major chemical reactions and PAH species involved in simulations contrasted with conventional theories. Simulations showed that PAH growth is characterized by complex sequences of highly reversible reactions, leading to a variety of species that far exceeds the relatively narrow range that has traditionally been the focus of investigations. SNAPS therefore represents an important tool for synthesizing experimental observations and theoretical predictions, towards building a comprehensive and accurate description of CNP growth. Most importantly, the current work is only one application of the software. The extensibility of SNAPS will enable modeling of many different systems involving heterogeneous nucleation and growth of nanoparticles, which illustrates its potential for wide impact. Altogether, this work represents a strong framework that will support and drive future investigations of nanoparticle growth and contribute to the development of novel combustion technologies that will positively impact society.

CHAPTER I

Introduction

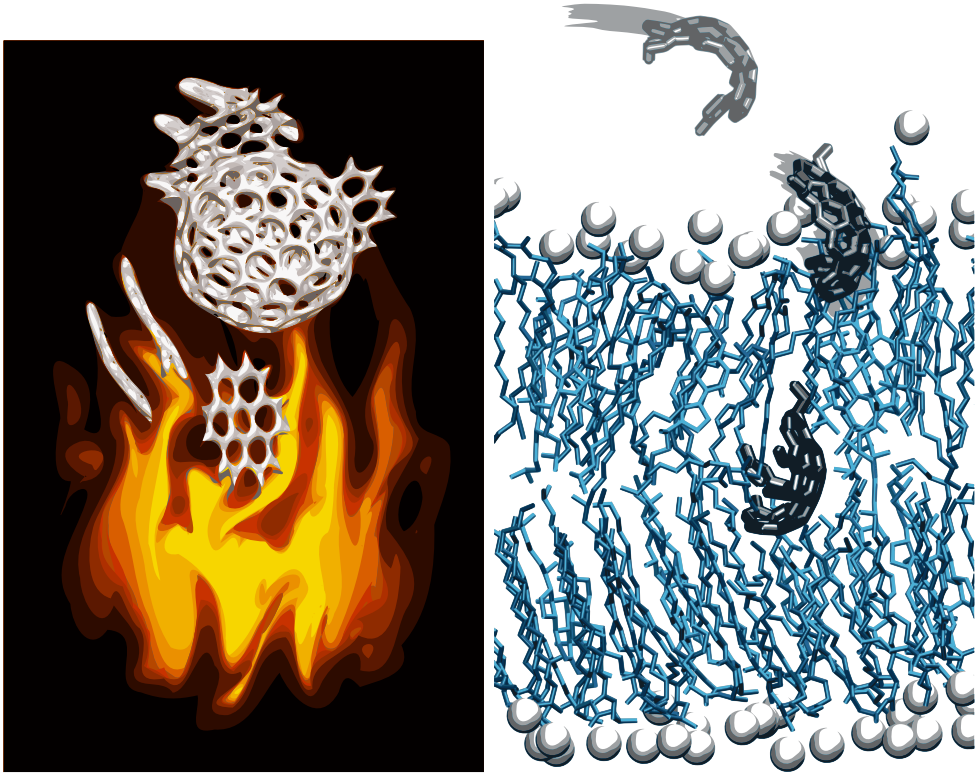

Figure 1.1: Nanoparticle genesis in combustion and interaction with a lipid membrane in a biological cell.

Nanoparticles formed in combustion are prevalent in modern society as both components in engineering and as harmful emissions from industrial processes [1]. Flame synthesis accounts for the majority of commercial nanoparticles, with typical production rates on the order of 100 metric tons per day [2]. In particular, carbonaceous

nanoparticles (CNPs), formed in the pyrolysis of combustion fuels, have a substantial impact on society. For example, carbon black is the most important commercial nanoparticle [2], and carbon nanoparticles can function as a cathode catalyst in solar cells [3]. Additionally, carbon nanotubes and fullerenes have important applications in composite materials that are both lightweight and strong.

However, CNPs also pose significant danger as a human health hazard, as they are emitted from combustion sources such as internal combustion engines, both as nanoparticles and as larger aggregates known as soot. Soot primarily consists of aggregated particles of polycyclic aromatic hydrocarbons (PAHs) and is classified as carcinogenic by the International Agency for Research on Cancer [4]. Carbon black, too, has also been classified as potentially carcinogenic [5]. Airborne emissions of this class of "ultrafine" particles (diameter ≤ 100 nm) is currently unregulated, in contrast with larger particulate classes like PM_{10} (between 2.5 and 10 μm) and $PM_{2.5}$ (≤ 2.5 μm), despite questions about increased toxicity [6–8] due to their small size. Indeed, there have been efforts [9–12] to understand the transport of CNPs in biological systems as a way to assess toxicity. These studies utilize a computational framework to investigate the interactions of CNPs cellular membranes. Since morphology greatly influences these interactions and toxicity [7, 8], there is strong motivation to understand the formation and composition of CNPs. Moreover, although CNPs may represent only 0.1 to 1.5% of emissions from engines by particle volume, they represent 35 to 97% of particle number [13]. As a result, toxicological assessment of these particles is a critical public health issue. Importantly, the formation of CNPs is greatly influenced by the combustion conditions, including temperature, pressure, and fuel composition. Therefore, in order to better assess health risks, develop cleaner combustion, or improve flame synthesis yields, there is strong motivation to understand the formation of CNPs, especially the influence of the combustion environment on chemical composition and morphology.

Despite the importance of nanoparticles in society, understanding the fundamental processes governing their growth remains a challenge. Indeed, there is still substantial uncertainty in the growth mechanisms, chemical composition, morphology of nascent CNPs in combustion. The difficulty in experimentally studying these processes has motivated the development of computational tools for exploring and characterizing the growth of nanoparticles in gas phase environments. The current work describes the development and application of the Stochastic Nanoparticle Simulator (SNAPS), a new software for the simulation of gas phase chemical growth of nanoparticles. SNAPS was applied to characterize the formation and chemical composition of PAHs in combustion, towards elucidating the process of particle inception, or nucleation, which is a key knowledge gap in understanding properties of of larger CNPs and soot. The characterization of PAHs included identification of important PAH molecular structures, chemical reaction pathways, as well as the investigation of the influence of the combustion environment.

This work represents a significant step in the investigation of CNP formation. Elucidating the relationships between combustion environment and CNP growth will have substantial engineering impact in toxicological assessment, pollutant control strategies in engines, and improvement of flame synthesis processes for nanomaterials. Moreover, SNAPS could also be used to investigate the formation of other nanoparticle growth systems, such as titania, silica, or transition (t)-aluminas, which are also formed through flame processes [14, 15]. Engineering of these types of nanoparticles will also benefit from a deeper understanding of the underlying phenomena that govern their formation. SNAPS, therefore, has potential for even wider impact in the study of nanoparticle growth.

1.1 Inception of Carbonaceous Nanoparticles

The formation of CNPs in flames, depicted in Figure 1.2, process begins with fuel oxidation and precursor formation, such as acetylene and benzene, and proceeds through PAH formation, particle inception, surface reaction and coagulation, agglomeration, and finally oxidation [16]. An important area of uncertainty in CNP formation is particle inception, or nucleation, which delineates the gas to solid phase transition. The inception process is complex, involves both chemical and physical phenomena [17], and has a significant impact on the growth of combustion-emitted particles, especially their size distribution [18] and morphology. Indeed, experiments have shown that flame conditions and fuel affect the structure of nascent particles [19–21], which reflects the complexity and impact of the inception process.

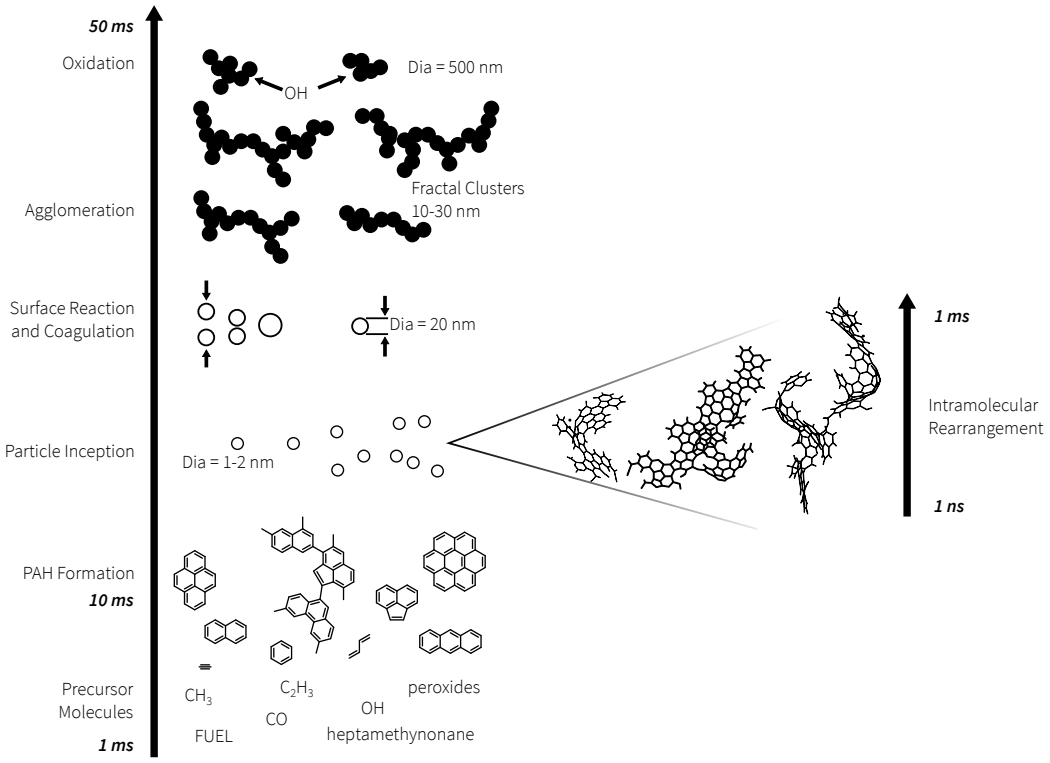

Figure 1.2: Particle formation in flames. Adapted from Izvekov and Violi [16].

There is a substantial body of further work, reviewed many times previously [14, 17, 20, 22–27], that has investigated CNP and soot formation in combustion. This

array of work, as well as proposed inception mechanisms, illustrates the considerable uncertainty in the chemical composition and morphology of incipient PAHs, as well as the difficulty involved with experimentally studying nucleation. Many experiments have probed flames and detected nascent particles ranging in size from 1.5 nm to 5 nm [28–40]. These experiments provided important insight into size distributions of nascent particles, but limited information concerning their chemical composition, morphology, and inception mechanisms.

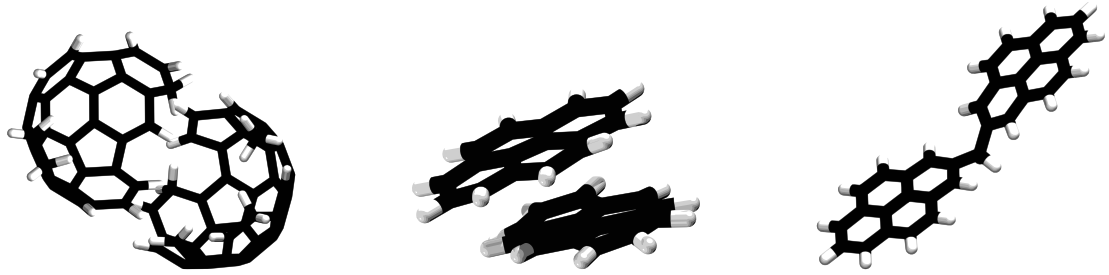

Figure 1.3: Depictions of proposed mechanisms for inception: (a) chemical growth of fullerene-like structures (b) dimerization of PAHs (c) aliphatic linking of PAHs

There are a variety of proposed mechanisms for particle inception; some examples are depicted in Figure 1.3. One mechanism is the chemical growth of PAHs into curved, fullerene-like structures [41, 42], shown in Figure 1.3a. The observation of mass spectra suggesting fullerene-like structures in flames [43, 44] ostensibly supports this pathway, but it is controversial [45]. In particular, purely chemical growth has been suggested to be too slow to account for observed soot nucleation rates, and that physical coagulation must play a role [46].

The most prominent mechanism for nucleation is the physical agglomeration of moderately sized PAHs into clusters, depicted in Figure 1.3b. As reviewed by Wang, models of CNP nucleation involving dimerization of PAHs predict a bimodal size distribution [14], which has been observed experimentally [34, 37]. Calculations of electrostatic and dispersive binding energies of PAHs have also shown an increase in dimer stability with size that could stabilize dimers at flame temperatures, especially

in stacked planar configurations [47]. The irreversible dimerization of pyrene ($C_{16}H_{10}$) is the most widely used definition of inception in numerical models [48]. However, there has been subsequent work that contradicts the plausibility of the pyrene dimerization inception mechanism.

While the existence of dimers of pyrene has been suggested to be plausible due to van der Waals forces [48], or aromatic excimer configuration [49], other work has argued against this phenomenon [14, 50–54]. Computed equilibrium constants for dimerization of benzene, coronene, and circumcoronene [55] predicted dimer number densities far below those experimentally observed in flames. Later, computed size-dependent lifetimes of PAH dimers were observed to approach the scale of chemical reaction times only for PAHs of mass 800 amu or greater, approximately four times the mass of pyrene [50]. More recent computation of equilibrium constants using an updated PAH interaction potential corroborates that pyrene dimerization is unlikely to play a role in nucleation [54]. Accordingly, experimental observation of pyrene dimerization kinetics showed that at high temperatures, equilibrium favors pyrene dissociation [51]. Molecular dynamics simulation of PAH clustering [52] suggests, based on lifetimes, that pyrene dimers are too unstable at flame temperatures to act as soot nuclei. Computation of free energy surfaces [53] further corroborates this observation, showing that, even at 1000 K, pyrene dimerization is thermodynamically unfavorable.

Theoretical arguments have suggested that physical agglomeration of species other than pyrene may be involved in nucleation. These species include unsubstituted peri-condensed aromatics with larger mass [50], such as ovalene ($C_{32}H_{14}$) [53], or circumcoronene ($C_{54}H_{18}$) [54]; however, these species may not contribute in all flames, as experiments show that in non-premixed co-flow flames, spatial profiles of PAHs peak higher in the flame than those of soot particles [33]. These species also include:PAHs with substituted aliphatic chains [53], which stabilize dimers through entropic effects;

chemically linked PAHs [52], depicted in Figure 1.3c; and fullerenes with at least 80 carbons [56]. Experiment corroborates the involvement of substituted aliphatic chains through the observation of aliphatic fragments in the mass spectra of particles collected from premixed laminar flames [57, 58].

Another proposed mechanism of nucleation is the chemical linking of smaller, two-ring PAHs with aliphatic chains or oxygen, similarly to the depiction in Figure 1.3c, based on experiments involving ultraviolet absorption and fluorescence spectra of CNP precursors [31, 59–61], kinetic modeling [62], time-resolved fluorescence polarization anisotropy [63], and aerosol mass spectrometry [64]. These structures could arise via reactions between aromatic molecules and aryl radicals; for example, benzene reacting with phenyl to form biphenyl. This mechanism is plausible in regions close to the main flame zone, where H atoms are abundant to produce aryl radicals via hydrogen abstraction [14]; however, experimental observation of persistent nucleation in the post flame zone [36, 37] raises concerns, as H atom concentrations are far lower [14]. Nevertheless, chemically linked PAHs could physically coalesce and so this mechanism may also play a role in CNP nucleation.

1.2 Composition, Morphology, and Growth of PAHs

Although nucleation is expected to involve PAHs, the variety of proposed inception mechanisms demonstrates that the exact species involved remain poorly understood. Although a significant amount of work has attempted to characterize particle inception, much of this effort typically involves the investigation of particle size and mass, not necessarily detailed chemical composition and morphology. As a result, the molecular structures of PAH species are typically inferred based on measurable properties combined with chemical intuition. Most commonly, PAHs are assumed to be the most thermodynamically stable pericondensed aromatics defined by Stein and Fahr [65], also termed "stabilomers." This assumption is rooted in the idea that the most

energetically favourable species will be present in the highest concentration. Thus, the prevailing characterization of PAHs growing in combustion are pericondensed aromatics consisting of almost exclusively 6-membered rings. For example, PAHs with a mass of 202 amu are most commonly associated with pyrene and those with mass 300 amu are commonly associated with coronene. These stabilomers are similarly utilized for even larger PAH masses, such as ovalene ($C_{32}H_{14}$) and circumcoronene ($C_{54}H_{18}$).

For example, Dobbins et al. [29, 30] observed PAH masses between 202 and 472 amu in coannular ethylene flames using laser microprobe mass spectrometry. Since these masses decrease significantly with height within the flame, they suggest a mechanism of inception, namely coalescence of PAHs in this mass range. Since this experiment did not measure isomeric information, peaks in mass spectra were matched with Stein's stabilomers. Importantly, this analysis was limited to matching mass based on the expected chemical formula, C_xH_y, and presumed expectations for the species and growth pathways involved. Indeed, the authors noted ambiguity with respect to the specific PAH isomers involved. Nevertheless, this analysis was used to support the idea that PAH growth occurs through a sequence of 6-membered pericondensed aromatics. Other efforts have further argued, using similar arguments, for the prevalence of these 6-membered ring PAHs based on mass spectra measured in low pressure premixed acetylene [66], benzene [67, 68], *n*-butane [69], and napthalene [70] flames, based on the thermodynamic favourability of reaction pathways involving the formation of 6-membered aromatic rings. More recently, Miller et al. [71] measured optical band gaps in a non-premixed ethylene/air flame and compared with computed values for pericondensed aromatic species. The authors concluded that measured values best corresponded with PAHs with at least ten rings. Nevertheless, this experiment did not did not provide detailed chemical information about these PAHs.

Other experimental work has also attempted to elucidate the chemical growth and composition of PAHs and nascent soot. Tregrossi et al. [72] identified specific

condensed PAHs produced in atmospheric pressure premixed benzene flames and measured concentration profiles for each relative to flame height. These species profiles suggested potential chemical reaction pathways. For example, measured peaks for acenaphthylene occured spatially after those for naphthalene, which is consistent with the reaction of naphthalene with acetylene to form acenaphthylene. Other studies have identified significant aliphatic content in nascent soot produced in various flames [57, 69, 73–75], which corroborates the idea that PAH species in flames are not entirely pericondensed. Skeen et al. [58] further supported this idea, based on aerosol mass spectrometry, by studying the isomeric distribution of species corresponding to specific masses, and showing that a combination of species best represents the photoionization efficiency curves corresponding with specific masses. The variance in PAH composition is even further supported by measured Hydrogen:Carbon ratios of soot samples [66, 75] that do not necessarily correspond with pericondensed stabilomers. Various low pressure premixed flame experiments have noted [67–69], based on measurements of H:C ratios, that PAHs growth does not strictly follow a narrow band of PAHs on the stabilomer table, but rather PAHs with a variety of H:C ratios.

Despite efforts made to characterize the chemical composition of PAHs, the prevailing concept remains sequential chemical growth of exclusively 6-membered ring pericondensed aromatics, such as from pyrene to coronene and beyond. This concept has dominated and heavily influenced understanding of particle inception. The conventional stabilomer table remains a standard tool for interpretation of experimental observations, despite persistent ambiguity with respect to the multitude of potential PAH isomers, which grows with mass. Consequently, the body of work in this area illustrates that characterizing the growth, composition, and morphology of nascent PAHs remains a vital step in understanding particle inception.

The uncertainty in chemical composition of nascent PAHs has motivated study of the chemical reaction pathways involved in their growth. The first step in this

process, especially for non-aromatic fuels, is generally considered to be the formation of the first aromatic ring or rings, namely benzene (C_6H_6) or phenyl (C_6H_5), which subsequently grows into larger PAHs. Important reactions have been proposed for ring formation that involve acetylene are $C_4H_3 + C_2H_2 \rightleftharpoons C_6H_5$ [76]; and $nC_4H_5 + C_2H_2 \rightleftharpoons C_6H_6 + H$. Additionally, propargyl radical recombination, $2\,C_3H_3 \rightleftharpoons C_6H_6$, is also considered to be an important aromatic formation pathway [77]. Alternate routes to the first rings, including ring formation from linear six carbon species or from cyclopentadienyl radicals (e.g. $2\,C_5H_5 \rightleftharpoons C_{10}H_8$), could also be important depending on environmental conditions, as reviewed by Frenklach [17].

PAH chemical growth beyond the first aromatic ring involves a large number of proposed chemical reaction pathways [17, 22]. The primary growth mechanism of aromatics has been proposed to be a repetitive sequence of hydrogen abstractions and acetylene additions, named the hydrogen abstraction, acetylene addition (HACA) or hydrogen abstraction, carbon addition mechanism [46]. This mechanism is important because H atoms and acetylene are typically among the most abundant species in flame environments [14]. The HACA mechanism, as its name implies, is a repetitive sequence of hydrogen abstractions and acetylene additions that result in an increasing number of aromatic rings. This sequence can be generally summarized by the following example reactions, where A represents a PAH with i rings:

$$A_i + H \rightleftharpoons A_i\cdot + H_2$$

$$A_i\cdot + C_2H_2 \rightleftharpoons A_iC_2H_2$$

$$A_iC_2H_2 + C_2H_2 \rightleftharpoons A_{i+1} + H$$

The HACA mechanism combined with the stabilomer table of Stein and Fahr [65], form the foundation for proposed reaction mechanisms for PAH growth. By a large

margin, the growth of 6-membered ring stabilomer species via the HACA mechanism comprises the majority of proposed PAH reaction mechanisms. For example, Figure 1.4 shows the growth of a napthyl radical to anthracene, via sequential addition of acetylene and ring closure.

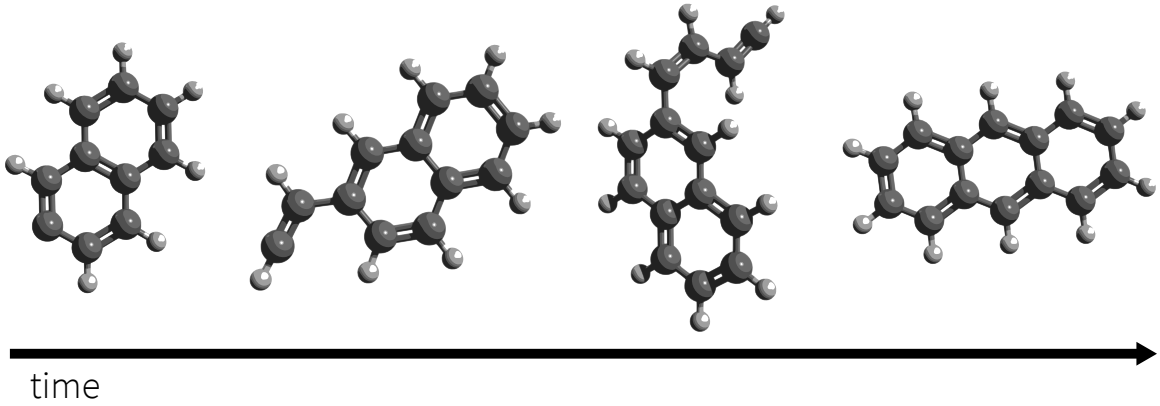

Figure 1.4: Depiction of the HACA mechanism, showing the sequential addition of acetylene atoms and formation of anthracene.

These growth pathways have been supported by experimentally measured mass spectra [29, 30, 66, 67, 72, 78], which typically exhibit dominant mass peaks separated by approximately 24 amu, or the mass of 2 carbon atoms. For example, the mass spectra measured by Dobbins et al. [30] showed the dominant sequential mass peaks 252, 276, and 300 amu and so are ostensibly separated by the addition of an acetylene and the abstraction of hydrogen atoms. Growth via formation of 6-membered rings has also been supported using thermodynamic arguments. Weilmünster et al. argued that the formation of a 6-membered ring via acetylene addition is energetically favourable to the formation of a 5-membered ring, due to the lower activation energies of its constituent elementary reaction steps. This suggestion is reasonable given that the formation of a 5-membered ring involves a higher ring strain energy.

Nevertheless, since the ambient species in a flame can vary significantly, especially depending on fuel, many other pathways could potentially contribute to aromatic growth. Pathways proposed include the addition of benzene [17, 22], phenyl [79], propargyl [62], cyclopentadienyl radicals [62], or vinyl radicals [80]. The variety of

possible growth mechanisms reflects the number of PAH intermediates that can be produced.

1.3 Deterministic Simulation of Chemical Growth

Theoretical and computational models complement experiment and provide predictive capability that facilitates the synthesis of observations and informs the design of novel technologies. Consequently, there has been a significant amount of work that has aimed to model the entire process of CNP and soot formation. This work primarily consists of models for chemical growth of PAHs, often coupled with soot particle dynamics models that describe the coagulation and reaction of increasingly larger particles.

Proposed chemical reactions for PAH growth and combustion have been combined and utilized in simulations to understand the underlying chemical phenomena in combustion and CNP formation. The most common method to study the chemical evolution of PAHs is through deterministic simulations of chemical kinetics in combustion systems. These models solve the time evolution of all chemical species simultaneously as a system of coupled ordinary differential equations derived from chemical rate laws. As a result, formulating a kinetic mechanism for such a purpose requires the specification of all expected intermediate species and their corresponding chemical reactions. Typically, reaction pathways are combined into a chemical kinetic model, or mechanism, which is a list of chemical reactions, each with a corresponding kinetic rate constant, that describes a chemically reacting system, such as combustion and PAH growth. This method fundamentally assumes that the time evolution of concentrations of all species is continuous and deterministic, which is accurate when describing systems in the thermodynamic limit [81].

However, since this assumption is sufficient for many traditional engineering problems and these models are computationally efficient, they are a commonly used in

simulations of PAH chemical growth, as extensions to existing models for the combustion of fuels. For example, chemical mechanisms are often used in continuous, deterministic combustion models, such as those in the CHEMKIN [82] software, to describe time evolution of species concentrations in a variety of combustion environments. These types of models have proven useful in studying the combustion chemistry of a wide variety of fuels. Leveraging this expertise, a substantial number of kinetic mechanisms have been formulated to describe hydrocarbon combustion and the chemical growth of PAHs from the formation of the first aromatic ring to larger PAHs such as pyrene ($C_{16}H_{10}$), or coronene ($C_{24}H_{12}$) [46, 77, 83–89].

One drawback of these types of models is their complexity, especially for large reaction networks. Chemical mechanisms are typically compiled in terms of reaction pathways that are considered to be important, based on chemical intuition and comparison with experiments. Any pathway branching or interactions between intermediate species must be explicitly specified. While this approach has been reasonable for smaller networks, issues arise when attempting to describe large reaction networks, such as PAH growth. For example, the reaction steps for the growth of benzene to naphthalene via the HACA mechanism are relatively simple to specify and alternate routes to naphthalene may also be feasibly specified. Moreover, as these species are relatively small, definition of pathway branching to other species, as well as interactions with other intermediates, is still a feasible, if challenging task. However, this same process will become difficult, if not intractable when attempting to describe growth to increasingly large PAH species, as a complete description of all potential chemical reactions and intermediate species will involve an extremely large quantity of each. Therefore, the formulation of a practical chemical mechanism for PAH growth requires simplification and consequently, a significant amount of pathway branching and interaction of intermediate species tends to be omitted out of necessity.

Ultimately, due to the computational efficiency of these types of mechanisms,

they are prevalent at foundation of particle growth simulations, providing PAH and gas phase species concentrations. Moreover, the wide number of reactions and rates available can be leveraged to facilitate the development of a PAH growth model for SNAPS. Moreover, these deterministic models, along with software like CHEMKIN, can be used to compute flame properties and chemistry that are used as input data for SNAPS. As a result, these models have significant utility, but will also benefit from alternate simulation methods to explore PAH growth, especially those than can identify the most important PAH growth pathways, which will greatly improve the specification of deterministic PAH chemical models. A simplified but accurate deterministic chemical model will provide a computationally efficient tool to study growth of PAHs in combustion.

1.4 Stochastic Simulation of Chemical Growth

Stochastic models for chemical kinetics offer a vastly different perspective and aim to model the discrete and random behaviour of chemically reacting systems of molecules. The discreteness and randomness of a system can be important in systems where reaction species are present in small quantities [81]. Generally, a stochastic perspective of chemical kinetics follows from the chemical master equation, described further by McQuarrie [90], which describes the probability that a reacting system originally in state x_0, which can undergo a number of reaction events, is in a given state i at time t.

Formally, consider a system comprising N chemical species, $S_1, ..., S_N$ whose molecules can undergo M chemical reactions $R_1, ..., R_M$. Also, let $X_i(t)$ be defined as the integer number of S_i molecules in the system at time t. Then, the chemical master equation describes the time evolution of $P(\mathbf{x}, t|\mathbf{x}_0, t_0)$, which is the probability that $\mathbf{X}(t) \equiv (X_1, ..., X_N)$ will be equal to $\mathbf{x} = (x_1, ..., x_N)$ at time t, given that the system began in the state corresponding to $\mathbf{X}(t_0) = \mathbf{x}_0$, where $t_0 \leq t$:

$$\frac{\partial P(\mathbf{x}, t|\mathbf{x}_0, t_0)}{\partial t} = \sum_{j=1}^{M} [a_j(\mathbf{x} - \nu_j) P(\mathbf{x} - \nu_j, t|\mathbf{x}_0, t_0) - a_j(\mathbf{x}) P(\mathbf{x}, t|\mathbf{x}_0, t_0)] \tag{1.1}$$

$\nu_j \equiv (\nu_{1j}, ..., \nu_{Nj})$, where ν_{ij} is the integer number change in the population of species S_i in the system as a result of a single reaction R_j. The quantity a_j, which is called the propensity function for reaction R_j, is defined as, for an infinitesimal time interval dt, the probability that an reaction event R_j, $j = 1, ..., M$, will occur somewhere inside the system, given that $\mathbf{X}(t) = \mathbf{x}$. The first term of equation 1.1 represents an increase in probability that the system is in state $\mathbf{x}$, while the second term represents a decrease in probability. Since the chemical master equation is difficult to solve even for simple systems, the common approach to understanding the evolution of a system is to simulate an ensemble of temporal trajectories that obey the master equation [81]. Then, ensemble averaging these trajectories yields information about the time evolution of the reacting system. Importantly, ensembles of trajectories represent macroscopic information about the system, equivalent to the deterministic formulation in the thermodynamic limit.

The motivation for applying a stochastic methodology to PAH growth has several benefits. First, a stochastic simulation offers detail about the trajectories of individual molecules, while retaining the ability to gain macroscopic insight through ensemble averages. In the context of PAHs, this detail is valuable, as chemical composition heavily influences particle nucleation mechanisms and thus the morphology of subsequently grown nanoparticles. Most importantly, a stochastic model requires a focus on the chemical reactivity of a system at any given time. By utilizing a set of rules that govern the chemical reactivity of any PAH at any time, a stochastic simulation can be used to explore growth without having to specify all reaction pathways and intermediate species beforehand. Moreover, due to the probabilistic nature

of each simulation, ensemble averages of trajectories enables discovery of the most common reaction pathways and species. A drawback of this approach is that simulating a system in this way can require more computational time than a conventional deterministic model. However, the benefits of stochastic exploration outweigh the computational costs.

There have been previous efforts in stochastically simulating carbonaceous systems. For example, Frenklach et al. [91–93] have employed kinetic Monte Carlo (kMC) to describe the edge-growth of graphene-sheets. The kinetic Monte Carlo – aromatic site (KMC-ARS) model [94, 95], which has focused on simulating planar PAH growth. For simplicity, the KMC–ARS model lumps elementary reaction steps into global reactions called "jump processes." These jump processes generally describe planar PAH growth using reactions that add or remove complete rings such as: the addition or desorption of five- and six-membered rings; five- to six-membered ring conversion; ring removal by oxidation; and benzene addition. More recently, this model has been updated to describe physical stacking of these planar PAHs, concurrent to their chemical growth [96]. As well, the KMC–ARS model has also been coupled with soot particle dynamics in the PAH-PP model [97, 98], with the aim of describing soot formation with a more detailed model for inception. However, this model has important restrictions in describing CNP growth, namely that it describes only planar PAH growth. This restriction limits the description of PAH and may neglect important structural features such as curvature or attached aliphatic chains that influence the inception process.

The Atomistic Model for Particle Inception (AMPI) [99–104], based on kMC and Molecular Dynamics, aims to describe more complex particle morphology. In contrast with the KMC-ARS model, AMPI describes particle growth through elementary reactions that include: hydrogen abstraction; addition and removal of major ambient species including acetylene, benzene, phenyl, and propargyl; and generic ring closure.

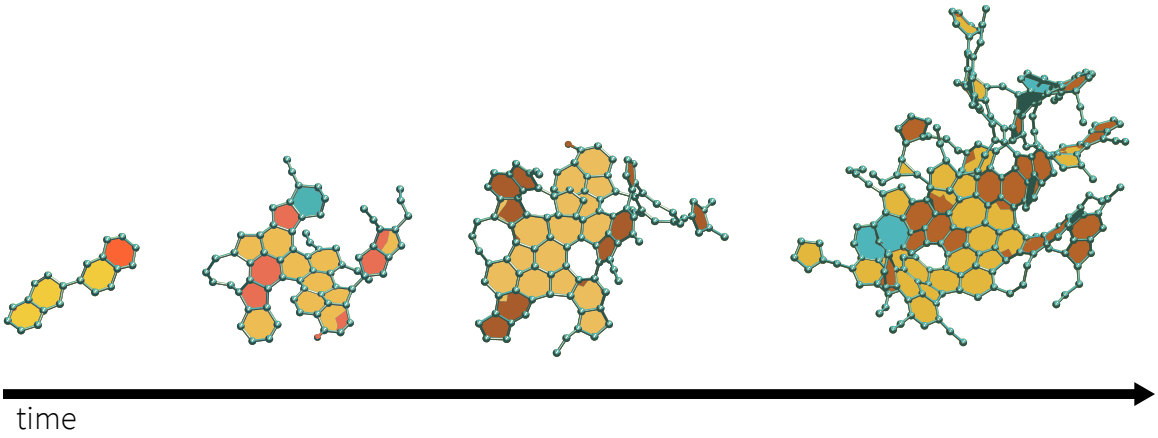

Figure 1.5: Selected snapshots from an AMPI trajectory showing a growing particle.

The goal of this strategy is to explore the various particle morphologies that are produced from different sequences of elementary reactions. As a result, AMPI simulates three-dimensional particles with arbitrary structure and links these structures with reaction pathways. This flexibility allows the description of features such as curvature and attached species on PAH edges, which also affect inception. AMPI has been utilized to study particle growth in flames, elucidating features such as aspect ratio, porosity, and density. For example, Figure 1.5 shows snapshots of a growing particle during an AMPI simulation. This model represents an important first step in stochastic simulation of PAH growth, but there remains significant room for improvement. While the KMC–ARS model was limited primarily to planar PAHs, AMPI demonstrated the utility of exploring particle growth using a set of reactions governing the chemical reactivity of any given intermediate species. Further development of stochastic models will provide deeper insight into the particle inception and soot formation.

1.5 Soot Particle Dynamics Models for Larger Particles

Currently, chemical kinetic mechanisms are utilized in conjunction with soot particle dynamics models to simulate the soot formation process in combustion. These

models, reviewed in detail previously, [14, 17, 20], utilize the kinetic mechanisms to simulate smaller PAH growth, and use the results to simulate particle inception, physical coagulation, and surface growth in the formation of larger soot particles. Importantly, the definition of inception in these models remains relatively simple. Many models continue to define the first soot nuclei as the irreversible dimerization of pyrene or larger molecules [17, 20]. For example, the Polycyclic Aromatic Hydrocarbon - Primary Particle (PAH-PP) model [97, 98] describes the formation, growth, and oxidation of soot particles in premixed laminar flames. The PAH-PP model defines an incipient particle nucleus as a dimer of two PAHs. Dimerization occurs upon collision of planar PAHs with a sticking probability that depends on the surface area and mass of the colliding particles [96]. A model created by D'Anna et al. [105] similarly uses a sticking coefficient that is dependent on the interaction potential between colliding particles, related to mass and particle chemistry through the Hamacker constant. The latter model aims to relate dimerization efficiency with the dispersion forces between colliding particles and consider species beyond pyrene. However, there are still potential improvements. For example, dimerization is still considered to be irreversible in both example models and the PAH-PP model only considers planar pericondensed PAHs. Given the uncertainty surrounding inception and the impact of nucleation on particle size distribution and morphology [18] a deeper understanding of inception will greatly benefit current CNP models.

1.6 Scope, Objectives, and Achievements

Towards elucidating an important component of CNP nucleation, this investigation aims to develop and apply a novel methodology for characterizing the composition, morphology, and growth of PAHs in combustion. The first step in this work was the development of a new software, SNAPS, for stochastic simulation of gas phase particle growth via chemical reactions, using a kinetic Monte Carlo framework. While

the SNAPS methodology can theoretically be applied to any system of interest, the software was developed with the primary aim of simulating PAH growth in combustion. As a result, a new chemical reaction mechanism was formulated, incorporating the most commonly proposed pathways for PAH growth in literature. After verifying the functionality of the software, especially comparing stochastic results against equivalent deterministic solutions, SNAPS was used to study PAH growth in flames of benzene/air, ethylene/oxygen, and acetylene/oxygen. Simulations successfully predicted experimental measurements of species concentration ratios and mass spectra, corroborating the accuracy of SNAPS predictions. Then, the simulations were analyzed to provide insight into the PAH growth process in combustion, especially major reaction pathways and PAH.

Importantly, the major species predicted by simulations contrasted conventional concepts of PAH growth. Moreover, this analysis revealed a common theme for PAH growth across all flame environments, involving a prominent role of acetylene and the HACA mechanism. Altogether, this investigation revealed substantial aspects of complex PAH growth process, and contributed significantly to the understanding of PAH, particle inception, and soot formation. Finally, the results demonstrated areas for future exploration, especially previously unexplored PAH reaction pathways. This work demonstrated a framework that will provide a strong foundation for future investigations. This framework enables synthesis of experimental and theoretical observations and greatly facilitates investigations of not just carbonaceous nanoparticle and soot formation, but nanoparticle growth beyond the current scope. Certainly, this dissertation will strongly benefit the engineering of novel combustion technologies, from toxicological assessment and emission control of nanoparticles, to efficient production of novel nanomaterials.

CHAPTER II

SNAPS: The Stochasic Nanoparticle Simulator

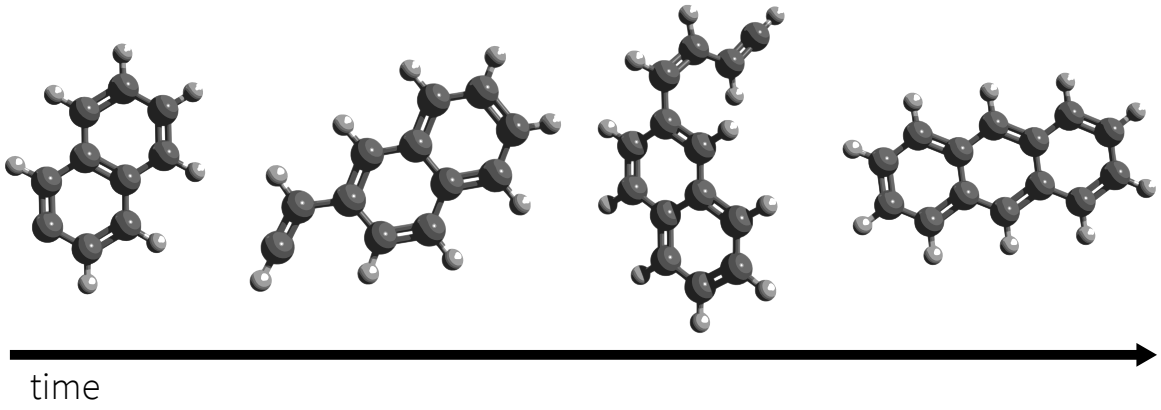

Figure 2.1: Selected snapshots of an example SNAPS trajectory.

The Stochastic Nanoparticle Simulator (SNAPS) is a new software for stochastic simulation of the chemical growth of single molecules or particles. Given a set of chemical reactions, environmental conditions, and an initial molecule, called a seed, SNAPS simulates the trajectory of sequential reactions of a single molecule, depicted in Figure 2.1. In this example, a naphthalene ($C_{10}H_8$) radical undergoes consecutive acetylene additions followed by ring closure to form anthracene ($C_{14}H_{10}$). A typical SNAPS trajectory will contain more steps and will represent one of many possibilities, due to the probabilistic nature of the method. A large ensemble of trajectories will contain macroscopic information about particle growth.

SNAPS has a completely new code base and represents substantial development

over the AMPI methodology, including a new scheme for defining chemical reactivity and the compartmentalization of growth chemistry as a component or input to the code; a new potential energy scheme to account for steric factors and imperfect reaction definition; and greatly increased computational speed. These developments address scientific and practical issues and also greatly expand the extensibility of the code, towards the secondary goal of applying the software to other growth systems, both chemical and physical.

2.1 Kinetic Monte Carlo

The foundation for SNAPS is kinetic Monte Carlo, which has been previously described in detail [106–109], due to its computational efficiency in modeling the long time scales of CNP growth. The desire to resolve atomic detail in simulations naturally suggests a method like molecular dynamics, which directly computes the dynamical evolution of a system of atoms. However, molecular dynamics (MD) is typically limited to modeling phenomena that occur on a time-scale of less than 1 microsecond due to computational requirements [106]. This issue is commonly referred to as the "time-scale problem" and motivates the application of alternate simulation methods to access longer time scales, such as kMC.

The kMC method is a stochastic algorithm that is able to efficiently model much longer time scales than MD for rare-event systems, which are characterized by fast transition events that are interspersed between relatively long periods of inactivity. While modeling such a system with MD can be inefficient due to the expenditure of large amounts of computational time on relatively uninteresting periods of inactivity, kMC focuses on describing the transition events directly, resulting in significant computational savings while retaining essential detail. Since the gas phase chemical growth of a molecule can be considered as a rare-event system, kMC will efficiently produce a time dependent trajectory.

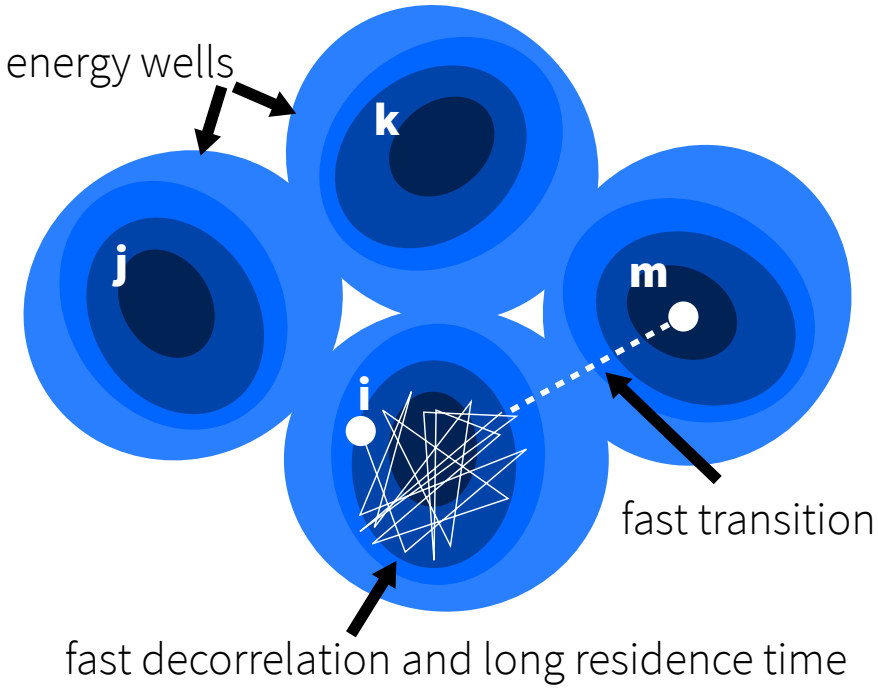

Figure 2.2: The fluctuations of a system within an energy well i. The green dot represents the state of the system at a given time. After some time, the system will eventually transition into state m. Adapted from [106]

KMC exploits the property that a rare-event system stays in any particular state for a relatively long period of time, such that the system exhibits no hysteresis. Consequently, the transitions of the system only depend on the state of the system at a given time. Consider a rare-event system, depicted in Figure 2.2, that begins in a potential energy well corresponding to a given state i. The system can be called relaxed and will spend relatively long periods of time in this energy well, but can also escape to an adjacent well, for example j, k, or m. An important assumption of kMC is that the system is ergodic; namely, over an infinite period of time, the system will explore all microstates, such that a time average over such a sequence of states is equivalent to an ensemble average for the system. Ultimately, transitions between wells characterize the evolution of this system. For a system in a given state i, each possible escape to an adjacent well j has an associated rate constant k_{ij}. A second important assumption of kMC is that the system decorrelates on a time scale that is

far shorter than the time spent in a relaxed state in the well. This assumption means that as the system "wanders" within a given well, it exhibits no hysteresis and the probability of escape through each pathway remains constant. This behaviour results in a first-order process, where the probability distribution function for the time of first escape from the well is

$$p(t) = k_{tot} \exp(-k_{tot} t)$$

$$k_{tot} = \sum_{j} k_{ij}$$

Similarly, the probability of escape for each pathway is:

$$p_{ij}(t) = k_{ij} \exp(-k_{ij} t)$$

A kinetic Monte Carlo simulation involves stepping through the transitions of the system, selecting a transition, such as a chemical reaction, amongst many possibilities, each weighted by its corresponding rate constant. The result of such a simulation represents a single trajectory that obeys the dynamics of the system. The kMC algorithm implemented in SNAPS is the Bortz, Kalos, and Lebowitz (BKL) algorithm [107], also known as the "direct" Gillespie algorithm [108, 109], which selects an escape pathway from a given set of possibilities, M. To select a pathway in a given kMC step, each is assigned a value with magnitude equal to its corresponding rate k_{ij}, which is proportional to its probability of selection. Summation of each of these values sequentially creates an array, s, of partial sums, where element $s(j)$ represents the sum of all pathways up to and including pathway j,

$$s(j) = \sum_{q}^{j} k_{iq}$$

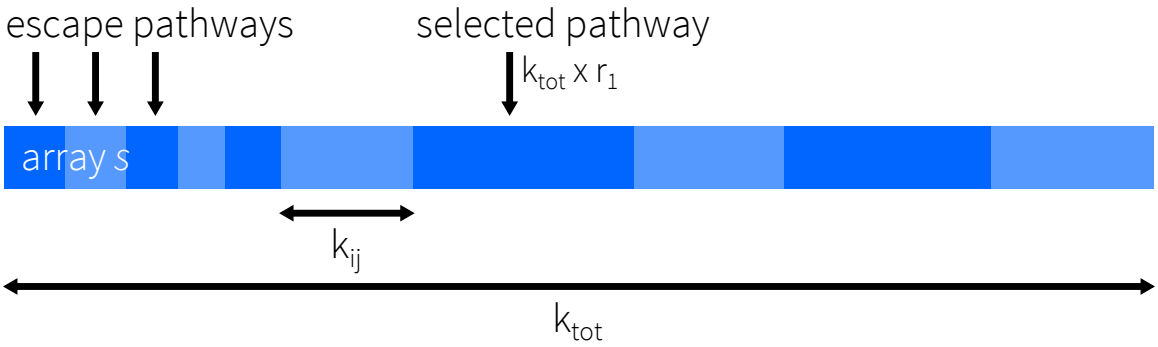

Figure 2.3: The BKL pathway selection algorithm.

Figure 2.3 depicts the BKL algorithm. The array s is analogous to a one dimensional object of length k_{tot} that is divided into sections. Each section corresponds to a specific escape pathway and has a length equal to k_{ij}. Selection of a pathway amounts to randomly choosing a point along this object and retrieving the pathway corresponding to the section containing this point. Algorithmically, a random number r_1 is drawn from a uniform distribution in the range (0,1] and multiplied by k_{tot}. The first element in the array s for which $s(j) > r_1 k_{tot}$ represents the selected pathway. The time of the simulation is then advanced according to

$$\delta t_{kMC} = \frac{-\ln(r_2)}{k_{tot}}$$

where r_2 is a second randomly chosen number from a uniform distribution in the range (0,1].

2.2 The SNAPS Algorithm

A SNAPS trajectory will consist of a time series of molecule structures, describing the chemical reaction steps in the growth of a single particle. SNAPS employs an iterative algorithm to compute each successive reaction step. Given an initial molecule seed, chemical growth model, and environmental parameters, SNAPS employs an iterative algorithm, shown in Figure 2.4, that broadly proceeds as follows:

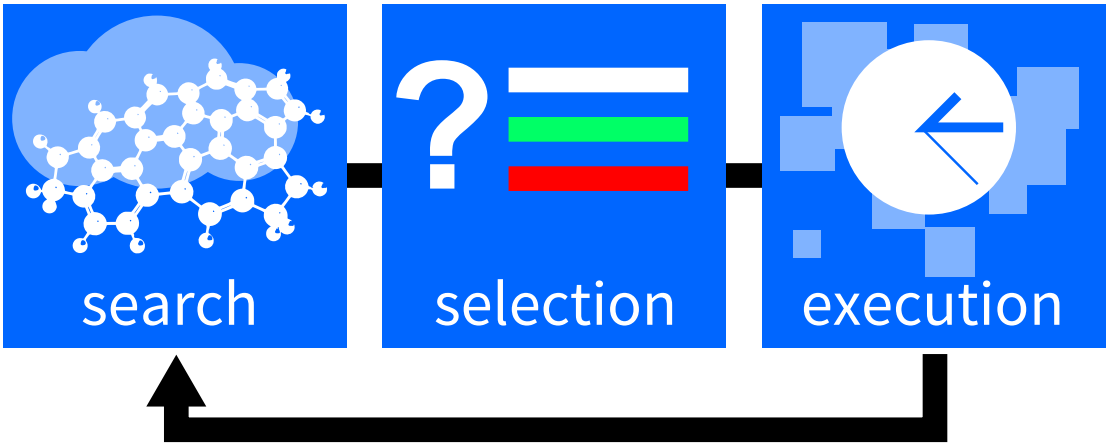

Figure 2.4: Schematic of the SNAPS algorithm.

1. **Search**: Based on a given mechanism and the gas phase environment, builds a list of possible chemical reactions weighted by their kinetic rates, computed using input rate constants and gas phase concentrations in the case of a bi-molecular reaction.

2. **Selection**: Selects a reaction using the BKL algorithm. Tests this choice based on the change in energy of reaction, ΔE, and accepts or rejects the reaction based on a chosen threshold placed on the Boltzmann factor $\exp(-\beta \Delta E_{reaction})$. Upon rejection, this step is repeated, omitting the rejected reaction.

3. **Execution**: Applies appropriate modifications to the molecular structure, advances the time of simulation according to the BKL algorithm, $\delta t_{kMC} = \frac{-\ln(r)}{k_{tot}}$, $k_{tot} = \sum_j k_{ij}$, and checks for termination of simulation based on a specified stop criterion, e.g. time of simulation, size of molecule, or number of kMC steps.

Figure 2.5 shows some examples of molecules produced by simulation of PAH growth in combustion using SNAPS and identical initial conditions. These examples illustrate the range in composition and morphology of particles that grow from a given a set of chemical reactions. In particular, these results show a significant variance in PAH mass, as well as the formation of both curved and planar PAHs.

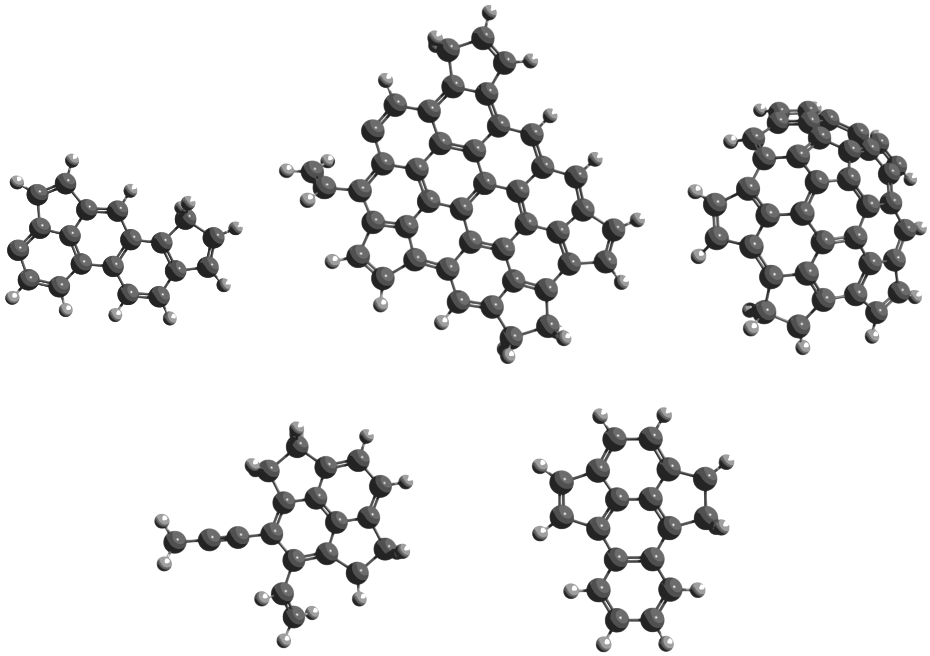

Figure 2.5: Selected molecules produced by SNAPS simulation of PAH chemical growth.

The SNAPS algorithm has been implemented in Python 2.7 to leverage its extensive collection of scientific and helper libraries, namely Open Babel 2.3.2 [110], Pybel [111], SciPy 0.12, and PyParsing 1.5.4. Furthermore, the new codebase utilizes an object-oriented approach and has been designed to be highly extensible to facilitate future development. A single growing molecule is represented by an instance of the particle class, which contains attributes and functions to simulate growth.

2.3 Gas Phase Environment

Strictly speaking, SNAPS simulates the growth of a seed molecule in well mixed, dilute, and ideal gas phase systems. Parameters that describe the environment for growth must be provided as inputs to the algorithm. These parameters include temperature, pressure, and ambient gas phase species, such as hydrogen radicals, hydroxyl radicals, or acetylene. While direct simulation of combustion is not within the scope of SNAPS, the program can simulate representative growth of particles in such environments given appropriate profiles. For example, an SNAPS simulation can represent

the growth of a single particle in a zero-dimensional homogeneous combustion reactor, or one as it travels along a streamline in a flame. These types of systems involve temporally changing temperature, pressure, and species molar concentrations. However, the previous version of AMPI restricted simulation to the growth of particles in environments where these parameters remained constant. Consequently, SNAPS includes the capability to model systems with time dependent environmental profiles.

An important assumption of SNAPS is that the growth of the particle has a negligible effect on its environment. Namely, while profiles for temperature, pressure, and ambient gas phase species may change, SNAPS does not account for changes in these parameters as a result of the growth of the particle. This assumption is reasonable when the concentration of growing particles is small relative to other ambient species. For example, the formation of PAHs in flames consumes species such as hydrogen radicals and acetylene; however, the concentration of PAHs is expected to drop by orders of magnitude with increasing number of rings [14]. Therefore, it is reasonable to infer that the concentration of these PAHs is small and that their growth has a negligible effect on the environment relative to other combustion processes.

2.4 Chemical Growth Mechanism

Conventional kinetic mechanisms, such as those used with the CHEMKIN software, specify all reactants, products, and intermediate species, as well as the chemical reactions that form and consume each one. Such a model is consistent with the macroscopic formulation of a deterministic simulation. However, since SNAPS employs a stochastic formulation of chemical kinetics, it requires a significantly different description of reactivity in the specification of a growth model. Namely, SNAPS describes chemical reactivity from the perspective of the single growing molecule, rather than the reacting system as a whole. Consequently, the chemical growth model must be defined in SNAPS such that it describes the reactivity of the growing molecule at any

step in its trajectory. This requirement necessitates flexibility and consistency in the specified growth model.

SNAPS defines chemical reactivity using a scheme that involves reactive sites on a molecule, atoms or groups of atoms, as well as corresponding reactions or transitions, each with an associated kinetic rate constant. For example, a reaction site in the current CNP growth mechanism is an aromatic carbon attached to a hydrogen atom. A corresponding reaction definition is the abstraction of this hydrogen by a radical, along with a corresponding chemical rate constant. SNAPS currently utilizes rate constants specified in terms of the parameters A, n, and E_a in the modified Arrhenius equation, where R is the universal gas constant:

$$k = AT^n \exp(\frac{E_a}{RT})$$

Definition of rate constants in Arrhenius form facilitates the use of a vast array of kinetic rate that have been formulated for combustion and PAH growth chemistry through experiment, as well as through *ab initio* and reaction rate theory. Using these rate constants, SNAPS computes rates for its kMC module using phenomenological first- and second-order rate equations for unimolecular and bimolecular reactions respectively.

A significant upgrade in SNAPS is the utilization of the Open Babel cheminformatics library and Pybel extensions [110, 111]. Beyond providing molecular modeling functionality, Open Babel provides cheminformatics capability that enables SNAPS to search for reactive sites in a molecule based on a diverse set of chemical criteria. SNAPS searches for reaction sites defined using the Smiles Arbitrary Target Specification (SMARTS) [112] language for specifying substructure patterns within a molecule. Using SMARTS, reaction sites can be specified in terms of properties including atom type (e.g. aromatic, aliphatic, sp^3 hybridized), bond type, and molecular connectivity

(e.g. membership in ring(s) or specific aliphatic group). This functionality enables far greater precision and flexibility in reaction definition compared with previous versions of AMPI. For example, SNAPS can detect attached aliphatic chains such as acetylene; groups of rings within the structure of the particle; atoms with unpaired electrons; and atoms that could form a ring-closing bond. This flexibility greatly facilitates the translation of proposed chemical mechanisms for PAH growth into an SNAPS compatible model.

In general, the kMC method requires the specification of corresponding forward and reverse rates in order to correctly simulate the dynamics of a system. Therefore, specifying both forward and reverse reactions is an important consideration when creating a chemical growth model. A drawback of emphasizing reaction reversibility is a common issue in kMC applications where some reactions have significantly lower barriers than competing reactions. These low barrier reactions are the most likely to be chosen by the kMC algorithm, leading to inefficiency in sampling states separated by higher barriers. Consequently in SNAPS, the specified growth model greatly impacts computational performance. Corresponding forward and reverse reactions with large rates in the growth model, due to low barriers or faster kinetics, lead to trajectories where particles spend substantial time switching between the same two structures. For example, a particle may experience repeated cycles of hydrogen abstraction followed by hydrogen addition. While this behaviour is physically correct, it results in computational inefficiency, especially in growing particles of large size. Currently, this issue is mitigated by the significant speed improvement of SNAPS, which enables the simulation of these reversible reactions while maintaining practical overall run times. Further amelioration of this problem could involve modifying the reaction model to define global reactions that jump over these elementary steps and obviate simulation of these repetitive cycles. However, this approach greatly hinders the exploration of PAH structures that may result from this reversibility and has been

avoided as much as possible.

Since time advancement in kMC is dependent on chemical rates, slower or fewer possible reactions lead to longer time steps in the simulation trajectory. As a result, the sampling efficiency of SNAPS also depends on the specified growth model and environmental conditions, which dictate the rate at which chemical reactions occur in simulation. Low rate constants, gas phase species concentrations, and temperature all slow the rate of particle growth. Consequently, more trajectories are required to resolve phenomena that occur on finer time scales. Moreover, a coarse time step can be particularly problematic if environmental parameters such as temperature are changing on a finer time scale.

2.5 Reaction Rejection

SNAPS employs a new means of reaction rejection to address growth model limitations, namely steric factors and imperfect reaction site definitions. Steric hindrance occurs when the algorithm attempts an addition reaction at a position of the particle where there is insufficient physical space to accommodate the incoming species. Additionally, there are instances where the algorithm erroneously identifies unphysical chemical reactions, such as for ring closures, that have identical connectivity to a legitimate chemical reaction. Figure 2.6 depicts examples of steric hindrance and an unphysical reactions that SNAPS will reject. Figure 2.6a shows that the SNAPS algorithm will reject a reaction that resulted in the addition of benzene that overlaps with the particle structure, but will allow the addition of benzene where there is sufficient volume. Figure 2.6b shows an expected ring closure to pyrene, and an unphysical one that has identical connectivity as specified in the growth model. In theory, the kinetic rates for these incorrect reactions should be vanishingly low and they should not be available for selection; inclusion of these reactions is an unfortunate result of the simplifications made in the chemical growth mechanism, which assigns them the

same rate as a legitimate reaction.

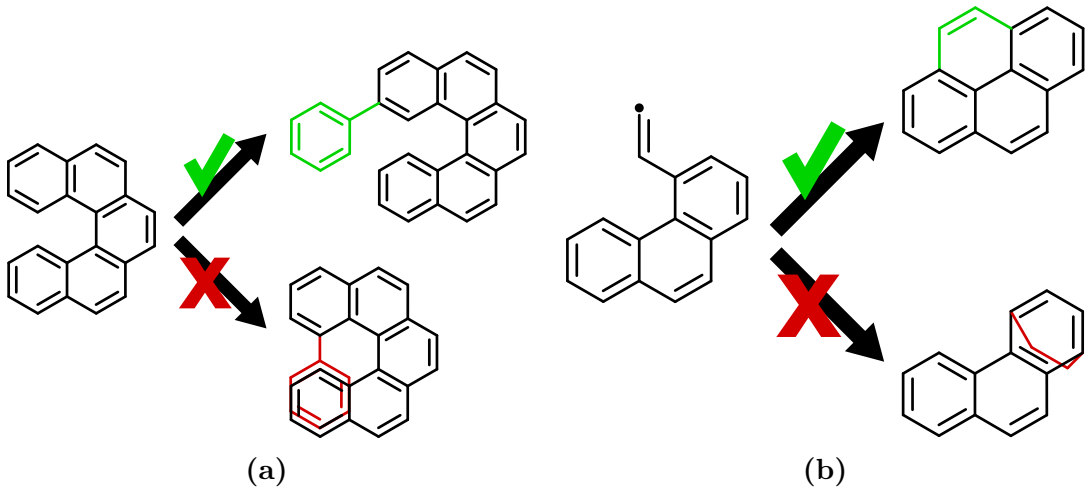

Figure 2.6: Examples of scenarios for reaction rejection in SNAPS: (a) steric hindrance in benzene addition (b) improper ring closure.

The original AMPI accounts for steric hindrance through a volume check on the particle and the species to be added. The SNAPS software implements a scheme that exploits the large changes in the potential energy that accompany these unphysical reactions. In each kMC step following minimization, SNAPS computes the change in potential energy, $\Delta E_{reaction}$, between initial and final states of the system due to the chosen reaction, including all reactants and products in a given reaction. For example, a hydrogen abstraction from a molecule such as benzene has the formula $C_6H_6 + H \longrightarrow C_6H_5 + H_2$ and the quantity $\Delta E_{reaction}$ includes the change in energy of the molecule, as well as the molecular and radical hydrogen.

The change in potential energy is then related to a probability of reaction, $P(\Delta E_{reaction})$, and is rejected based on a chosen threshold as follows:

$$P(\Delta E_{reaction}) = \exp(-\beta \Delta E_{reaction})$$

$$Accepted : P(\Delta E_{reaction}) \geq threshold$$

$$Rejected : P(\Delta E_{reaction}) < threshold$$

$P(\Delta E_{reaction})$ is the ratio of the Boltzmann factors for the initial and final states and gives a measure of the likelyhood that the particle would experience a reaction with a given change in energy. Using this rejection criterion, SNAPS recognizes and rejects unphysical reactions that are associated with large changes in energy and thus low probabilities of reaction. This scheme was chosen because it enables the specification of a threshold that accounts for the temperature of the system.

2.6 Energy Minimization

The most significant change in SNAPS is obviating the use of molecular dynamics (MD), which was primarily motivated by the desire to significantly increase the computational performance of SNAPS. The MD component is integral to AMPI primarily because it is employed to produce a relaxed molecular structure at the simulation temperature. This structure is critical to detecting reaction sites, which relies heavily on atomic distances. In addition, AMPI utilizes this structure to perform a volumetric check for reactions to account for steric hindrance. The new scheme for the chemical growth component of SNAPS employs the molecular feature perception routines of Open Babel, which does not require an MD relaxed structure, as it relies primarily on explicit molecular connectivity. As a result, SNAPS replaces MD with a substantially faster energy minimization step, utilizing the molecular modeling capabilities of Open Babel. This step provides structures for visualization and computed potential energies that are used in the new reaction rejection scheme of SNAPS, which accounts for steric hindrance and reaction definition errors. In each kMC step, the algorithm minimizes the potential energy of the molecule after modification due to the chosen reaction. SNAPS currently utilizes both the conjugate gradients [113] and steepest descent [114–116] minimization methods. Furthermore, the algorithm minimizes the molecule multiple times to mitigate errors in this process. Before each minimization step, each atom of the molecule is translated randomly in direction and

by a magnitude between 0 and 1 Å. This arbitrary translation corrects for errors of the minimization algorithms, as well as scenarios where the molecule ends in a configuration corresponding to a local rather than global minimum.

Energy minimization and calculation requires a molecular modeling forcefield. Previously, AMPI utilized the Adaptive Intermolecular Reactive Empirical Bond Order (AIREBO) [117] forcefield, a reactive forcefield used to simulate hydrocarbon systems, and more recently, hydrocarbon-oxygen systems [118]. This forcefield was originally used as part of the molecular dynamics and ring closure routines of AMPI. However, since the MD component of AMPI is obviated by the new schemes of SNAPS, an alternate choice of forcefield is possible. The current work utilizes the static variant of the Merck Molecular Force Field 94 (MMFF94s) [119, 120], which is a classical all-atom forcefield designed for energy minimization studies. MMFF94s has been parametrized using a core of computational chemistry derived data, and further augmented with experimental data. MMFF94 aims to be applicable to a wide variety of species, including alkanes, alkenes, aromatics, and 5- or 6-membered ring heteroaromatic species. As a result, this forcefield is a reasonable choice to simulate PAH growth, which will include primarily these types of species. In addition, the wide scope of MMFF94s offers flexibility in potentially studying reactions with species other than carbon and hydrogen, or other growth systems. Moreover, the extensibility of the SNAPS code base allows the use of other forcefields included in the Open Babel toolkit, or even to other molecular modeling software, should the need arise.

2.7 Summary

The SNAPS software is a significant development in stochastic simulation of particle growth, building upon and refining the original AMPI methodology. Through a new code base and schemes for chemical reactivity and reaction rejection through po-

tential energy, SNAPS achieves significant improvement in computational efficiency, as well as flexibility and precision in the specification of chemical reactivity. The probabilistic nature of the kMC algorithm enables the exploration of detailed chemical reaction trajectories, which will greatly benefit the investigation of PAH growth by predicting isomers resulting from specific chemical reaction pathways. Through comparison with experimental data and observations, this level of detail will enable the evaluation of proposed PAH chemical mechanisms, as well as the characterization of species formed in combustion. The following chapters detail this effort, beginning with a description of the application to and evaluation of SNAPS in the context of PAH chemical growth in combustion.

CHAPTER III

A Framework for Investigating Gas Phase Chemical Growth of Polycyclic Aromatic Hydrocarbons

A methodology to investigate PAH growth in combustion was concurrently developed to the SNAPS software. A newly created chemical reaction mechanism was used to evaluate SNAPS in terms of: the accuracy of its kMC algorithm; the behaviour reaction rejection scheme; computational speed; and sensitivity to reaction pathways. In addition, a method was also defined to use SNAPS to simulate premixed laminar flames. Together, these components form a framework for subsequent characterization of PAHs in combustion.

3.1 A PAH Chemical Reaction Mechanism for SNAPS

A new chemical mechanism for SNAPS was developed to investigate PAH growth in combustion. While the model utilizes the reaction pathways and rates described by traditional chemical kinetic models, it differs dramatically, as it must describe the reactivity of any PAH molecule at any given time step, as described in Chapter II. A key goal in developing the current mechanism was to include major PAH chemical growth pathways in terms of elementary steps. Through implementing the growth

model in this way, a SNAPS simulation can be used to explore the PAHs produced by the combinations of specified reaction pathways. The base collection of pathways for the current PAH growth model is the hydrogen abstraction, acetylene addition (HACA) mechanism [17, 46]. This mechanism is important in PAH growth because it involves acetylene and hydrogen radicals, which are among the most abundant species in flames [14]. As a result, HACA is considered to be the most important PAH chemical growth mechanism and is the foundation of many PAH kinetic models. As the name implies, HACA is a repetitive sequence of hydrogen abstractions and acetylene additions that result in an increasing number of aromatic rings. The current implementation of this mechanism for SNAPS combines several variants of the HACA mechanism [46, 76, 83, 121, 122], utilizing chemical rate constants derived from Kislov et al. [123].

The growth model also includes addition reactions ethylene and vinyl radicals, which are 2 carbon species that may also contribute to growth via the HACA mechanism. Furthermore, the mechanism includes the addition of benzene, phenyl, and propargyl radicals, which can form biphenyl moieties; cyclopentadienyl radicals, forming phenanthrene moieties; and methyl radicals, which can, for example, contribute to the formation of indene moieties. Many different types of ring closures were also included in the mechanism, including creation of 5- and 6-membered rings at "zig zag," "armchair," and "bay" sites (nomenclature described by Celnik et al. [94]), using reactions and rates derived from Kislov et al. [123], Raj et al. [95], and Violi [124]. A full description of the PAH growth model is shown through reaction pathways in Figures 3.1 and 3.2, as well as rate constants in Tables 3.1 and 3.2.

Figure 3.1a shows the growth of benzene to naphthalene via the HACA mechanism. The mechanism utilizes chemical rate constants derived from work by Kislov et al. [123]. The growth model also includes the addition reactions of the vinyl radical (C_2H_3) and ethylene (C_2H_4). These reactions are alternative addition reactions

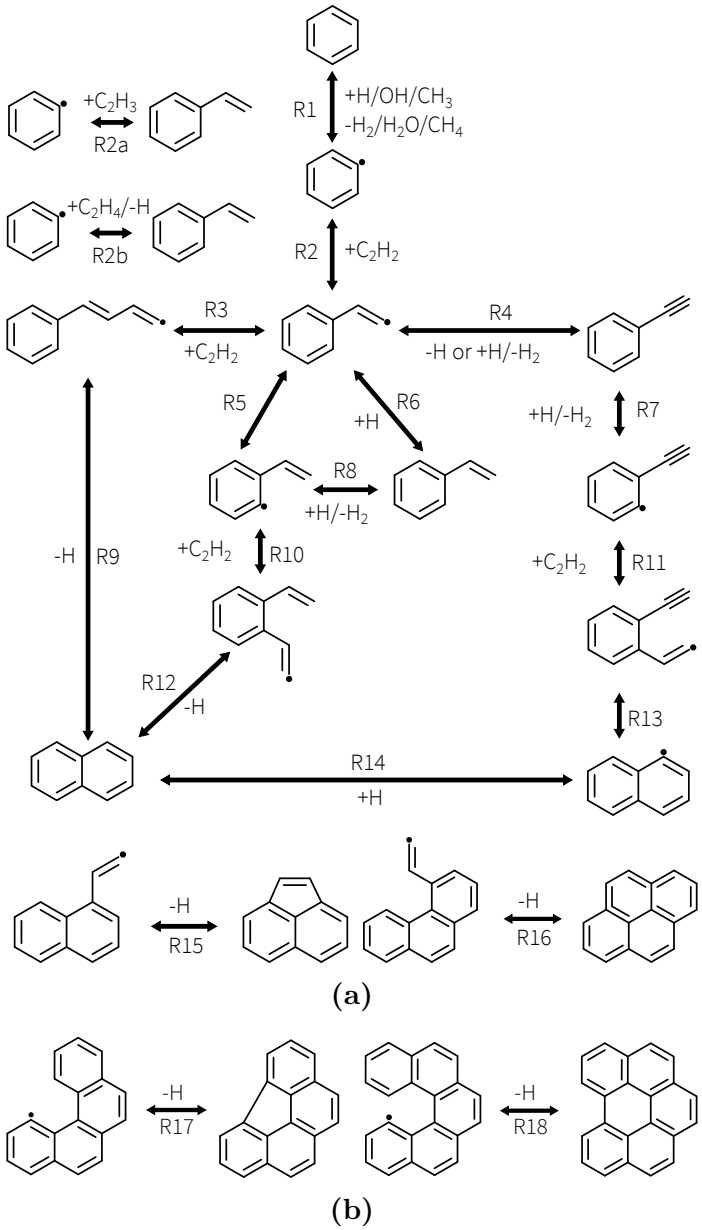

Figure 3.1: The reaction network of the HACA mechanism: (a) benzene growth to naphthalene and 5- and 6-membered ring closure at zig zag and armchair sites (b) 5- and 6-membered ring closure at bay sites.

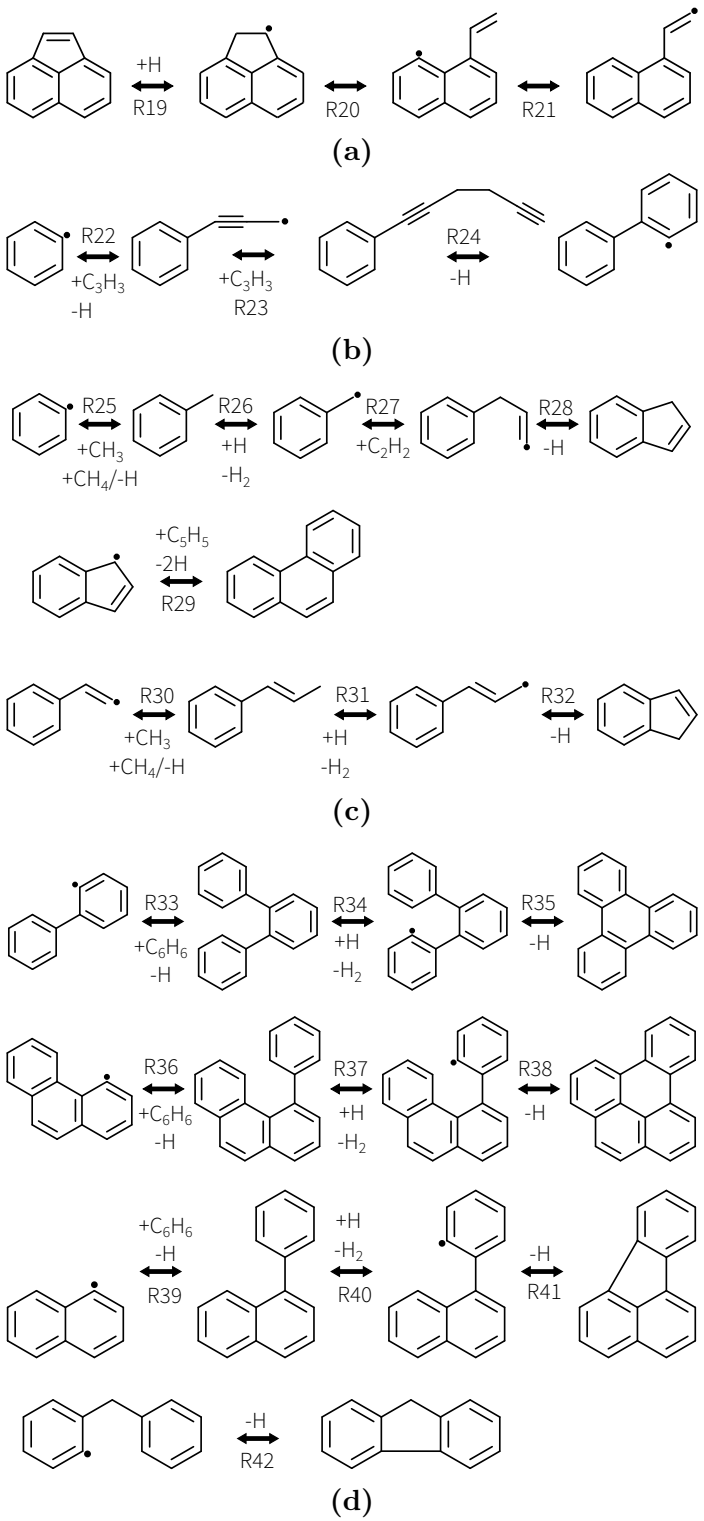

Figure 3.2: Additional reaction pathways in the PAH growth model: (a) 5-membered ring migration (b) propargyl addition to biphenyl (c) formation of indene and reaction with cyclopentadienyl radicals to phenanthrene (d) benzene and phenyl addition and ring closures.

Table 3.1: Chemical rates for reactions included in the HACA portion of the PAH growth model. The source "CR" refers to a reverse rate computed using thermodynamic equilbrium.

Reaction and Number(s)	Forward Rate A	n	E_a	Source	Reverse Rate A	n	E_a	Source
Units: A = [s^{-1}] for unimolecular reactions, [$cm^3 s^{-1} mol^{-1}$] for bimolecular reactions; $E_a = \frac{kcal}{mol}$								
Hydrogen Abstraction, Acetylene Addition								
H Abstraction by H e.g. R1, R6, R8, R14, R26, R31, R34, R37, R40	6.46E+07	1.86	15.98	[123]	9.23E+04	2.39	5.82	[123]
H Abstraction by OH e.g. R1, R6, R8, R14, R26, R31, R34, R37, R40	8.65E+02	3.04	3.68	[123]	5.59E+00	3.57	8.66	[123]
H Abstraction by CH_3 e.g. R1, R6, R8, R14, R26, R31, R34, R37, R40	8.65E+02	3.04	3.68	[123]	5.59E+00	3.57	8.66	[123]
Acetylene Addition e.g. R2, R3, R10	3.29E+06	2.05	3.16	[123]	2.48E+15	0.01	46.06	[123]
Vinyl (C_2H_3) Addition e.g. R2a	1.50E+22	-2.6	6.28	[125]	7.10E+21	-1.67	118.73	CR
Ethylene (C_2H_4) Addition e.g. R2b	2.51E+12	0	6.2	[125]	4.84E+20	-2.17	13.66	CR
Isomerization - Ethenyl to Acetyl e.g. R4	7.18E+10	1.02	38.67	[123]	1.06E+09	1.53	5.63	[123]
Isomerization - Ethenyl to Acetyl by H e.g. R4	1.65E+11	0.49	10.63	[123]	6.99E+08	1.32	87	[123]
Hydrogen Transfer e.g. R5	5.90E+10	0.55	27.57	[123]	2.32E+10	0.69	25.93	[123]
6-Membered Ring Closure e.g. R9	3.61E+09	0.6	3.64	[123]	3.91E+17	-1.51	67.91	CR
6-Membered Ring Closure e.g. R12	5.14E+12	0.06	2.13	[123]	4.16E+20	-2.05	66.35	CR
6-Membered Ring Closure e.g. R13	9.95E+11	0.05	5.4	[123]	2.22E+12	0.74	62.4	CR
5-Membered ring closure - Zig Zag e.g. R15	2.88E+11	0.23	17.03	[123]	6.67E+12	0.43	15.54	CR
6-Membered ring closure - Armchair e.g. R16	1.91E+09	1.14	1.63	[123]	3.29E+11	1.24	26.43	CR
Ring Closures at Bay Sites								
5-Membered Ring Closure - Bay e.g. R17	3.86E+11	0.21	17.7	[124]	6.67E+12	0.43	15.54	CR
6-Membered Ring Closure - Bay e.g. R18	1.11E+11	0.66	23.99	[95]	3.29E+11	1.24	26.43	CR

Table 3.2: Chemical rates for additional reactions included in the PAH growth model. The source "CR" refers to a reverse rate computed using thermodynamic equilbrium.

Reaction and Number(s)	Forward Rate A	n	Ea	Source	Reverse Rate A	n	Ea	Source
Units: A = [s^{-1}] for unimolecular reactions, [$cm^3 s^{-1} mol^{-1}$] for bimolecular reactions; $E_a = \frac{kcal}{mol}$								
5-Membered Ring Migration								
5-Membered Ring Hydrogenation e.g. R19	8.41E+08	1.49	0.99	[92]	1.00E+10	0.22	25.54	[92]
5-Membered Ring Opening - Hydrogenated e.g. R20	1.00E+10	-0.22	23.22	[92]	5.04E+06	0.74	6.57	[92]
Hydrogen Transfer e.g. R21	1.22E+06	1	8.01	[92]	3.22E+06	0.93	7.38	[92]
Propargyl Addition and Formation of Biphenyl								
Propargyl Addition e.g. R22	3.00E+12	0	0	[62]	3.39E+17	-1.06	-0.94	[62]
Propargyl Addition and 6-Membered Ring Closure to Biphenyl e.g. R23 + R24	3.00E+12	0	0	[62]	3.39E+17	-1.06	-0.94	[62]
Formation of Indene and Phenanthrene								
Methyl Addition e.g. R25,R30	2.82E+44	-9.36	14.31	[125]	1.03E+22	-1.8	106.82	CR
Acetylene Addition to Methyl e.g. R27	3.20E+11	0	7	[125]	2.48E+15	0.01	46.06	[123]
Ring Closure - Propenyl Chain e.g. R28,R32	2.88E+11	0.23	17.03	[123]	6.67E+12	0.43	15.54	CR
Indene to Phenanthrene e.g. R29	5.00E+12	0	8	[125]	1.00E+19	-1.05	-15.56	CR
Benzene, Phenyl Addition and Ring Closures								
Benzene Addition e.g. R33,R36,R39	2.22E+83	-20.79	46.89	[125]	1.79E+22	-2.45	23.59	CR
Phenyl Addition e.g. R33,R36,R39	2.00E+26	-3.9	6.32	[125]	7.06E+21	-1.56	119.01	CR
6-Membered Ring Closures e.g. R35,R38	1.11E+11	0.66	23.99	[123]	3.29E+11	1.24	26.43	CR
5-Membered Ring Closure e.g. R41,R42	3.86E+11	0.21	17.7	[123]	6.67E+12	0.43	15.54	CR

involving 2 carbons, which also lead to growth through the HACA mechanism shown in Figure 3.1. The growth model includes the ring closures depicted by R15 and R16, creating 5- and 6-membered rings at zig zag and armchair sites, respectively. The armchair and zig zag closure reactions utilize rates derived from Kislov et al. [123]. Figure 3.1b depicts 5- and 6-membered ring closures at bay sites, which utilize rates derived from Raj et al. [95] and Violi [124].

Figure 3.2 shows additional reaction pathways that have been translated into the PAH growth model which form several different moieties. These pathways include the 5-membered ring migration pathway proposed by Frenklach et al. [92], shown in Figure 3.2a; the addition of propargyl sequentially to form biphenyl, shown in Figure 3.2b; the formation of indene through addition of methyl radicals and acetylene, shown in Figure 3.2c; the formation of phenanthrene by reaction with the cyclopentadienyl radicals, shown in Figure 3.2c; the addition of benzene and phenyl radicals to PAHs and subsequent ring closures involving attached benzyl groups, shown in Figure 3.2d. All of the elementary steps of these reactions are expected to mix in simulations, exploring complex reaction pathways beyond those illustrated.

The included pathways have been proposed in literature as significant contributors to PAH growth and have been included in previous chemical kinetic mechanisms [62, 83, 86, 125]. Moreover, the species involved in addition reactions in the growth model where also chosen considering their abundance throughout different flame environments. For example, Table 3.3 enumerates the maximum mole fractions of important addition species in the flame of Tregrossi et al. [72]. The most abundant species are acetylene and benzene, while the concentrations of other species are several orders of magnitude lower. While acetylene might be expected to dominate PAH growth, the remaining species were included to test their effect on growth, as their corresponding pathways have been posited to be significant. Moreover, a species like ethylene or the vinyl radical may be more abundant under different conditions, such

as in an ethylene flame.

Table 3.3: Maximum magnitudes of species mole fractions of species involved in addition reactions in the current PAH growth model in the premixed laminar benzene flame of Tregrossi et al. [72]

Species	**Maximum Mole Fraction Magnitude**
CH_3	1E-4
C_2H_2	1E-2
C_2H_3	1E-6
C_2H_4	1E-4
H_2CCCH	1E-4
C_5H_5	1E-4
C_6H_5	1E-6
C_6H_6	1E-2

The SNAPS PAH mechanism is relatively simple compared with existing kinetic mechanisms for PAH growth, which can contain hundreds or thousands of species and reactions, and is advantageous for modeling larger and more varied PAHs. In a traditional deterministic kinetic model, the number of required species and reactions increases dramatically with size when describing the growth of PAHs, due to the complexity of the reaction network and the necessity to track the concentration of every intermediate species of interest. For example, the ABF PAH mechanism [83], which simulates pericondensed PAHs growth up to pyrene, as well as the oxidation of small hydrocarbons, contains 101 species and 544 reactions. A more recent mechanism created by Raj et al. [86] is based on the ABF mechanism and adds 26 species and 77 reactions to describe the growth of pyrene to coronene. These additions significantly grow the size of the mechanism, accounting for an increase of 25% and 14% in species and reactions respectively. Moreover, there may be additional intermediate species and reactions that would require an increasing amount of mechanism complexity. In contrast, the SNAPS growth model has just 28 reaction types that mix to predict intermediate species. Importantly, while the types of expected species are kept in mind during mechanism development, they do not need to be explicitly specified

beforehand. Therefore, specification of the growth model can be simplified.

Despite an increased requirement for computational time, there is an emphasis on reaction reversibility in the current model that arises from the desire to observe PAH growth as accurately as possible. Fundamentally, reversibility is a requirement of the kMC methodology when modeling a chemical system like PAH growth. Moreover, from an intuitive perspective, a given PAH does not necessarily grow in a linear sequence of growth reactions, for example, hydrogen abstraction and acetylene addition. Indeed, reversibility is a fundamental characteristic of the HACA mechanism [17]. Therefore, the inclusion of reverse reactions is important in describing the complex sequence of chemical reactions that comprise the growth trajectory of a given PAH and produces a more physically realistic growth trajectory. Reversibility enables the description of intramolecular structural rearrangements and enhances the mixing of the elementary steps in the growth model and therefore the variety of PAH structures that can be explored using SNAPS.

Reaction rates have been sourced from a variety of existing literature. Unimolecular rates in the current model have been used in the high pressure limit. While efforts were made to source accurate data, analogous chemical rates were used to estimate those for reactions where specific data was not available. In particular, many rates for reverse reactions have not been explicitly computed or reported, but the emphasis on reaction reversibility in the current model necessitated their estimation. Each missing reverse reaction rate was estimated by using the relationship between forward and reverse rate constants at equilibrium, namely:

$$\frac{k_{fwd}}{k_{rev}} = K_{eq}$$

where k_{fwd} and k_{rev} are the forward and reverse rate constants and K_{eq} is the equilbrium constant for the reaction. These calculations use the concentration quotient

K_c, which is defined for a reaction $\mathrm{aA} + \mathrm{bB} \rightleftharpoons \mathrm{cC} + \mathrm{dD}$ as:

$$K_c = \frac{[\mathrm{A}]^a[\mathrm{B}]^b}{[\mathrm{C}]^c[\mathrm{D}]^d}$$

Equilibrium constants were computed using existing thermodynamic data in the NASA polynomial format for calculation of molar enthalpy and entropy. While there is error associated with this type of estimation, this method aligns the calculated rates with existing deterministic chemical mechanisms which estimate reverse rates in the same way. As a result, these computed reaction rates will have equivalent accuracy to implicitly computed reverse reaction rates in a traditional deterministic chemical kinetics simulation, such as in CHEMKIN.

Since SNAPS uses the growth model to specify potential reactions for any intermediate species, it necessitates the definition of lumped reaction types to produce a manageable mechanism size. For example, instead of defining separate rates for hydrogen abstraction from benzene and naphthalene, these chemical reactions are lumped and defined as hydrogen abstraction from an aromatic carbon-hydrogen pair. Lumping such reactions requires the choice of a single rate to approximate all reactions in the set. For hydrogen abstraction by H, Kislov et al. [123] computed different chemical rates for benzene and naphthalene. To derive a single rate for the corresponding SNAPS hydrogen abstraction reactions, these rates must be adjusted for reaction path degeneracy. The current SNAPS model approximates the rates of hydrogen abstraction from an aromatic carbon as the rate for benzene. Other reactions, such as ring closures or acetylene addition, have been similarly simplified to be applicable to any intermediate structure. Ultimately, the simplification of the HACA mechanism in this manner is a design choice, balancing the size of the overall mechanism with accuracy of the simulation and computational performance. The SNAPS mechanism has been formulated to be a "best estimate" of PAH growth and

its application in the current work also represents an evaluation of its constituent pathways.

3.2 Simulation of PAH Growth in a Premixed Laminar Flame

An important part of the application of SNAPS to PAH growth is simulation of the combustion environments in which PAHs and soot are formed. One such environment is the premixed laminar flame, an important experimental apparatus in which many studies have investigated PAH growth and CNP formation. Since SNAPS itself does not directly model the flame environment, it was necessary to develop a methodology using the software to simulate particle growth.

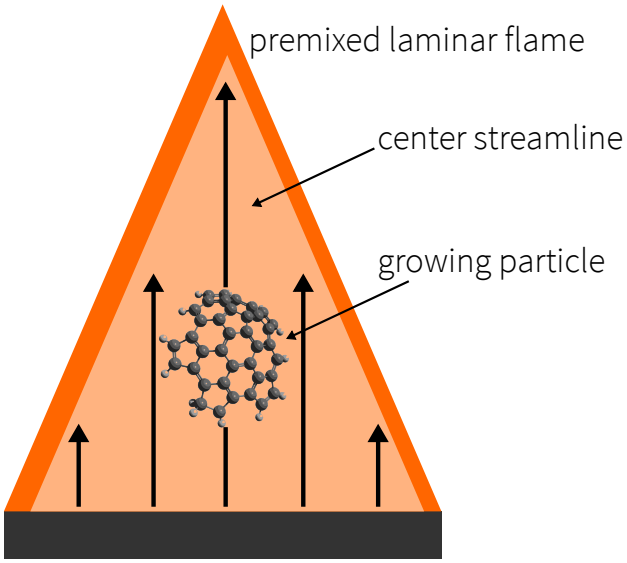

Figure 3.3: Schematic of a premixed laminar flame showing the center streamline used for simulating PAH growth using SNAPS.

To simulate growth in a premixed laminar flame, particles were assumed to travel along the center streamline of the flame, as depicted in Figure 3.3. Then the flame was modeled as a homogeneous ideal gas system that changes with time, using time dependent profiles for temperature and ambient gas phase species. These profiles were first computed as spatially dependent outputs from the premixed laminar flame

model in CHEMKIN [82]. The solution for the flame consists of a series of spatial intervals, each with a corresponding temperature and gas phase composition. Assuming a particle moving along the streamline of the flame, a "residence time" for each grid interval of the CHEMKIN solution was computed using its length and corresponding axial velocity of the mass flow. Then, a sequence of cumulative sums of these residence times, each with a corresponding temperature and gas phase composition, represents the time dependent profiles required as inputs for SNAPS simulations. A key assumption of this methodology is that the reactions governing the growth of the particle occur much faster than the flame environment changes. This assumption is particularly important because the time step of a kMC simulation is variable. If the temperature and gas phase species within an interval of the flame result in slow reactions, the average kMC time step can be greater than the residence time of that interval. This phenomenon physically corresponds to a scenario in which the particle does not have time to react before it moves out of a particular region of a flame.

Related to the dependence of the kMC time step on the gas phase environment, there is a strong correlation between SNAPS trajectories, and the choice of initial conditions for simulations of PAH growth in flames. Physically, this choice corresponds to a height in the flame where the particle is assumed to begin growth. An important issue is that at low heights in the flame, particularly before the main chemical reaction zone, are characterized by low temperature and gas phase species concentrations. Within a given spatial interval of the flame, this environment leads to long average kMC time steps that are longer than the residence time of the particle within this region. This phenomenon can be physically interpreted as the average particle moving through such a region without experiencing a reaction. Therefore, the starting point can be chosen such that adequate growth can be achieved within the starting grid interval.

For example, consider the simulation of the premixed laminar benzene flame pre-

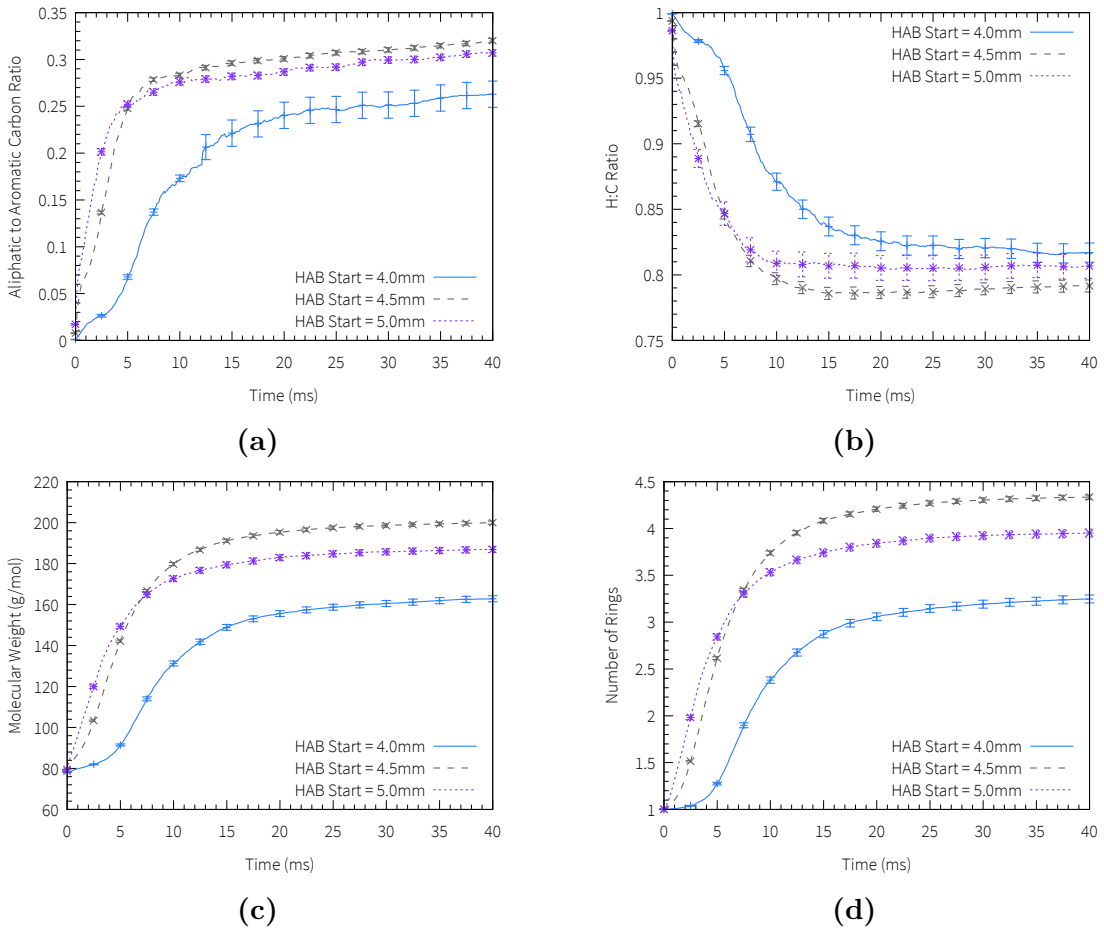

Figure 3.4: Time evolution of ensemble-averaged quantities of particles simulated with SNAPS, starting at 3 different heights above burner (HAB): (a) aliphatic:aromatic carbon ratio (b) H:C ratio (c) molecular mass (d) number of rings.

viously studied experimentally by Tregrossi et al. [72]. Figure 3.4 shows the time evolution of ensemble averaged quantities for three simulations starting at different heights above the burner. The substantial differences between the averaged quantities illustrates the strong correlation between the starting point of the simulation and simulated trajectories. The maximum growth by average molecular mass, shown in Figure 3.4c, occurs for the simulation starting at 4.5 mm. This height approximately locates the maximum rate of production of H, OH, and CH_3 radicals, which are key to particle chemical growth and can be considered to mark the beginning of the main chemical reaction zone. Simulations started before and after this point result in lower average mass growth. For simulations starting at 4.0 mm, the average first time step was 6.82 ms, which corresponds to the particle traveling well past the next starting point, 4.5 mm, before experiencing a reaction. As a result, this starting point can be considered "too early" for SNAPS to successfully model. Simulations starting at 5.0 mm also show lower overall mass growth, even though this point corresponds to the maximum concentration of H radicals. The lower growth of these trajectories can be ascribed to smaller residence time within the main chemical reaction zone of the flame. This result suggests that a particle would have experienced substantial growth before reaching this point in the flame. As a result, this point can be considered to be "too late." This example shows that, for the current implementation of SNAPS, the starting point should be chosen carefully when performing SNAPS simulations.

3.3 Verifying the SNAPS Algorithm

The SNAPS algorithm was verified by comparing an ensemble of simulated trajectories with an equivalent deterministic solution. Specifically, SNAPS predictions for the time dependent consumption of benzene and the production of naphthalene were verified against those computed using the CHEMKIN [82] closed homogeneous reactor. This reactor isolates the time evolution of chemical kinetics for comparison

between models. CHEMKIN is a well known combustion simulation software and served as a reliable benchmark. The HACA component of the PAH growth model was translated into an equivalent chemical mechanism compatible with CHEMKIN. Since CHEMKIN requires the specification of all intermediate species, the translated CHEMKIN mechanism was limited to growth between benzene and naphthalene. Then, given this mechanism and chosen set of environmental conditions (temperature, pressure, initial concentrations of fuel, etc.), CHEMKIN simulated combustion, including fuel breakdown and oxidation, and computes time histories of mole fractions for reactions and products. Of particular interest are the gas phase species involved in the HACA growth mechanism, namely acetylene, H, H_2, OH, H_2O, CH_3, and CH_4. Importantly, SNAPS is still reliant on external data for ambient gas phase species, so these profiles were used as input to SNAPS simulations. The CHEMKIN results for the time history of the mole fraction of benzene was used for comparison with SNAPS results. Using benzene as the seed molecule, a single SNAPS trajectory can be analyzed to determine a time history of when the particle exists as benzene. An ensemble of such trajectories can be averaged to produce a time dependent probability distribution for the likelihood that a particle is benzene at a given time. Multiplication of this distribution by the initial benzene concentration produces a time dependent profile that directly compares with the CHEMKIN solution. Similarly, a probability distribution for naphthalene can be computed from SNAPS trajectories, multiplied by the initial benzene concentration, and compared with the CHEMKIN solution.

The first conditions compared were at a constant temperature and pressure of 1490 K and 1 atm respectively. Initial species mole fractions, enumerated in Table 3.4, were chosen as a point at the maximum H concentration, as predicted by the ABF soot mechanism, for a a premixed ethylene flame, "C5," studied by Abid et al. [126]. The second conditions evaluated were for a variable temperature profile, which was taken from the premixed laminar benzene flame studied by Tregrossi et al. [72].

Table 3.4: Species mole fractions at the point of maximum H concentration, as predicted by the ABF mechanism, in the premixed laminar flames. The constant temperature case is for and ethylene flame "C5," studied by Abid et al. [126]. The variable temperature case is for the benzene flame, C/O = 0.77, studied by Tregrossi et al. [72]

Species	**Initial Mole Fraction**	
	Constant Temperature	**Variable Temperature**
C_6H_6	1.80E-4	3.46E-03
H	2.20E-4	7.02E-05
H_2	9.17E-2	3.04E-02
OH	1.58E-5	1.11E-05
H_2O	1.31E-1	7.29E-02
CH_3	5.86E-4	1.81E-04
CH_4	1.26E-2	3.89E-03
C_2H_2	1.42E-2	6.87E-03
Ar	7.49E-1	N/A
N_2	N/A	8.82E-01

This flame was modeled using the ABF [83] soot mechanism and the CHEMKIN premixed laminar flame solver. Species mole fractions, enumerated in Table 3.4, were recorded at the height of maximum H concentration, approximately 0.53 cm. A second CHEMKIN simulation was run in the closed homogeneous reactor using these concentrations, the CHEMKIN compatible SNAPS HACA mechanism, and the flame temperature profile beginning at this point. The spatial dependence of the temperature was related to time through the computed axial velocity of the first simulation (described in Section 3.2). This simulation was intended to isolate the HACA growth chemistry of a particle for comparison with SNAPS.

Figures 3.5a and 3.5b compare CHEMKIN and SNAPS solutions for the decay of benzene concentration for the constant and variable temperature cases, respectively. Figure 3.5b also shows the temperature profile for the variable case. Under both sets of conditions, the solutions matched. Moreover, SNAPS produced reasonably correct benzene decay with an ensemble of only 100 trajectories, but with significant statistical error. This error was reduced substantially with an ensemble of 1000

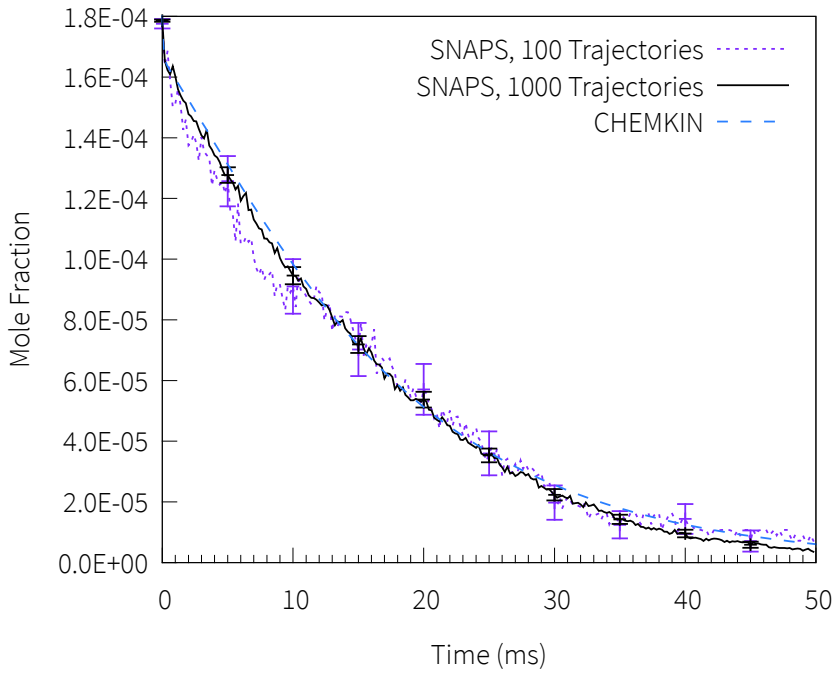

(a)

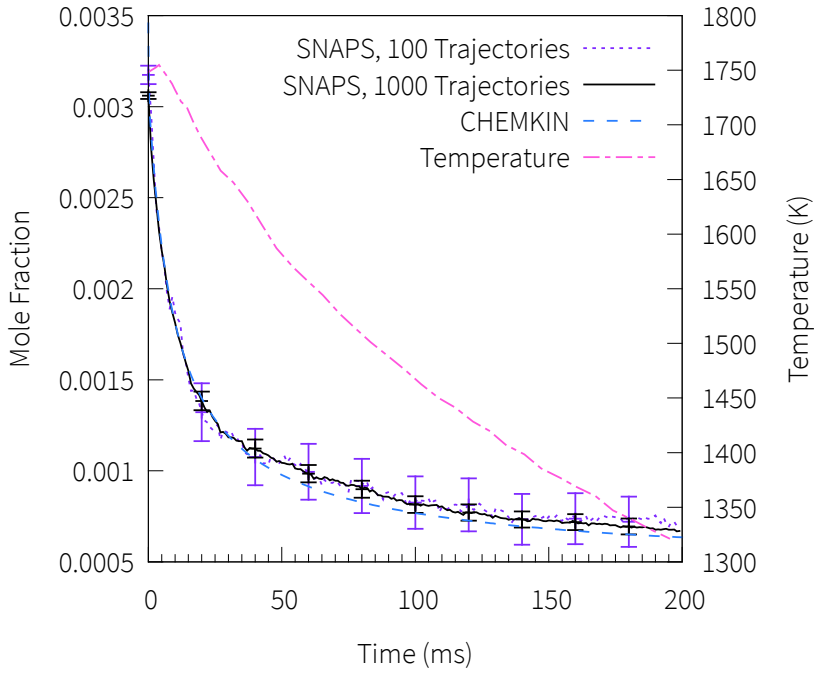

(b)

Figure 3.5: Comparison of SNAPS and CHEMKIN predictions of benzene concentration profiles with (a) constant temperature profile, $T = 1490$ K and $P = 1$ atm (b) varying temperature profile as shown in the plot. Error bars represent the standard error of the mean of the ensemble.

trajectories. The kMC algorithm in SNAPS is also theoretically accurate under conditions of varying pressure. However, since the current HACA model contains only high pressure limit rate constants, a simulation with varying pressure would not be any more illustrative of accuracy than one with constant pressure.

An important characteristic of SNAPS is that it only simulates the chemical reactions of the seed molecule and not the system in which the particle is growing. As shown in current evaluations, SNAPS requires environmental inputs that describe how the combustion environment evolves with time. If the results of a CHEMKIN simulation using a detailed chemical mechanism, such as the ABF model, were used as input to SNAPS, the solutions for the benzene concentration profile would not necessarily match. This discrepancy exists because SNAPS does not account for contributions from chemical reactions involving benzene that are unrelated to particle growth, such as benzene production from propargyl radical recombination. By restricting the CHEMKIN mechanism input to the benzene HACA growth implemented in SNAPS, the CHEMKIN simulations shown in Figures 3.5a and 3.5b provide a direct comparison to evaluate the underlying algorithm. As a result, the CHEMKIN and SNAPS solutions for benzene decay become equivalent.

By explicitly simulating only seed growth, SNAPS implicitly assumes that this growth has a negligible effect on the flame environment through its consumption of ambient species, compared with other chemical and thermodynamic processes in the flame. This assumption could be addressed by extending SNAPS to interface with software that simulates flames and combustion chemistry. Nevertheless, separating particle growth from flame chemistry is reasonable in the context of using SNAPS as an exploratory tool to link specific growth mechanisms, such as HACA, with CNP morphology.

Figure 3.6 compared SNAPS and CHEMKIN solutions for the production of naphthalene. At short times (0 to 2 ms) the solutions match, then subsequently begin to

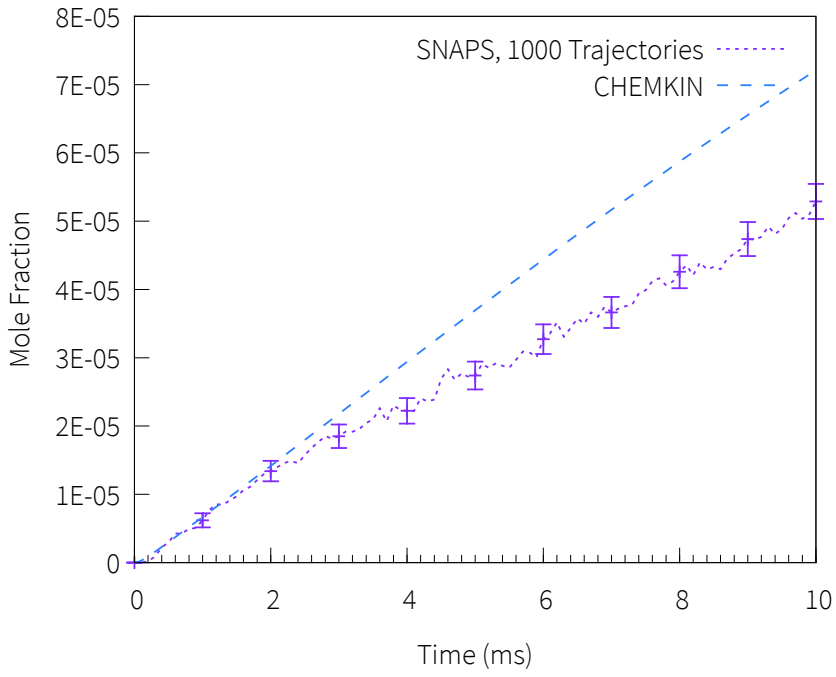

(a)

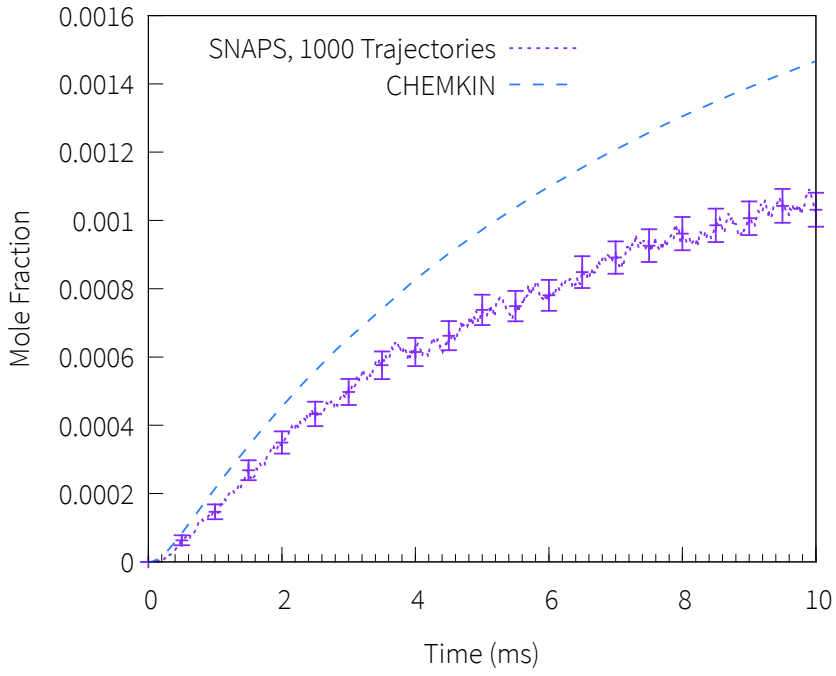

(b)

Figure 3.6: Comparison of SNAPS and CHEMKIN predictions of naphthalene concentration profiles with (a) constant temperature profile, $T = 1490$ K and $P = 1$ atm (b) varying temperature profile as shown in the plot. Error bars represent the standard error of the mean of the ensemble.

deviate from each other. This deviation is due difficulty in translating between reaction mechanisms, namely the fact that the CHEMKIN mechanism is limited to growth from benzene to naphthalene, while the SNAPS mechanism is unlimited in its growth. Consequently, the concentration of naphthalene predicted by SNAPS simulations is lower, due to consumption of naphthalene by further growth. Nevertheless, this effect is negligible early in simulations ($\leq$ 2 ms) as the production of naphthalene is expected to be much higher than its consumption. In this range, both solutions match, which corroborates the SNAPS algorithm. Altogether, the current comparisons demonstrate that SNAPS correctly describes particle chemical growth, as dictated by the growth model and the environment described by input parameters. The absolute accuracy of SNAPS with respect to real combustion systems will depend on the choice of the chemical growth model and environmental inputs.

3.4 Computational Performance

The computational speed of SNAPS was compared with AMPI in order to demonstrate its substantial performance improvement. SNAPS is a substantially faster software than AMPI, but a direct comparison of absolute speed is difficult, due to the difference in chemical growth mechanisms implemented in each software. Nevertheless, performance per kMC cycle was evaluated against AMPI simulations for 100 trajectories of chemical growth up to 30 atoms. The average times per kMC cycle for AMPI and SNAPS were 48.56 and 0.4273 seconds per cycle, respectively. The average kMC cycle time illustrates the efficiency of the SNAPS algorithm. SNAPS outperformed AMPI by approximately 113 times on a per cycle basis.

3.5 Reaction Rejection Threshold

The new scheme for reaction rejection in SNAPS requires a defined "reaction probability" threshold. To elucidate the significance of this threshold, consider the probability of reaction computed by SNAPS and a threshold defined by 10^{-x}, where x is an integer value.

$$\begin{aligned} P(\Delta E_{reaction}) &= \exp(-\beta \Delta E_{reaction}) \\ 10^{-x} &= \exp(-\beta \Delta E_{reaction}) \\ x \ln(10) &= \beta \Delta E_{reaction}; \beta = \frac{1}{k_B T} \\ x \ln(10) k_B T &= \Delta E_{reaction} \end{aligned}$$

This result shows that x effectively sets the allowable change in energy per particle as a multiple of $k_B T$, or the average kinetic energy of a particle at temperature T. The SNAPS rejection scheme was evaluated by comparing the energies of accepted and rejected reactions in 1000 SNAPS trajectories simulating particle growth in the C/O = 0.77 flame studied by Tregrossi et al. [72], using the detailed PAH growth model. This comparison was performed for a range of thresholds to illustrate their impact on SNAPS simulations. Figure 3.7 summarizes the range in energies that were accepted or rejected for 5 threshold values from 10^{-5} to 10^{-9}.

Figure 3.7 shows a clear distinction between the energies of accepted and rejected reactions, which confirms the intended behaviour of the reaction rejection scheme. In all cases, there is slight overlap between the maximum accepted energy and the minimum rejected energy. This phenomenon reflects the dependency of reaction likelihood on the temperature of the system. Namely, at a higher temperature, a reaction is more likely to be accepted, or at a lower temperature, a reaction is more likely to be rejected. Additionally, the clear distinction between accepted and rejected energies

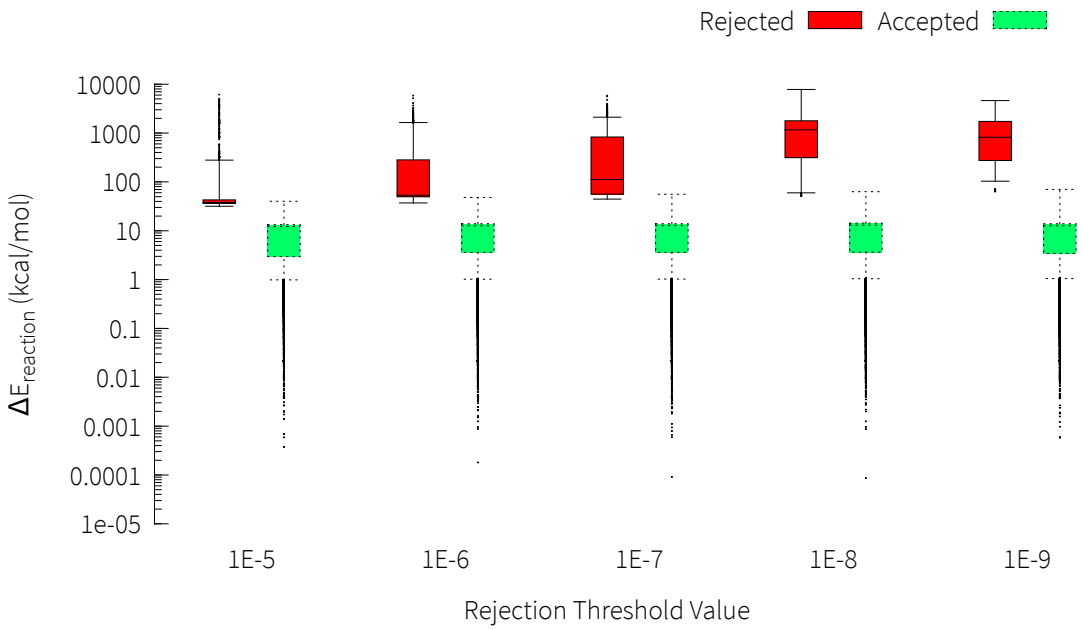

Figure 3.7: Ranges of accepted and rejected reaction energies for different rejection thresholds. Boxes are drawn to encompass data within the first and third quartiles. The median is drawn as a horizontal line within each box. Whiskers are drawn to maximum and minimum values that encompass 95% of data points. The remaining 5% are considered outliers and are drawn as points.

shows that reaction rejection is not particularly sensitive to the choice of threshold. Rejected energies tend to be orders of magnitude greater than their accepted counterparts. This behaviour reflects the goal of the rejection scheme to filter out unphysical reactions that have extreme changes in energy. These results show that the rejection scheme functions as intended in SNAPS simulations.

3.6 Sensitivity to Reaction Pathways

SNAPS simulations were also used to demonstrate its sensitivity to reaction pathways. Accordingly, the current work examined the relationship between the HACA model and the increase in CNP particle mass with time. The chosen environment for this investigation was the premixed ethylene flame, "C1," studied by Abid et al. [127]. This flame is characterized by high temperature and acetylene concentration,

which enhances growth via the HACA mechanism. Temperature and species concentration profiles for this flame, shown in Figure 3.8, were computed using CHEMKIN and the ABF chemical mechanism. SNAPS simulations were run starting at a point corresponding to a height of 0.05 cm above the burner surface. This position approximately locates the maximum rate of production of benzene, as the slope of its concentration begins to decrease after this point, and suggests significant benzene growth to larger PAHs. Similarly, the concentration profiles of acetylene, as well as radicals such as H, OH, and CH_3, show similar trends. SNAPS simulations beginning at this position describe the growth of benzene in an environment where the HACA mechanism is expected to be important. The spatial dependence of all profiles was related to time dependence through the computed axial velocity of the CHEMKIN simulation.

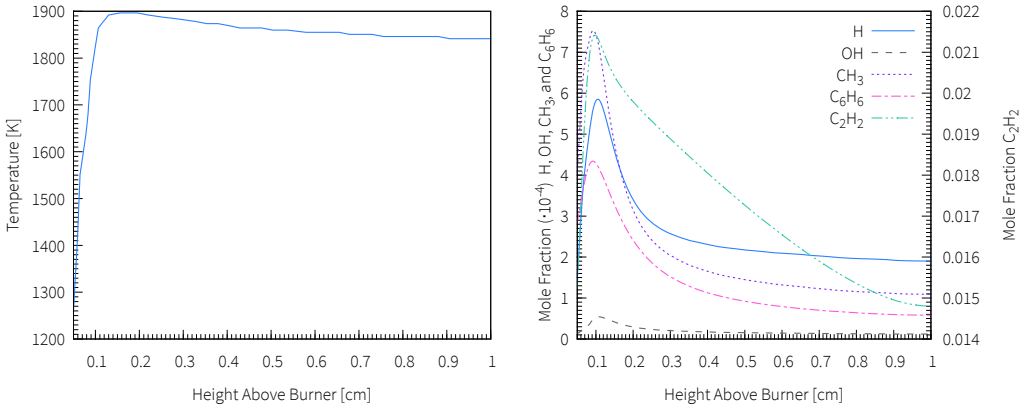

Figure 3.8: Temperature and species profiles used in SNAPS simulations for chemical growth model comparison. Profiles were computed using the ABF soot mechanism, simulating flame "C1" studied by Abid et al. [127]

Ensembles of 500 SNAPS trajectories utilizing three different growth models illustrate the impact of chemistry on accumulation of CNP mass. The growth models compared were: the HACA growth model, without closure of zig zag sites; the HACA growth model with closure of zig zag sites, depicted in Figure 3.1a; and the HACA growth model including 5-membered ring migration as proposed by Frenklach et al.

[92], shown in Figure 3.2a. Figure 3.9 compares the increase in average mass with time among simulations using the three growth models. The results show that even small changes in the growth model have significant impact on CNP mass accumulation. Addition of the zig zag closure reaction to the base HACA mechanism significantly reduces the rate of mass accumulation. Ostensibly, this result suggests that growth through the closure of 5-membered ring sites is inefficient and that particles of larger mass are less likely to contain a large number of 5-membered rings. However, this result could arise from mechanism inconsistency. Importantly, the current model considers ring closures to be directly irreversible, due to the high barriers involved in ring opening [128]. Consequently, when SNAPS closes a 5-membered ring at a zig zag site, the options for further reaction are limited, which could lead to a lower rate of mass growth. This decrease suggests that simply adding the zig zag closure reaction alone leads to structures with reactivity that the growth model cannot adequately describe.

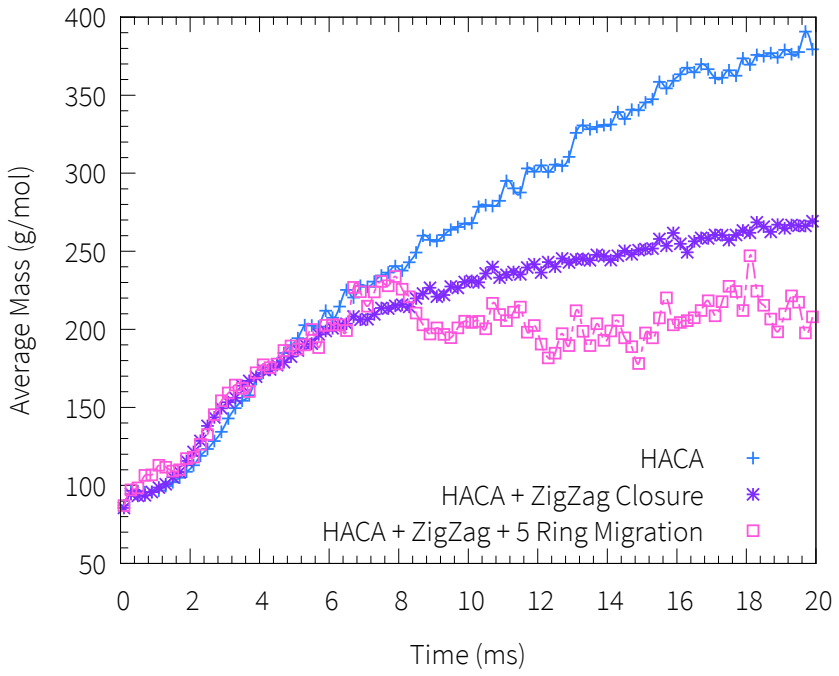

Figure 3.9: Comparison of mass growth over time for SNAPS ensembles using three different growth mechanisms.

The included reactions shown in Figure 3.2a ostensibly enable SNAPS to better

describe the reactivity of species including 5-membered rings. This growth model is always able to describe the reactivity of 5-membered rings, such that particle growth should not be as hindered by this particular inconsistency. However, Figure 3.9 shows that the addition of 5-membered ring migration further stagnates the average mass growth. This result corroborates the notion that growth through 5-membered ring closure at zig zag sites may be inefficient relative to growth through the base HACA pathways, which primarily involve 6-membered rings. However, this conclusion should be qualified inasmuch as the rates for the reactions included are uncertain. Changes in any of the reaction rates in the growth could potentially alter the resulting description of particle growth. Moreover, the reaction mechanism could be missing reaction pathways involving 5-membered rings, which could further alter growth. This result does show, however, that SNAPS can capture the effects of even small changes in the input reaction mechanism and serves a means to investigate the effects of proposed chemical reaction pathways.

3.7 Summary

SNAPS was evaluated using a newly developed PAH chemical growth mechanism. The kMC algorithm was successfully verified against the deterministic solutions of CHEMKIN and the reaction rejection scheme performed correctly as expected in prohibiting extreme changes in potential energy due to incorrect reactions. In addition, SNAPS improved computational speed per cycle by 113 times compared with AMPI and was able to capture the effect of small changes in the input chemical reaction mechanism. As well, a methodology was created for simulation of premixed laminar benzene flames using SNAPS. The development of a new chemical reaction mechanism, a flame simulation methodology, and the successful evaluation of the SNAPS algorithm represent the framework used to explore the growth of PAHs in combustion.

CHAPTER IV

PAH Growth in a Premixed Laminar Benzene/Air Flame

Motivated by the uncertainty in the composition of combustion-generated PAHs, SNAPS and the new PAH growth model were applied to study the formation of PAHs in a premixed laminar benzene flame [129]. The laminar flame environment and the benzene fuel were ideal for simulation using the current stochastic methodology. The goal of these simulations was to verify the accuracy of SNAPS simulations through comparison with existing experimental data; and investigate PAH growth and composition at an atomistic scale beyond what has been measured. Towards this goal, an experiment was chosen, originally conducted by Tregrossi et al. [72], who characterized PAH and soot formation in a premixed laminar benzene flame using gas chromatography and mass spectrometry. This experiment provided valuable measurements of species concentrations and mass spectra with which to verify simulation accuracy. Furthermore, analysis of SNAPS trajectories provided insight into the composition of nascent PAHs and the important chemical reaction pathways involved in their growth. Importantly, the results of this investigation demonstrate the accuracy of SNAPS and challenge prevailing concepts of PAH growth, revealing that even a relatively small group of chemical pathways will combine to produce complex reaction trajectories, which ultimately lead to a variety of PAH species that increases further

with mass.

4.1 Methodology

In order to prepare inputs for SNAPS simulations of PAH ensembles, namely spatially dependent temperature and gas phase species profiles, the premixed laminar benzene flame, studied by Tregrossi et al. [72], was first simulated using CHEMKIN [82]. This step is necessary as profiles of important species, such as H, OH, and CH_3, were not measured experimentally. A number of chemical mechanisms were compared to inform the choice of mechanism for this purpose, namely Appel et al. [83], Richter et al. [125], Raj et al. [86], and Sirignano et al.[89] Figure 4.1 shows a comparison of the predictions of the four kinetic models for the concentrations of acetylene, benzene, carbon dioxide, naphthalene, cyclopentadiene, and acenaphthylene in a premixed laminar flame, C/O = 0.77, studied by Tregrossi et al. [72]. The concentration profiles were computed using the laminar flame model in CHEMKIN [82].

The concentration profiles for benzene and carbon dioxide, shown in Figures 4.1b and 4.1c respectively, match reasonably well with experimental measurements. However, Figure 4.1a shows that these models, excluding that of Richter et al., have difficulty predicting acetylene concentrations. Furthermore, Figure 4.1d shows that all of these models have difficulty predicting the concentrations of naphthalene, cyclopentadiene, and acenaphthylene, substantially over predicting each. The ability of these mechanisms to reasonably describe the concentrations of carbon dioxide and benzene corroborates the performance of their underlying oxidation mechanisms, but the discrepancies in predictions of the larger ring species suggests error in their descriptions of PAH growth. This level of performance is suitable for the current simulations, which rely only on accurate description of small gas phase species rather than larger PAHs. Ultimately, the Richter et al. mechanism was chosen as it best predicted the concentration profile of acetylene, which is a key species in the HACA mechanism.

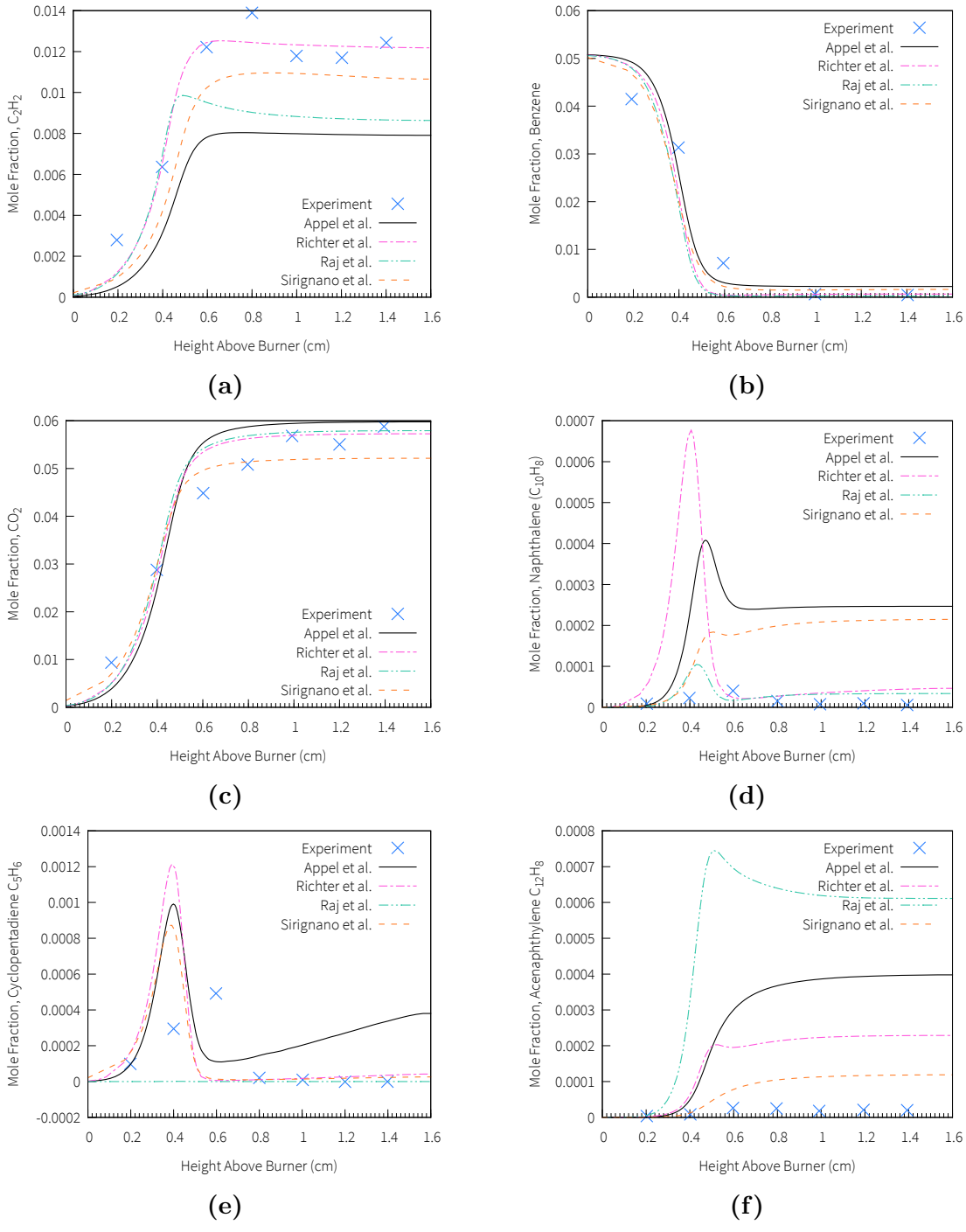

Figure 4.1: Comparison of species predictions by different chemical kinetic models for PAH growth in the premixed benzene flame, C/O = 0.77, studied by Tregrossi et al. [72] (a) acetylene (b) benzene (c) carbon dioxide (d) naphthalene (e) cyclopentadiene (C_5H_6) (f) acenaphthylene ($C_{12}H_8$).

Spatial profiles for both were converted to temporally dependent ones following the methodology described in Chapter III, Section 3.2, assuming a PAH traveling downstream along the center streamline with computed axial velocities within each spatial grid interval. Furthermore, SNAPS simulations were started at a height of 4.5 mm above the burner, which corresponds to a point just before the peak concentration of H radicals and acetylene concentration, as shown in Figure 4.2. This point approximately locates the maximum rate of production of H radicals and acetylene, suggesting that they are consumed significantly after this point. Simulations started at this point in the flame traverse the main reaction zone of the flame and this location therefore can be considered to be the main starting point for PAH growth. Simulations were stopped at a simulation time corresponding to the end of the laminar flame environment, or the end of the computed temporal temperature and gas phase species profiles. The seed molecule for simulations was chosen to be benzene. Since SNAPS currently does not directly simulate the combustion environment, the implicit assumption of the current trajectories is that the distribution of PAHs downstream primarily consist of those that began as benzene at this point in the flame. This assumption was consistent with the fact that the first aromatic ring is considered to be the first step towards larger PAH formation.

SNAPS simulations were analyzed to classify the most important PAH structures for specific mass ranges. To simplify analysis of the vast amount of potential structures, PAHs were classified by carbon configuration using social permutation invariant topological coordinates (SPRINT) [130]. SPRINT coordinates are a useful application of spectral graph theory to the classification of atomic structures for molecular simulation. These coordinates are quantitative descriptors of molecular structure, and contain information about the short and long range topology of a molecule. The quantitative nature of SPRINT coordinates greatly facilitates computational differentiation and grouping of molecular structures produced in SNAPS simulations. Further

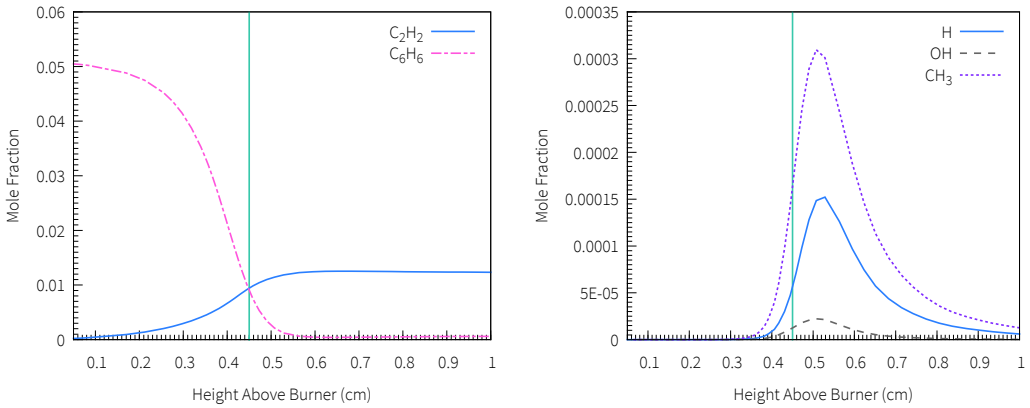

(a) **(b)**

Figure 4.2: Mole fraction profiles for species impacting growth of particles in the premixed benzene flame, C/O = 0.77, studied by Tregrossi et al. [72]: (a) acetylene and benzene (b) H, OH, and CH_3. The vertical lines mark the starting point of simulations.

details of SPRINT coordinates are provided in Appendix A.

SPRINT coordinates were computed for selected molecules (e.g. at a given height in the flame) in each SNAPS trajectory, focusing specifically on carbon-carbon connectivity. A given structure is characterized by a vector containing as many SPRINT coordinates as the number of carbons in the molecule. Importantly, PAHs with equivalent connectivity will have almost identical SPRINT coordinates, which are invariant under all permutations of a set of N atoms. Figure 4.3 shows SPRINT coordinates calculated for three example molecules with 16 carbons. The computed coordinates demonstrate how each molecule has a distinct set of values, enabling quantitative differentiation between different molecules. Therefore, molecular structures with specific carbon numbers were grouped by placing a limit on the magnitude, specifically the p-2 norm, of the difference between the vectors representing the SPRINT coordinates of each pair of PAHs in the target ensemble. This p-2 norm threshold was adjusted to produce distinct carbon configurations for the top 5 most frequently observed PAH structures.

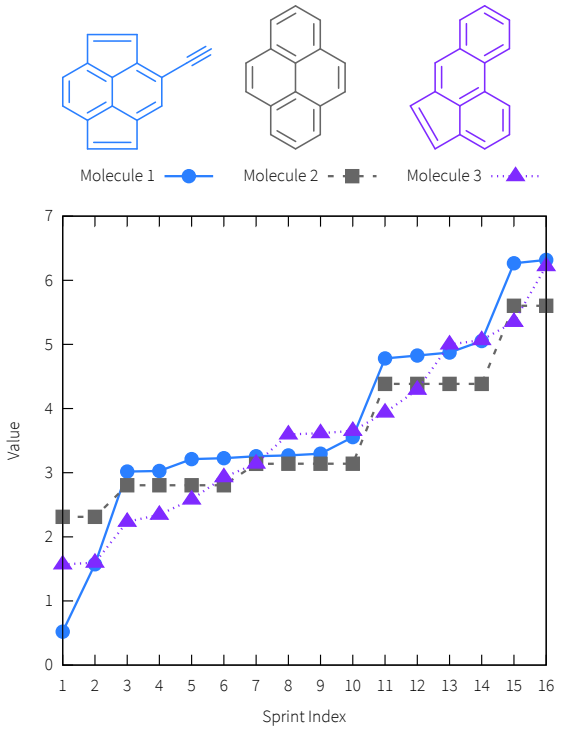

Figure 4.3: SPRINT coordinates computed for three example molecules with 16 carbons.

4.2 Results and Discussion

4.2.1 Comparison with Experimentally Measured Quantities

In order to evaluate the performance of the SNAPS algorithm and the PAH reaction mechanism, simulations of PAH growth were analyzed and compared with experimentally measured data [72]. An ensemble of 30000 SNAPS trajectories was used to compute a distribution of species, which was compared with ratios of experimentally measured concentrations in the flame of Tregrossi et al. [72], including naphthalene, acenaphthylene, biphenyl, indene, phenanthrene, and anthracene. These ratios were computed in order to be able to compare results among the CHEMKIN, experimental, and SNAPS results. In addition, the chosen set of ratios include species that are formed through different reactions. For example, the formation of indene can occur through the addition of methyl and acetylene radicals; biphenyl can be produced through the addition of a phenyl radical or benzene; and acenaphthylene, naphthalene,

phenanthrene, and anthracene can be produced through HACA mechanism. This set of comparisons demonstrates the functionality of SNAPS and the PAH mechanism. The same trajectories were also used to compute PAH mass distributions at heights of 8 and 10 mm above the burner, which correspond to simulation times of 15 and 23 ms, respectively. Figure 4.4 compares experimentally measured concentration ratios with those computed using CHEMKIN and SNAPS. Additionally, Figure 4.5 shows a comparison of computed and experimentally measured mass distributions.

In the comparison of species concentration ratios shown in Figure 4.4, the time evolution of the SNAPS species ratios at the short simulation times (before approximately 5 ms) show a correlation with the chosen starting point, resulting in significant deviation from both CHEMKIN and experimental profiles. Compared with CHEMKIN, SNAPS predictions are very similar in performance to the deterministic solutions. This result is consistent with the fact that the SNAPS results are limited in accuracy by their environmental inputs, which in this case come from CHEMKIN solutions. Ultimately, the simulations are able to reproduce the experimental ratios within an order of magnitude after approximately 5 ms, which corresponds to the regions of primary interest. Additionally, as shown in Figure 4.5, mass distributions computed from SNAPS compare well by visual inspection with experimental measurements at both heights above the burner. In particular, the simulated mass distribution reproduces the most frequent mass (226 amu) as well as the relative frequencies of peaks in the mass spectra. Altogether, within the assumptions of the current simulation methodology, the quantities derived from SNAPS simulations agree well with experiment, which supports the credibility of the simulations produced by SNAPS and PAH growth model. Therefore, the detailed trajectories of these simulations were further analyzed provide insight into the PAH growth process, specifically important reaction pathways and species.

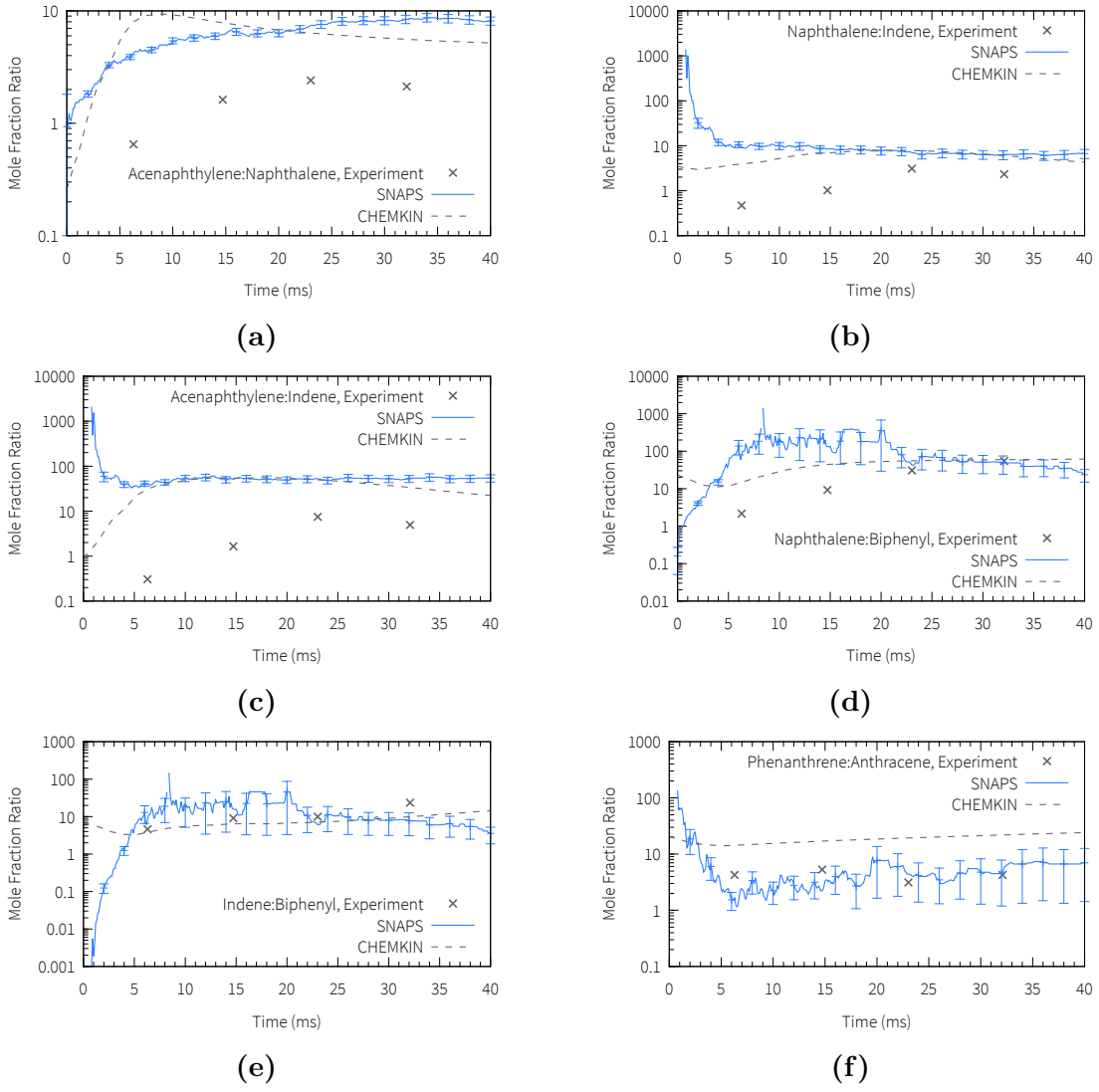

Figure 4.4: Time evolution of ensemble-averaged species mole fraction ratios computed with SNAPS (30000 trajectories) compared with of CHEMKIN computed and experimentally measured values in the flame of Tregrossi et al. [72]: (a) acenaphthylene:naphthalene (b) naphthalene:indene (c) acenaphthylene:indene (d) naphthalene:biphenyl (e) indene:biphenyl (f) phenanthrene:anthracene. Error bars represent the standard error of the mean.

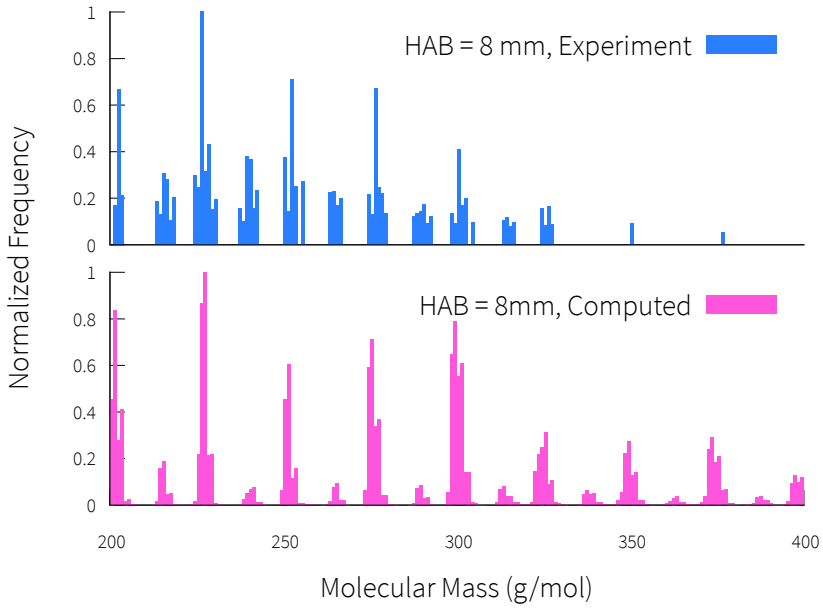

(a)

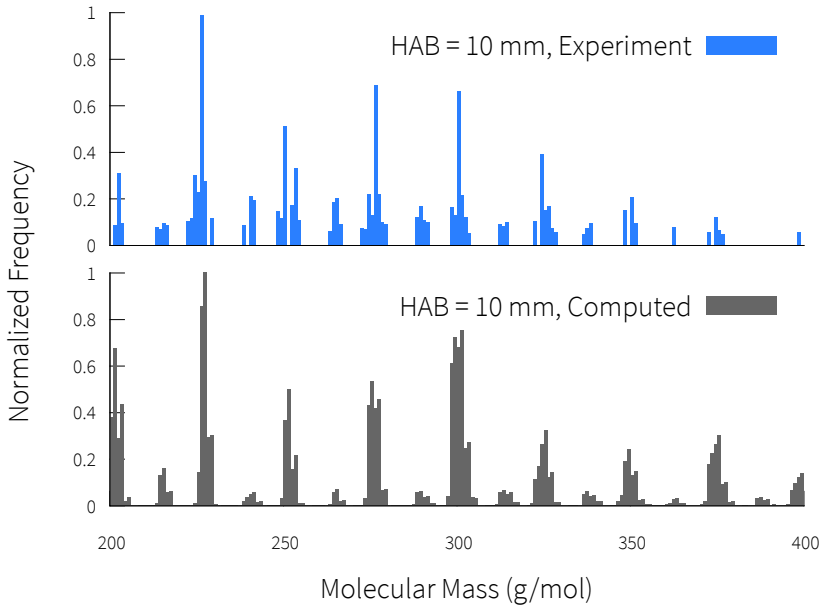

(b)

Figure 4.5: Comparison of ensemble-averaged mass distributions computed by SNAPS (30000 trajectories) compared with experimentally measured values in the flame of Tregrossi et al. [72]: (a) 8 mm above burner (15 ms) (b) 10 mm above burner (23 ms).

4.2.2 Mass Accumulation

An important aspect of particle inception and soot formation is the rate of mass growth. The role of the current chemical reaction pathways in PAH mass growth was investigated by comparing the time evolution of average mass growth predicted by SNAPS simulations in two different environments related to the current benzene flame. The first environment was time dependent corresponding to the benzene flame. The second environment was constant, corresponding to the flame conditions at a height of 5.2 mm above the burner. The latter conditions were chosen to represent the ideal environment for maximum chemical growth in this flame. Figure 4.6 compares the average mass over time for both simulations. While PAHs in the ideal environment grow steadily, those growing in the real flame environment reach a plateau. This stagnation in growth corresponds to the depletion of H radicals and decrease in temperature outside of the main chemical reaction zone of the flame. These high radical concentrations are therefore very important to the chemical growth of PAHs, which can be ascribed to the importance of hydrogen abstraction reactions in the HACA mechanism. Therefore, although these chemical reactions, in ideal conditions, lead to continuous particle growth, they have a limited role under the current flame conditions, specifically in regions of high radical concentration and temperature.

Since experiments have observed particles much larger than the approximate 200 amu plateau shown in Figure 4.6, a reasonable conclusion from these simulations is that additional mechanisms must be involved in particle inception and growth, including, for example, hitherto neglected chemical reactions or faster kinetic rates. Another potential mechanism is growth via physical agglomeration of PAHs. Previous work [14, 17, 46] has argued that particle inception by purely chemical reactions is insufficient to predict observed nucleation rates, suggesting physical agglomeration as a complementary process. In addition, comparison with experimentally measured bimodal particle size distributions [14, 37] shows that nucleation models using physi-

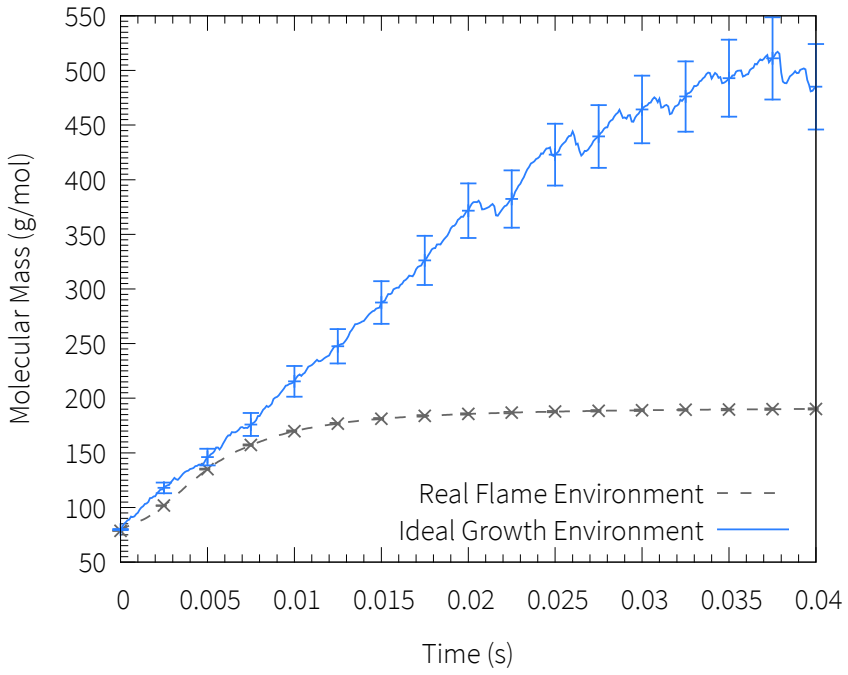

Figure 4.6: Comparison of average mass growth in simulations under two environments: the flame of Tregrossi et al. [72] (30000 trajectories, dashed/grey line) and ideal growth conditions (100 trajectories, continuous/blue line). Error bars represent the standard error of the mean.

cal agglomeration correctly predict this bimodality, while those using purely chemical growth erroneously predict a unimodal distribution. These SNAPS simulations therefore show that additional work must investigate and quantify more growth pathways to deepen our understanding of particle inception.

4.2.3 PAH Structures and Reaction Pathways

Understanding the composition and morphology of PAHs formed in combustion is a key step in understanding particle inception and soot formation. This task is an ideal application of SNAPS, which explores detailed molecular structures. Accordingly, the distribution of PAH structures was investigated for the mass frequency peaks between 200 and 400 amu. Figure 4.7 shows the top 5 most frequently observed carbon structures in 5000 trajectories for carbon counts between C16 and C32 at a height of 8 mm above the burner (simulation time of 15 ms), which correspond to masses around

202 and 400 amu, respectively. There is a range of PAH masses around each peak that correspond to species with the same number of carbons, but a different number of hydrogen atoms. Since the carbon skeleton of these PAHs are of the most interest, hydrogens were neglected and these species were analyzed as a group. The most important feature of these structures is the prevalence of 5-membered rings, which contrasts with conventional assumptions about the composition of PAHs. Prominent PAH masses have traditionally been associated with almost exclusively 6-membered ring PAHs, such as pyrene, or coronene. These types of species are commonly referred to as "Stein's Stabilomers" and are considered to be prevalent based on their high thermodynamic stability, as argued by Stein and Fahr [65].

In the current results, several observed structures do correspond with proposed stabilomers, but these species contain 5-membered rings. For example, the structure for C16 column A in Figure 4.7 and pyrene (C16 column D), were identified as a stabilomer by Stein and Fahr. Interestingly, the former structure was observed with 74.9% frequency, while pyrene was observed far less often, with a frequency of 0.948%. Likewise, C18 column C, C22 column A, and C24 column A correspond to proposed stabilomer species that do not contain exclusively 6-membered rings. These results suggest the importance of 5-membered rings in PAH growth and also support the exploration of additional reaction mechanisms for 5-membered rings, including their conversion to 6-membered rings, to better simulate PAH growth. Figure 4.7 also shows a wide variety of structures that are not contained in the traditional PAH stabilomer grid. This phenomenon is particularly notable for a carbon count of 32, where the most commonly observed structure occurred with a frequency of only 17.4%, the top 5 most frequent structures accounted for only 39.4% all those observed, and the total number of distinct structures classified was 166. Physically, this variety of structures arises from a substantial increase in potential reactions and branching pathways with molecule size. The five structures shown in Figure 4.7 illustrate the

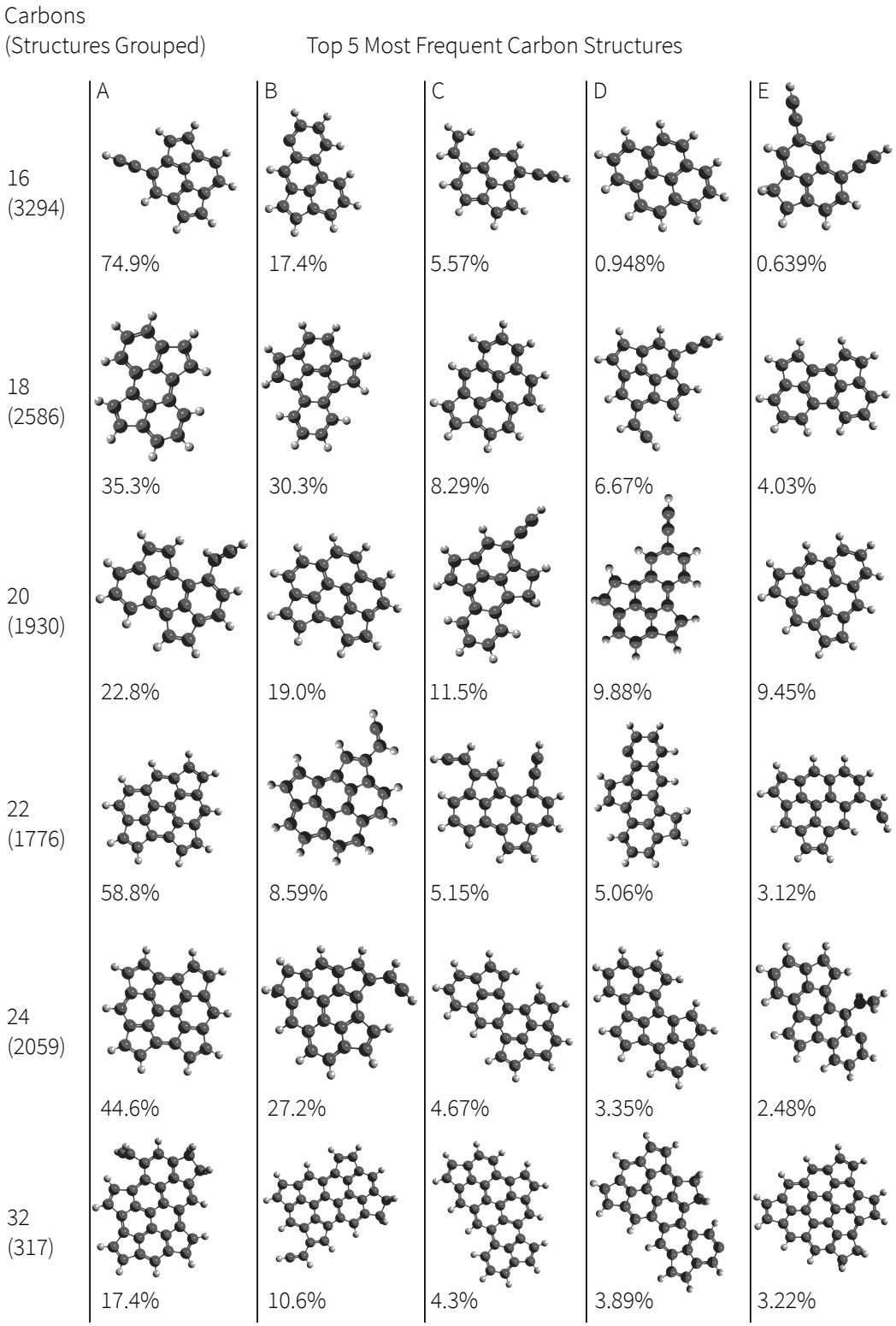

Figure 4.7: Top 5 most frequent carbon structures observed at 8mm above the burner (simulation time of 15 ms) in 30000 simulations for varying number of carbons. The value "Structures Grouped", shown in parenthesis on the left below the number of carbons in each row, represents the quantity of trajectories with structures matching the specified number of carbons at this height.

variety in possible PAH features, including both planar molecules, attached chains, and configuration of of 5- and 6-membered rings. Additionally, curved species, where a 5-membered ring is encircled by 6-membered rings were also observed in simulations, but in significantly smaller quantities than the most frequently observed structures.

The variety of structures in Figure 4.7 arise from complex sequences of reactions, which were recorded throughout SNAPS simulations. Simulation trajectories were analyzed to determine the relative frequencies of each reaction. Figure 4.8 illustrates some of the most common reaction pathways observed throughout simulations. Each forward and reverse reaction is annotated with its frequency relative to all recorded reactions. The most common reactions were the forward and reverse hydrogenation of 5-membered rings, the first step of the ring opening pathway shown in Figure 4.8a, with a frequency of 26.8% and 24.8% respectively. The uncertainty in all rates included in the PAH mechanism leads to the question of whether the importance of this hydrogenation reaction is correct. The rate for hydrogenation was taken from the work of Frenklach et al. [92] who assigned it based on analogy with the reaction $C_2H_4 + H \rightleftharpoons C_2H_5$ in the GRI mechanism [131]. This rate is much higher than those assigned for hydrogen abstraction and thus tends to dominate whenever 5-membered rings are present. The simulation is accurate within the input reaction rates and therefore, part of this analysis is the evaluation of these reaction pathway and rates.

An argument could be made that the dominance of 5-membered ring opening and migration hinders PAH growth by preventing particles from following other reaction pathways, such as growth through the HACA pathway. To test this argument, simulations were run without the 5-membered ring migration pathway in Figure 4.8a. These simulations were unable to reproduce the experimental mass distributions shown in Figure 4.5. Instead, the predicted mass distributions, shown in Figure 4.9, exhibits reduced PAH growth, namely substantial decreases in higher masses and increases of lower masses, especially those with 16 carbons. This increase can be ascribed to the

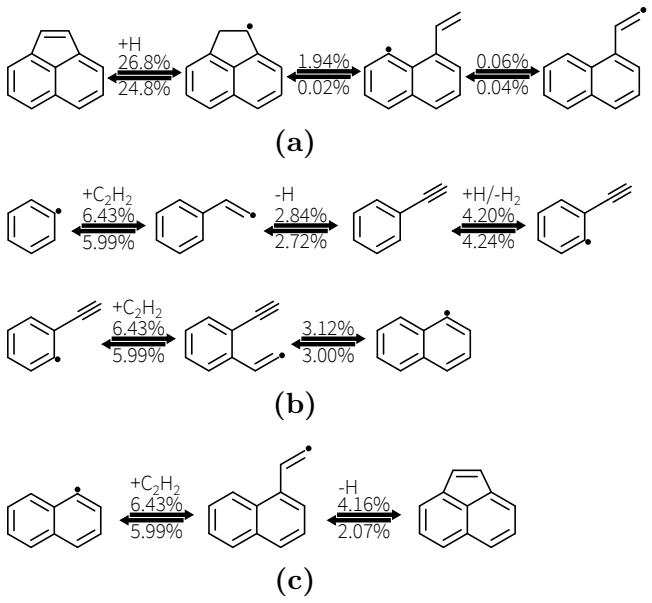

Figure 4.8: Important reaction pathways occurring throughout all simulations. Forward and reverse reactions are each annotated with their frequency relative to all recorded reactions. (a) 5-membered ring opening/migration pathway [92] (b) the most commonly observed 6-membered ring HACA pathway (c) acetylene addition and 5-membered ring closure at a zig zag site.

high frequency of the structure C16 column A in Figure 4.7, which contains two 5-membered rings. Without 5-membered ring migration, the particle has fewer reaction pathways to follow, leading to the observed stagnation in growth. Consequently, these results highlight the importance of reaction pathways involving 5-membered rings, regardless of the absolute accuracy of the specific migration pathway investigated. Future work should aim to deepen understanding of all PAH chemical pathways, especially those involving 5-membered rings.

In addition, reversibility was prominent throughout simulations, as corresponding forward and reverse reactions occured with almost equal frequencies. For example, as shown in Figure 4.8b, acetylene addition had a frequency of 6.43%, while its reverse reaction had a frequency of 5.99%. As well, ring closures were similarly reversible, exhibited in the last step of Figure 4.8b, where the forward and reverse reactions forming napthyl had frequencies of 3.12% and 3.00%, respectively. This reversibility illustrates the high degree of reaction pathway mixing and intramolecular rearrangement. For

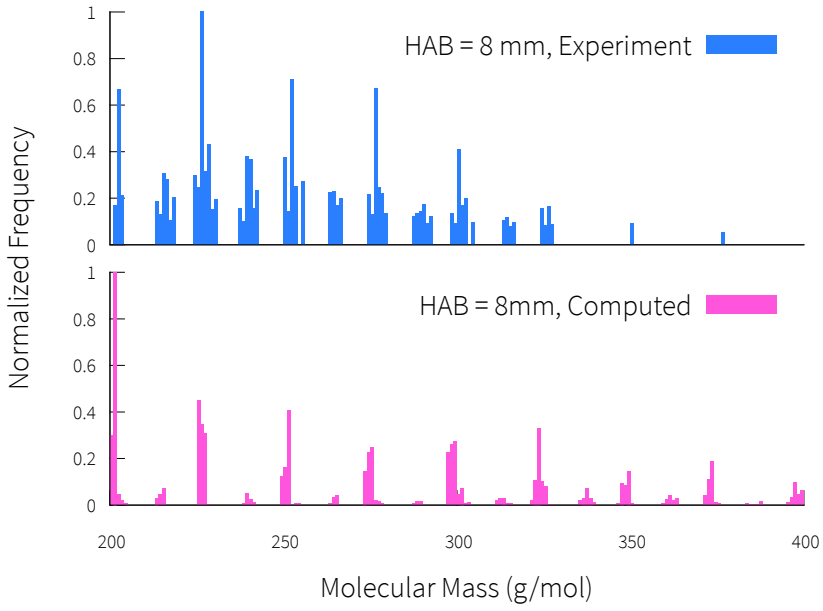

(a)

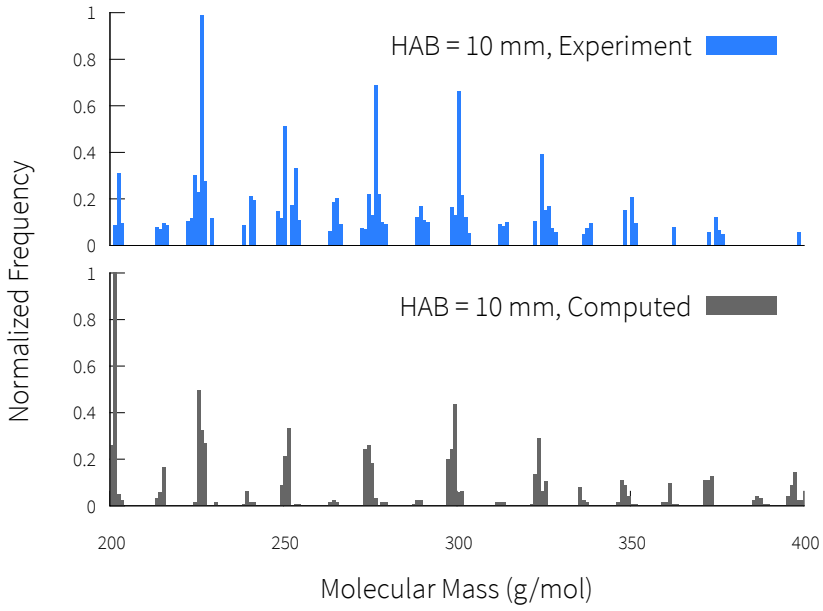

(b)

Figure 4.9: Comparison of ensemble-averaged mass distributions computed by SNAPS (1000 trajectories), without 5-membered ring migration (see text) compared with experimentally measured values in the flame of Tregrossi et al. [72]: (a) 8 mm above burner (b) 10 mm above burner.

example, in Figure 4.7 there is no obvious direct route, such as an acetylene addition and ring closure, between the species in C18 column B and those in C20 columns A and B. Instead, the simulations suggest that much of the growth from C18 to C20 requires a more complex sequence of forward and reverse reaction steps, including such as ring closure/opening and acetylene addition/removal.

Out of all the addition reactions in the current mechanism, acetylene accounted for the majority, 98%, of all addition reactions. This dominance can be ascribed to the far greater concentration of acetylene in the flame, typically at least 2 orders of magnitude greater than species such as propargyl or vinyl radicals. Benzene and phenyl were expected to make an important contribution to PAH growth based on their expected abundance as fuel components, but CHEMKIN simulations show that their concentrations fall below acetylene in the regions of major PAH chemical growth. This phenomenon corroborates the importance of the HACA pathway in PAH chemical growth.

These simulations also demonstrate the importance of kinetics in PAH growth. Previously, in an investigation of a low pressure benzene flame, Weilmünster et al. [66] proposed PAH growth pathways involving both 6-membered and 5-membered rings. These pathways are analogous to those shown in Figures 4.8c (5-membered ring closure at a zig zag site) and 4.8b (6-membered ring closure). Weilmünster et al. argued that the 6-membered ring growth pathway is more prominent based on the relatively lower activation energies of its constituent reactions compared with the 5-membered ring growth pathway. However, the formation of a 6-membered ring typically involves the addition of 2 acetylenes, as in Figure 4.8b. Conversely, only a single acetylene addition reaction is required to create a potential 5-membered ring zig zag closure site, as in Figure 4.8c. Once this acetylene is added, SNAPS simulations show that the particle is far more likely to experience the unimolecular ring closure step before it reacts with an additional acetylene that would enable a

6-membered ring closure. Therefore, while the closure of a 6-membered ring may have a lower activation energy than a 5-membered ring, due to lower ring strain, the closure of 5-membered rings tends to be more kinetically favourable. Corroborating this conclusion, Weilmünster et al. previously observed that, for a given reaction pathway branch between 5- and 6-membered ring species, the maximum concentration associated with the 5-membered branch was double that of the 6-membered one [66].

4.3 Summary

The validity of SNAPS simulations was corroborated by comparison with experimentally measured species concentration ratios and mass distributions in a premixed laminar benzene flame [72]. These simulations were analyzed to further characterize PAH growth in this flame. The time evolution of average particle mass showed that PAHs do not grow infinitely via chemical reactions, instead only experiencing significant growth in the region of the flame with high radical concentrations and temperature. Furthermore, SPRINT topological coordinates were used to group PAH isomers associated with mass distribution peaks by carbon-carbon connectivity. These isomers exhibited significant presence of 5-membered rings, which correspond to species on the stabilomer grid of Stein and Fahr [65]. Importantly, these PAHs are different from those commonly associated with important PAH masses, such as pyrene or coronene, which have exclusively 6-membered rings. The prevalence of 5-membered rings can be ascribed to the faster kinetics of 5-membered ring pathways that require only a single acetylene addition, compared with 6-membered ring pathways that require two. Analysis of reaction pathways showed the importance of acetylene addition, reversible reactions, and molecular rearrangement, which was also reflected in observed PAH structures that are not connected via a direct growth pathway. These results demonstrate the utility of atomistic simulation in elucidating features of PAH growth typically inaccessible to experiment, as well as the complexity of PAH growth beyond

traditionally held assumptions. SNAPS is also useful in evaluating proposed chemical reaction pathways. This worked showed that the 5-membered migration pathway of Frenklach et al. [92] was necessary to properly predict experimental mass distributions of PAH growing in a premixed laminar benzene flame, and therefore supports continued exploration of PAH growth pathways involving 5-membered rings. The characterization of PAHs in this work will inform future development of models for chemical and physical nanoparticle growth and deepen understanding of particle inception.

CHAPTER V

PAH Growth A Premixed Laminar Ethylene/Oxygen Flame

The insight revealed by investigation of a premixed laminar benzene flame motivated further study the important PAH reaction pathways and species involved in combustion. Towards this goal, the SNAPS methodology was employed to study PAH growth in a premixed laminar ethylene/oxygen flame, with conditions chosen correspond to a premixed laminar flame studied experimentally by Apicella et al. [78]. By modeling these conditions, simulation results could be compared directly with experimentally measured mass spectra. This work focuses on understanding the major reaction pathways and structures associated with PAH growth, in comparison with current conventions and knowledge. Furthermore, comparison of computed mass distributions with experimental results enabled the evaluation of the underlying chemical mechanism.

5.1 Methodology

A similar methodology to Chapter IV was employed to study PAHs in an atmospheric, fuel rich, premixed laminar ethylene/oxygen flame, C/O = 1. The conditions of the flame where chosen to match with one studied by Apicella et al., who performed

mass spectrometric analysis of large PAH species [78]. The experimental mass spectra of this work provides valuable data to compare with simulations. Like the previous investigation, this flame was simulated using CHEMKIN [82] and the combustion and PAH mechanism of Richter et al. [125] to compute spatially dependent temperature and gas phase species profiles. Spatial profiles were converted to temporally dependent inputs for SNAPS simulations of PAH ensembles, assuming a PAH traveling downstream along the center streamline with computed axial velocities within each spatial grid interval. SNAPS simulations were started at a height of 0.4 mm above the burner, which approximately locates the maximum rate of production of H radicals and acetylene and implies that they are consumed significantly after this point. Simulations started at this point in the flame traverse the main reaction zone of the flame. This location was considered to be the main starting point for PAH growth, due to the subsequent high radical concentrations and temperature relative to prior heights in the flame. The seed molecule for simulations was chosen to be benzene. As a result, the current PAH ensembles assume that the distribution of PAHs downstream primarily consist of those that began as benzene at this point in the flame.

SNAPS simulations were also analyzed to classify the most important PAH structures for specific mass ranges, grouped by carbon configuration by computing SPRINT topological coordinates [130], which utilize graph theory to describe the connectivity of an isomer. Since SPRINT coordinates are invariant under all permutations of a set of N atoms, they enable quantitative identification of PAHs with equivalent connectivity. Isomers with specific carbon numbers were grouped, focusing specifically on carbon-carbon connectivity, by placing a limit on the magnitude, specifically the p-2 norm, of the difference between the vectors representing the SPRINT coordinates of each pair of PAHs in the target ensemble. This p-2 norm threshold was adjusted to produce distinct carbon configurations for the top 5 most frequently observed PAH

structures.

5.2 Results and Discussion

5.2.1 Evaluation Against Experimental Mass Spectra

SNAPS and the current PAH growth mechanism have previously reproduced, with reasonable accuracy, the experimentally measured peaks of mass spectra in the range of 200–400 amu in a premixed laminar benzene flame, as shown in Chapter IV. Apicella et al. [78] measured mass spectra in an ethylene flame with an expanded range of masses, up to a maximum of 1700 amu. The current simulations focused on comparison in the mass range of 300–600 amu, which includes larger PAHs with which to further test SNAPS and the chemical mechanism. In addition to evaluating and improving the PAH reaction mechanism, these simulations serve to further characterize PAH growth in this flame in terms of molecular structures and reaction pathways.

Figure 5.1 compares experimentally measured mass spectra, for masses between 300–600 amu, with distributions computed using 30000 SNAPS trajectories, at heights of 6 mm and 8 mm, which correspond to SNAPS simulation times of 21 ms and 27.5 ms respectively. The simulation results differ substantially from experimental measurements. The computed mass distributions show dominant peaks for structures with a mass of approximately 300 amu, which suggests that the simulated PAH growth tends to stagnate around this mass. Moreover, the simulations are unable to reproduce mass peaks that are typically associated with an odd number of carbons (e.g. approximately 312 amu, 336 amu, 360 amu, etc.). The latter discrepancy can be ascribed to the fact that not all PAHs observed in experiment necessarily grow from benzene. Alternatively, PAHs could grow from other single aromatic species with an odd number of carbons such as toluene (C_7H_7). As such species grow via the addition of acetylene, they maintain an odd number of carbons, which would create the peaks

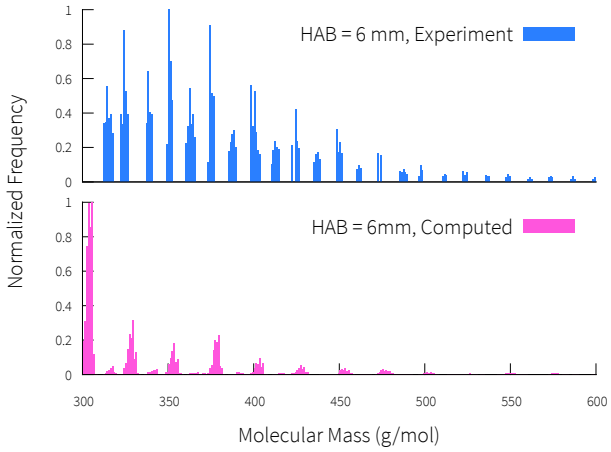

(a)

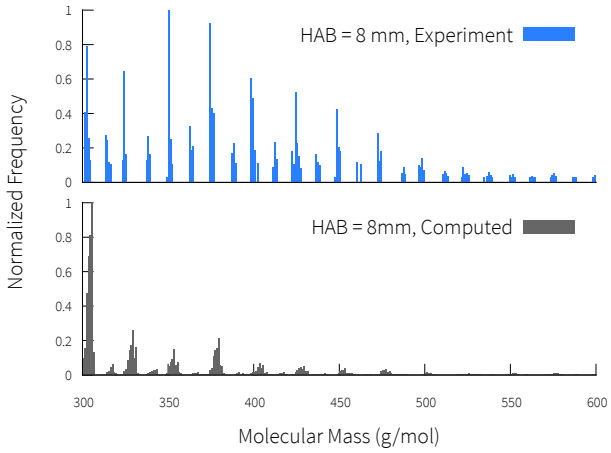

(b)

Figure 5.1: Comparison of ensemble-averaged mass distributions computed by SNAPS (30000 trajectories) compared with experimentally measured values in the flame of Apicella et al. [78]: (a) 6 mm above burner (b) 8 mm above burner.

observed experimentally. An example of including toluene-seeded simulations in mass distributions is discussed in Chapter VI.

The current chapter focused on understanding the sensitivity of mass distributions to reactions in the PAH growth mechanism. Although the current reaction mechanism aims to be inclusive of major growth mechanisms, the discrepancy between experimental and computed results suggests that additional pathways will be required to properly describe the growth chemistry of PAHs, especially those larger than 300 amu. Based on the successful application of this methodology to the previous study of a benzene/air flame, the current work as focused on the evaluation of the reaction mechanism as a means to improve simulation results.

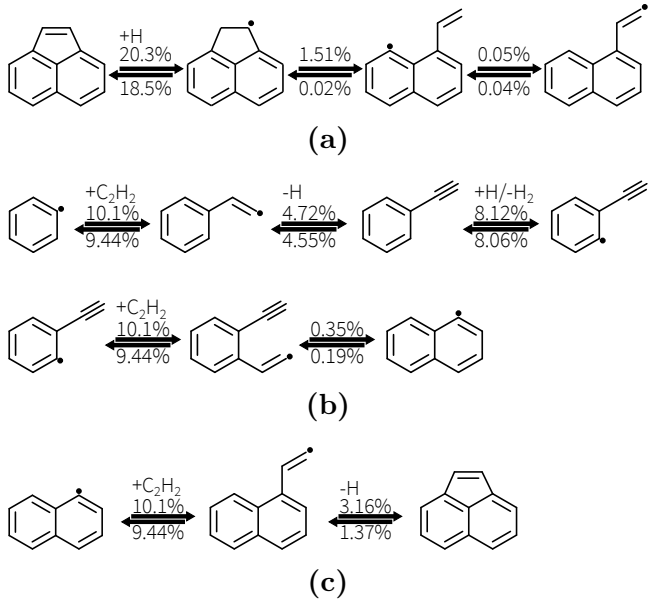

Figure 5.2: Important reaction pathways occurring throughout all simulations. Forward and reverse reactions are each annotated with their frequency relative to all recorded reactions. (a) 5-membered ring opening/migration pathway [92] (b) the most commonly observed 6-membered ring HACA pathway (c) acetylene addition and 5-membered ring closure at a zig zag site.

To investigate the discrepancy in simulated mass distributions, the most frequent reactions and molecular structures were tabulated to elucidate important growth pathways in the PAH mechanism. Figure 5.2 shows important pathways observed in all SNAPS simulations, with each reaction annotated with its corresponding fre-

quency as a percentage of all reactions. The most important reactions overall were the forward (20.3%) and reverse (18.5%) hydrogenation of a 5-membered ring, the first step of the migration pathway proposed by Frenklach et al. [92] shown in Figure 5.2a. Shown in Figure 5.2b, acetylene was the dominant addition reaction species, accounting for 10.1% of all reactions. The next most common addition reaction was by ethylene, occurring with only a 0.27% frequency. 5-membered ring closure at a "zig zag" reaction site, shown in Figure 5.2c was the most common ring closure reaction, occurring with a frequency of 3.16%. The next most common ring closure reaction was the 6-membered ring closure shown in Figure 5.2b, with a frequency of 0.35%.

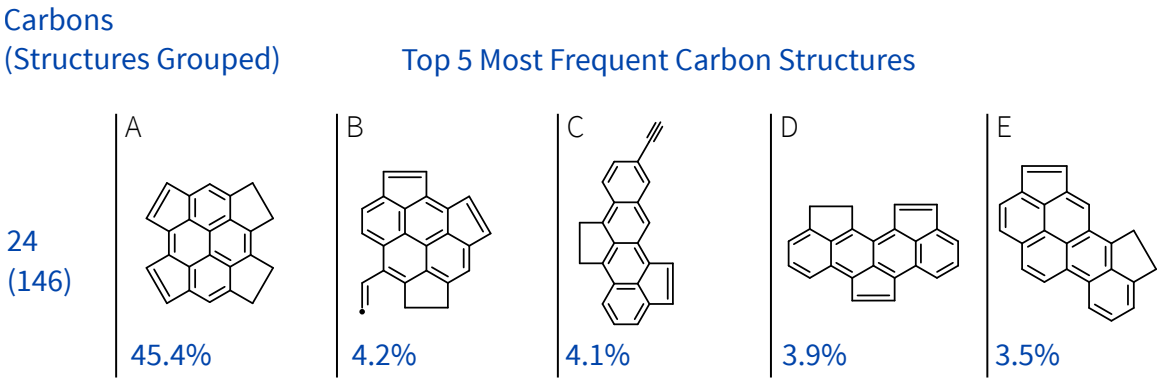

Figure 5.3: The top 5 most frequently observed PAH structures with 24 carbons observed in SNAPS simulations and the base growth mechanism (30000 trajectories) at a height of 8 mm above burner. The value "Structures Grouped", shown in parenthesis on the left below the number of carbons in each row, represents the quantity of trajectories with structures matching the specified number of carbons at this height.

These important reactions are strongly reflected in the most frequently observed PAH structures in simulations. Figure 5.3 shows the top 5 most frequently observed molecular structures with mass of approximately 300 amu, which correspond to PAHs with 24 carbons. Species were grouped using SPRINT coordinates, focusing on carbon–carbon connectivity. This mass range was chosen to investigate the ostensible stagnation in growth associated with the dominant peak in the computed mass distribution. The most frequently observed species reflect the high frequency of reactions involving 5-membered rings and exhibit variety beyond the commonly proposed

"stabilomer" PAHs studied by Stein and Fahr [65]. Conventionally, the most important PAHs are considered to be those stabilomers containing primarily 6-membered rings. For example, PAHs with 24 carbons are associated with coronene ($C_{24}H_{12}$). The simulation results show a variety of species that includes a stabilomer, the 24 carbon PAH shown in C24 column A, which contains a pyrene structure surrounded by four 5-membered rings. However, although this species was identified as a stabilomer, it has not been traditionally studied in chemical mechanisms. The remaining structures shown in Figure 5.3 are likewise unconventional species, further demonstrating departure from the traditional stabilomer table.

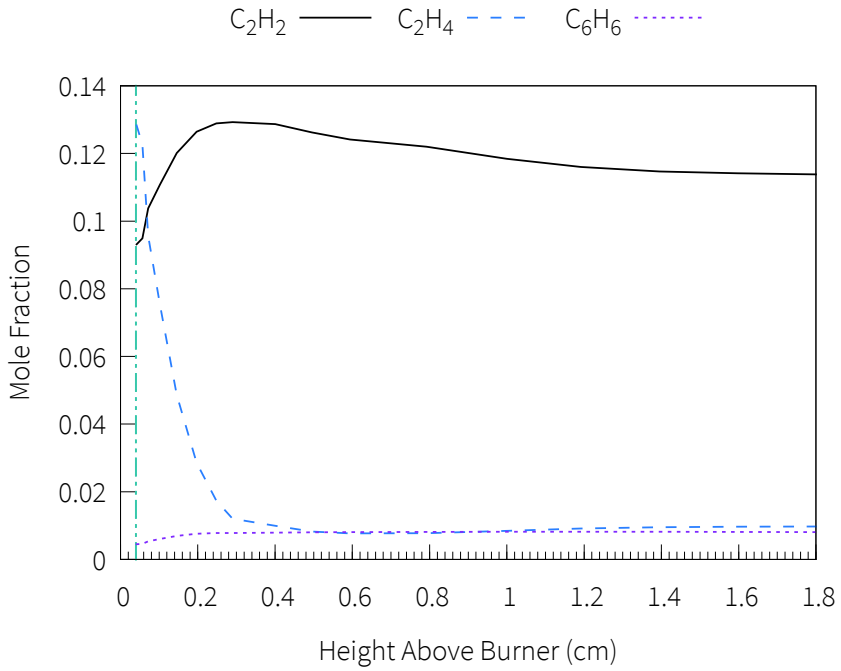

Figure 5.4: Concentration profiles in the ethylene flame of important gas phase species participating in addition reactions. The vertical line represents the starting point of SNAPS simulations.

The major reactions and species observed in these simulations strongly support the prominence of acetylene addition, as well as the prevalence of 5-membered rings, in the formation of PAHs. These results also emphasize the importance of several factors, beyond energetics, that influence reaction kinetics and determine important

growth pathways. The HACA reaction mechanism is considered to be important in soot formation, due to the high concentration of acetylene and H radicals in flames [14]. This theory is consistent with the current simulations, where acetylene was the most frequently added species by a large margin. In the current simulations, the gas phase concentration of acetylene is at least one order of magnitude higher relative to other potential addition species. Figure 5.4 shows concentration profiles in the flame of important species participating in addition reactions in SNAPS simulations. While the concentration of ethylene is initially competitive with acetylene, it is ostensibly quickly consumed by oxidation resulting in rapidly decreasing concentration. As a result, acetylene becomes the most prevalent species available for addition. Other species, such as methyl (CH_3), vinyl C_2H_3, propargyl (C_3H_3), and phenyl (C_6H_5) radicals have been omitted as their concentrations are 2-3 orders of magnitude lower than those in Figure 5.4. Within a given kMC step, the higher concentration of acetylene has a substantial effect on the reaction rates for species additions. Despite some variation in the rate constants for each potential addition reaction, concentration has the largest impact, leading to a much higher reaction probability for acetylene, with respect to any other species addition. Physically, the higher reaction probability, heavily impacted by gas phase concentrations, reflects the fact a particle is most likely to encounter and react with an acetylene molecule rather than another species such as benzene or even ethylene. The difference in reaction probability is reflected in the much higher frequency of acetylene addition, 10.1%, compared with the next most frequent, ethylene addition, 0.2%.

Similarly, the high frequency of 5-membered ring closure, as well as their prevalence in the observed PAH structures, can be ascribed to overall kinetics. Following an acetylene addition reaction, there are many competing growth pathways to follow. The particle may experience the ring closure forming a 5-membered ring shown in Figure 5.2c. This pathway was the most frequent ring closure. Alternatively, the

particle could follow the pathway shown in Figure 5.2b, involving isomerization of the attached ethenyl chain, hydrogen abstraction, acetylene addition, and ring closure. This pathway was the next most frequently observed ring closure. The first ring closure pathway requires a single unimolecular step, while the second requires 2 unimolecular and 2 bimolecular steps. SNAPS simulations show that the molecule is more likely to experience the first 5-membered ring closure, despite a higher energetic barrier, rather than follow the second pathway, which requires reaction with both a hydrogen radical and an acetylene molecule. Therefore, as a consequence of requiring only unimolecular step, the 5-membered ring closure pathway is highly kinetically favourable in comparison with 6-membered ring formation. This conclusion is consistent with the kinetic analysis of the HACA mechanism by Kislov et al. [132], who showed using *ab initio* calculations that 5-membered ring species such as acenapthylene ($C_{12}H_8$) are more kinetically favourable than 6-membered ones like phenanthrene (C14H10).

5.2.2 Sensitivity to 5-Membered Ring Migration

Motivated by these results, the role of 5-membered ring reaction pathways in PAH growth was investigated using SNAPS simulations to quantify adjustments to the chemical mechanism in terms of their impact on the computed PAH mass distributions and molecular structures. In particular, focus was placed on the migration pathway [92] shown in Figure 5.2a. SNAPS simulations were conducted for three adjusted mechanisms. First, the magnitude of the forward hydrogenation rate, shown as the first step in Figure 5.2a, was reduced by two orders of magnitude. This reduction was chosen to promote growth by making the magnitude of this rate similar to hydrogen abstraction by H radicals, a closely competing reaction. Moreover, there is some uncertainty in with respect to the accuracy of this particular rate constant, which was originally assigned by analogy with the hydrogenation of ethylene that produces

an ethyl radical, $C_2H_4 + H \rightleftharpoons C_2H_5$. Adjustment of this rate is reasonable within the context of assessing its impact on PAH growth. This mechanism will be referred to as the "reduced" case.

A second mechanism case was formulated to resemble the resembles the growth pathways followed by conventional kinetic models [83, 86, 88, 125]. These kinetic models describe PAH growth as the formation, through the HACA mechanism, of pericondensed species consisting of primarily 6-membered rings. Growth through species involving 5-membered rings in these mechanisms is limited. For example, the ABF mechanism [83] contains the formation of acenaphthylene (3 pericondensed rings, 2 6-membered and 1 5 membered) and the only subsequent growth pathway is the formation of phenanthrene (3 pericondensed 6-membered rings). Similarly, in the mechanism of Raj et al. [86], although the largest species considered is coronene (7 pericondensed 6-membered rings), the largest species involving a 5-membered ring contains a pyrene structure (4 pericondensed 6-membered rings) with one attached five membered ring, which does not grow further. To mimic this growth, 5-membered ring migration pathways were removed, along with the 5-membered ring closure reaction at zig zag sites, shown in Figure 5.2c. Although this change removes the ability of SNAPS simulations to produce acenaphthylene, this change was necessary to match the growth characteristics for larger PAH. This adjusted SNAPS mechanism will be referred to as the "conventional" case.

Comparison of simulations using these adjusted mechanisms elucidated the importance of 5-membered rings in PAH formation. Figure 5.5 compares experimentally measured mass spectra with the distributions computed at heights of 6mm and 8mm above the burner, using 30000 SNAPS trajectories for each adjusted mechanism. The simulations using the "conventional" mechanism exhibited a significant discrepancy with experimental results and a peak at a PAH mass of approximately 300 amu. As shown in Figure 5.6, the primary growth pathway is the same 6-membered ring

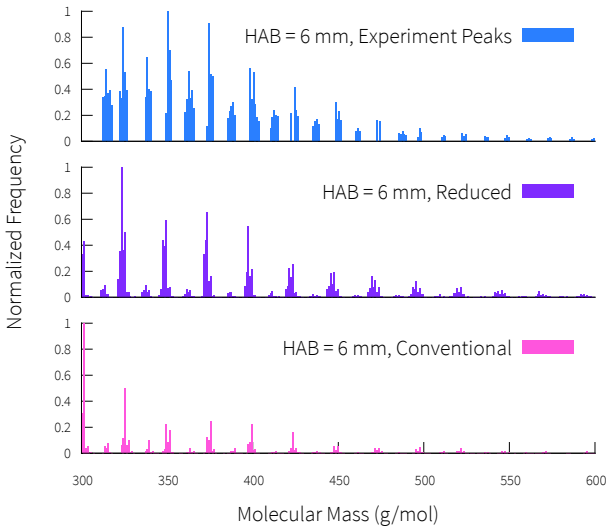

(a)

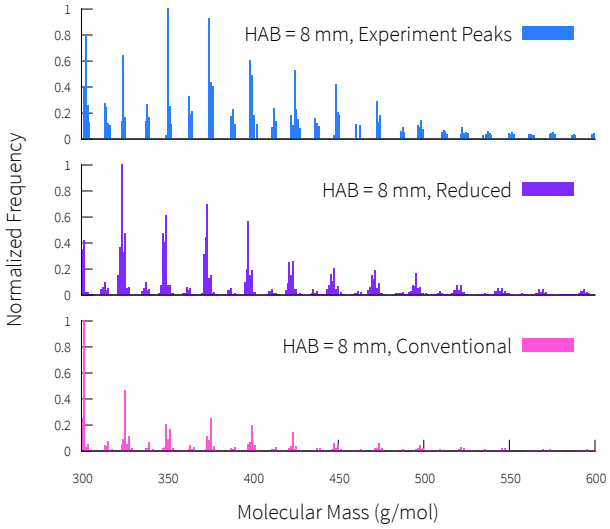

(b)

Figure 5.5: Comparison of ensemble-averaged mass distributions computed by SNAPS (30000 trajectories) using the "reduced" and "conventional" mechanisms (see text for definitions) with experimentally measured peaks in the flame of Apicella et al. [78]: (a) 6 mm above burner (b) 8 mm above burner.

reaction acetylene addition mechanism as the one shown in Figure 5.2b. Since the growth mechanism was specified to exclude 5-membered ring closure and migration, this result suggests that reaction pathways that consider only pericondensed species with 6-membered rings are insufficient to describe the chemical growth of PAHs with mass greater than 300 amu, where the mass distribution suggests a stagnation in growth.

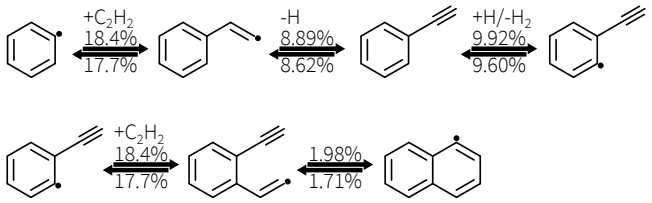

Figure 5.6: The most important reaction pathway, 6-membered ring formation via acetylene addition, occurring throughout all simulations in the "conventional" case (see text for definitions). Forward and reverse reactions are each annotated with their frequency relative to all recorded reactions.

In contrast, the best agreement with the experimental data was observed for the "reduced" case. The most frequently observed reactions for this case, shown in Figure 5.7 show that the migration pathway of Frenklach et al. [92] is substantially reduced in importance; the forward and reverse hydrogenation rates, shown in the first step of Figure 5.7a, are reduced in frequency from 20.1% and 18.3% in the original mechanism (Figure 5.2a) to 0.12% and 0.17% respectively. As a result, the primary mechanism for migration is a ring opening, or reverse of the 5-membered ring closure shown in Figure 5.7c. Despite this relatively simple method for migration, the computed mass distributions suggest more efficiency in growth and improves agreement with the experimental data. These results corroborate the importance of both 5-membered rings in PAHs that form in combustion and growth pathways involving these rings, including migration.

The results also demonstrate the need for further development of reaction mechanisms. In particular, the improvement in experimental agreement of computed mass distributions with the "reduced" adjustments is somewhat incongruous with previous

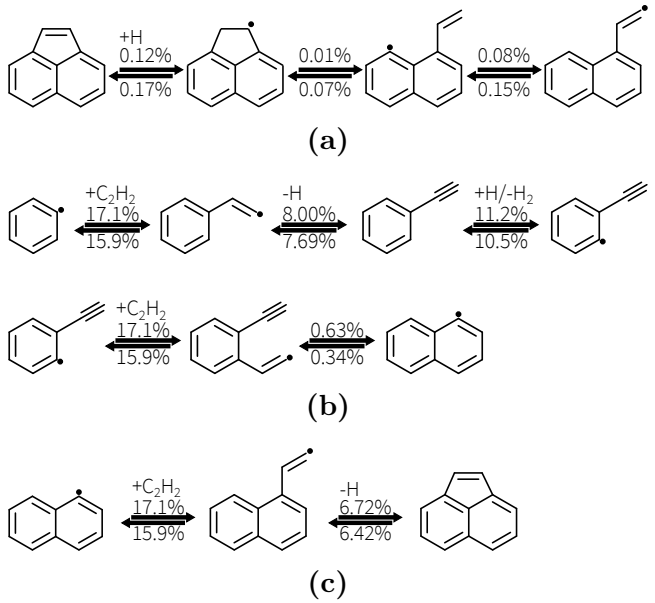

Figure 5.7: Important reaction pathways occurring throughout all simulations in the "reduced" case (see text for definitions). Forward and reverse reactions are each annotated with their frequency relative to all recorded reactions. (a) 5-membered ring opening/migration pathway [92] (b) the most commonly observed 6-membered ring HACA pathway (c) acetylene addition and 5-membered ring closure at a zig zag site.

results in a benzene/air flame (Chapter IV), where SNAPS simulations instead include the Frenklach et al. migration pathway and agreed well with experimental mass distributions in the range of 200–400 amu. Therefore, while this migration pathway may be useful for PAH masses from 200–300 amu, the ethylene flame results show that it may be insufficient to model growth beyond 300 amu. Further refinement of this and other reaction pathways involving 5-membered rings will further improve modeling of PAH growth. Nevertheless, the current results for the "reduced" case show reasonable agreement with experiment and better predict the experimental mass spectra for larger PAHs in comparison with the all other studied cases. The "reduced" simulations therefore currently represent a better estimate of PAHs in this 300–600 amu mass range and indicate a direction for future investigation of reaction pathways.

5.2.3 Comparison of PAH Structures

To further characterize the PAHs in this flame, SNAPS trajectories for all cases were analyzed, at a height of 8 mm above the burner, to determine the most frequently observed molecular structures, grouped using SPRINT coordinates. Figures 5.8 and 5.9 show the top five most frequently observed structures in SNAPS simulations at a height of 8 mm above the burner for the "conventional" and "reduced" cases. Despite the dominance of acetylene addition and the HACA mechanism, both sets of structures illustrate the variety of PAHs that can be produced in this ethylene/oxygen flame. Illustrating this variety, the 5 most important structures for 32 carbons in the "conventional" and "reduced" cases account for 49.6% and 28.9% of all observed structures respectively.

In addition, these results show the substantial differences in structures that can result from even small adjustments to the reaction mechanism. The structures in the "conventional" case, as expected, resemble PAHs several that exist in PAH kinetic models. For example, the species shown in C24 column B (coronene), C30 column A, and C32 column A (ovalene) are PAH stabilomers that are commonly associated with soot formation. Nevertheless, even the "conventional" results show a variety of PAHs that far extend beyond those in the stabilomer table. Figure 5.8 also shows a many species that are prevented from closing 5-membered rings in the "conventional" mechanism, such as C24 column E; C26 columns A and C; C28 column C; C30 column D; and C32 column C. These structures disappear in the "reduced" results shown in Figure 5.9, reflecting the kinetic favourability of 5-membered ring closure. The structures of the "reduced" case show a significant number of 5-membered rings that occur more frequently those seen in the "conventional" results.

Importantly, the presence of 5-membered rings does not exclude the formation of species with many pericondensed 6-membered rings, such as coronene or ovalene. Instead, the current results suggest that if such species form, they are more

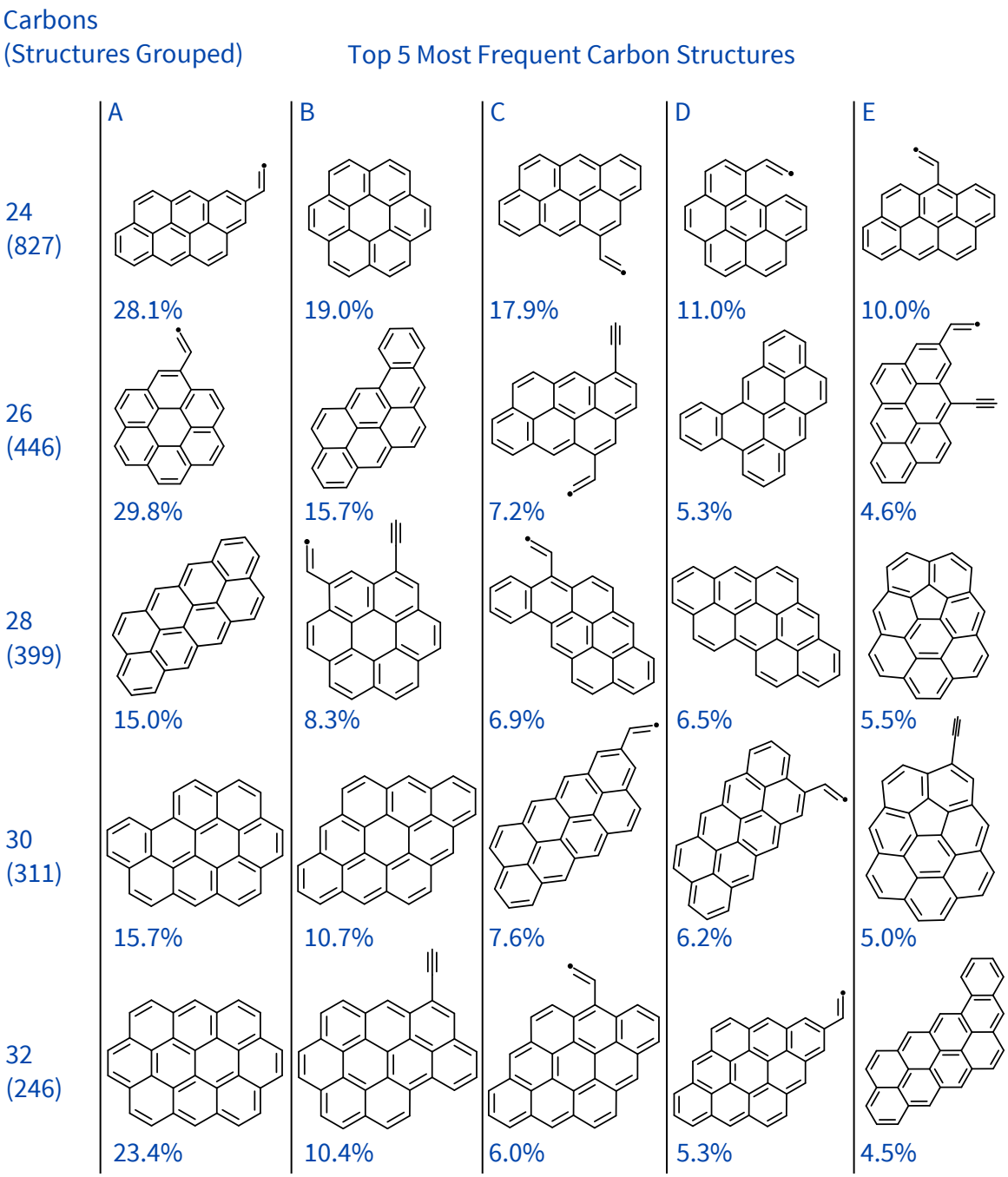

Figure 5.8: The top 5 most frequently observed PAH structures with 24 to 32 carbons observed in SNAPS simulations and the "conventional" growth mechanism (30000 trajectories) at a height of 8 mm above burner. The value "Structures Grouped", shown in parenthesis on the left below the number of carbons in each row, represents the quantity of trajectories with structures matching the specified number of carbons at this height.

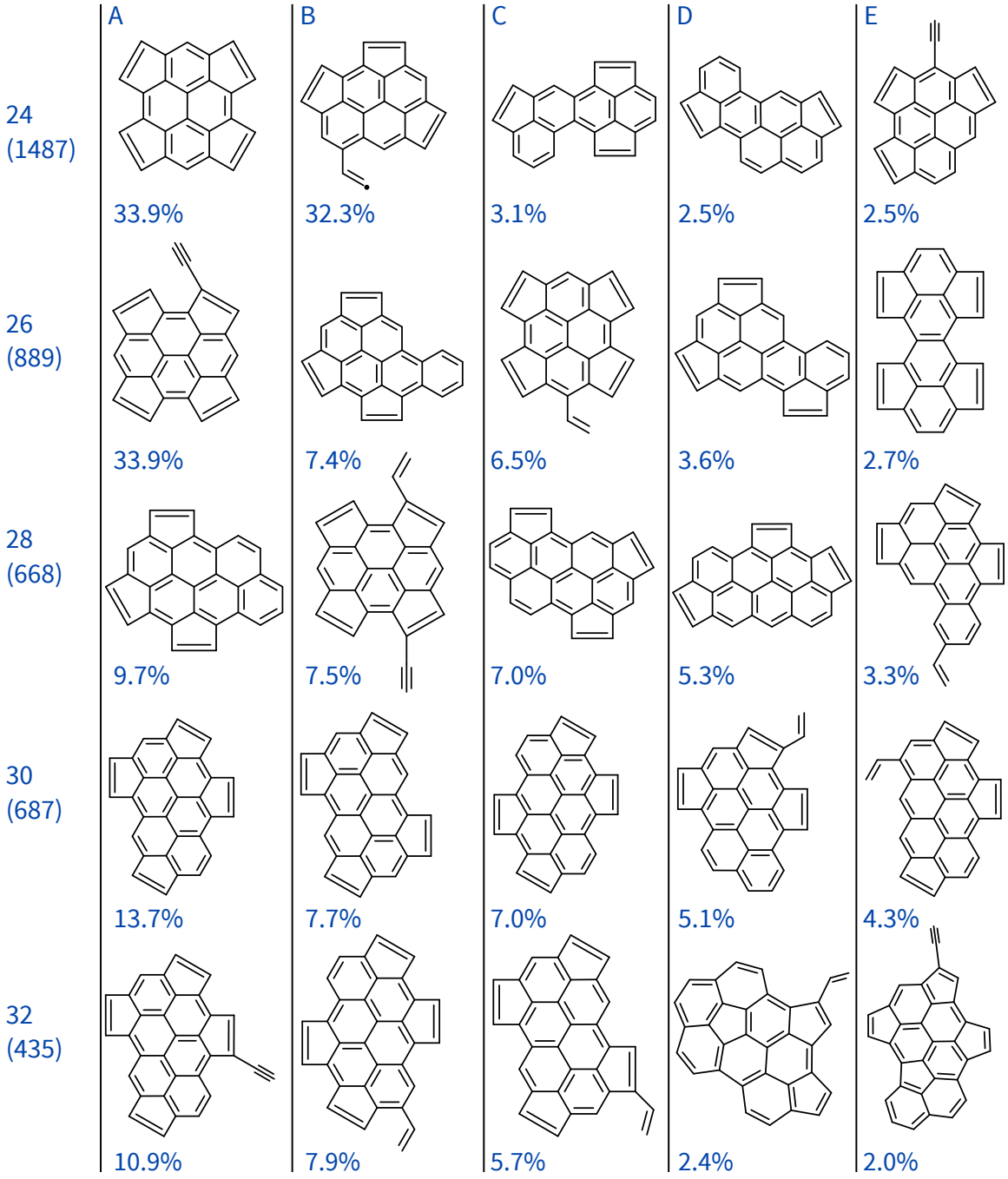

Figure 5.9: The top 5 most frequently observed PAH structures with 24 to 32 carbons observed in SNAPS simulations and the "reduced" growth mechanism (30000 trajectories) at a height of 8 mm above burner. The value "Structures Grouped", shown in parenthesis on the left below the number of carbons in each row, represents the quantity of trajectories with structures matching the specified number of carbons at this height.

likely to involve the migration or transformation of 5-membered rings to 6-membered ones. For example, the most common 24 carbon species (C24 column A) in the "reduced" case consists of a pyrene structure containing 4 pericondensed 6-membered rings, surrounded by 4 5-membered rings. Examining larger PAHs, the most common species from 28 to 32 carbons include many structures that contain 6 pericondensed 6-membered rings, for example C28 column A. The growth from 24 to 32 carbons suggests that some of the 5-membered rings open and migrate, creating new 6-membered rings.

5.2.4 Similarities with a Benzene/Air Flame

Comparison of the current results with those of Chapter IV in a benzene/air flame shows significant similarity between the characterizations of PAH growth in both flames. Both of these studies were for rich premixed laminar flames, with equivalence ratios of 1.925 and 3 for the benzene/air and ethylene/oxygen flames respectively. Temperature (a maximum of 1754 K and 1664 K for benzene and ethylene respectively) and pressure (1 atm) were similar between the two flames. In both flame simulations, acetylene dominated all other addition reactions, leading to PAHs that can be characterized as formed through the HACA mechanism. The PAH structures in both simulations are also similar, prominently featuring 5-membered rings. The similarities in growth between the two flames occur despite differences in both equivalence ratio and fuel. While both flames are fuel rich, the difference in fuel is notable, as both benzene and ethylene addition reactions are included in the current PAH mechanism. Although benzene and ethylene may be expected to contribute significantly to PAH growth, their respective gas phase concentrations are depleted prior to significant PAH formation in the current simulations. In the benzene/air flame, simulations were started at 4.5 mm, where temperatures and gas phase concentrations are favourable to PAH growth. At this height, the concentration of benzene is ap-

proximately equal to acetylene, but rapidly diminishes due to oxidation. Likewise, in the current ethylene flame, while the gas phase concentrations of ethylene and acetylene are similar at the beginning height of simulations, 0.4 mm, the concentration of ethylene rapidly decreases. Consequently, acetylene addition becomes the dominant gas phase species throughout the majority of simulation time. Ultimately, the similarity in PAH growth between these two flames further supports the importance of acetylene as an important soot precursor.

5.3 Summary

This analysis has significant implications on the understanding and development of chemical mechanisms for PAH growth, which has traditional focused on energetic arguments. Conventionally, the most common PAH have long been considered to be the 6-membered ring stabilomers of Stein and Fahr, due to their energetic stability. As a result, mechanism development has focused on pathways producing these types of species, reflected in many current kinetic models [83, 86, 88, 125]. However, the current simulations show that other kinetic factors beyond energetics can influence PAH growth.

In the ethylene/oxygen flame studied, the high gas phase concentration of acetylene, as well as the unimolecular 5-membered "zig zag" ring closure significantly influence SNAPS simulations, revealing a view of PAH growth prominently featuring the HACA mechanism as well as 5-membered rings. Computed mass distributions were highly sensitive to reactions involving 5-membered rings, and the best prediction of experimental mass spectra was achieved by adjusting important rates in a migration pathway originally proposed by Frenklach et al. [92]. Conversely, a mechanism created to mimic conventional PAH growth through pericondensed 6-membered ring species was unable to accurately model the experimental data. Examination of the most frequently formed PAH species in SNAPS simulations further corroborated the

important role of 5-membered rings and showed that transformation or migration of these rings is a more likely way to produce pericondensed 6-membered rings than direct formation through the HACA mechanism. Comparison of these results with a similar study of a benzene/air flame demonstrated similarities in PAH growth, despite the difference in fuel and corroborated the importance of acetylene as a soot precursor.

The importance of 5-membered rings contrasts with traditional mechanism development for PAHs. Importantly, reactions and accurate rates for such pathways in literature are relatively scarce, which limits the accuracy of the current work. Future investigation of these pathways will greatly benefit understanding of PAH growth. Altogether, the results of this work contribute to a better understanding of PAH growth and will greatly improve the future development of both chemical and physical growth pathways for PAHs and soot formation.

CHAPTER VI

PAH Growth in a Counterflow Acetylene/Oxygen Flame

SNAPS was used to study PAH growth in an counterflow diffusion acetylene/oxygen flame, which has been experimentally studied at Sandia National Laboratory by Skeen et al. [58] using aerosol mass spectrometry. Simulations were utilized to elucidate the chemical composition of species associated with experimentally observed peaks in mass spectra. Due to the separation of flows fuel and oxidizer and the increased complexity of the flame, simulating PAH growth in a counterflow diffusion flame using SNAPS presents more of a challenge than the previously studied premixed laminar flames. Particle motion in a counterflow setup is expected to involve both axial (*i.e.* parallel to the outlet) and radial (*i.e.* perpendicular to the outlet) components. Moreover, depending on the flow rates of fuel and oxidizer, the location of the flame may be either on the fuel or oxidizer side, leading to different sooting characteristics [133].

6.1 Methodology

Despite this complexity, a methodology was devised and tested for simulating PAH growth in a counterflow configuration. Since the sooting zone is expected to always be located on the fuel side [133], the methodology first focused on the assumption of

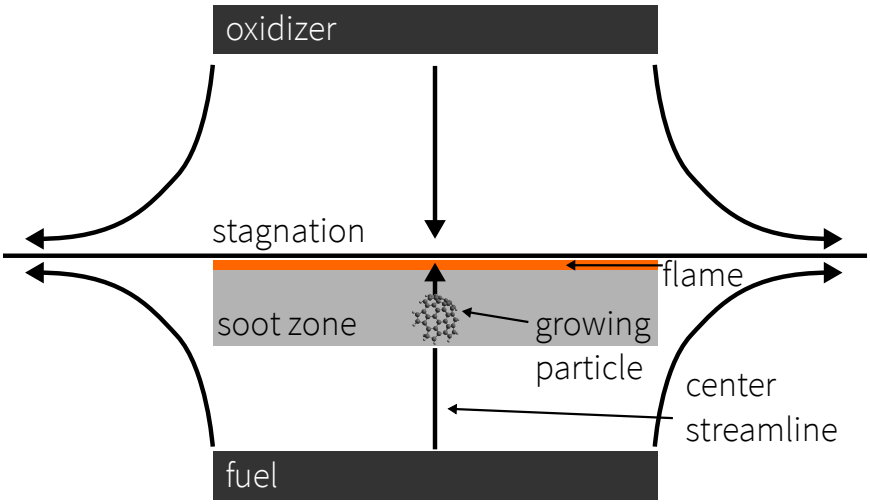

Figure 6.1: Schematic of a counterflow flame showing the center streamline and flame location used for simulating PAH growth using SNAPS.

particles growing as they move along the center streamline from the fuel outlet towards the flame. This assumption is consistent with the fact that soot precursors such as benzene and toluene can be expected to be present in relatively higher quantities on the fuel side than on the oxidizer side. Moreover, in the acetylene/oxygen flame studied by Skeen et al., the flame was located on the fuel side, providing favourable temperature and radical concentrations for simulating PAH growth using SNAPS. While soot particles will form in other counterflow configurations, these will likely involve more complex flow for which the current methodology is ill-suited. The current simulations also serve to test the suitability of this methodology to this counterflow configuration.

Table 6.1: Conditions of the counterflow acetylene/oxygen flame studied by Skeen et al. [58]

	Fuel Stream		**Oxidizer Stream**	
	C_2H_2	**Ar**	**O_2**	**Ar**
mol/min	0.0074	0.0803	0.0153	0.0535

The pressure of the flame was 700 torr and the burner separation was 14 mm. The conditions of the flame are given in Table 6.1. Temperature and gas phase species

profiles were computed using the OPPDIF program in CHEMKIN [82] and the ABF chemical mechanism [83]. Since the formation of the first aromatic ring is considered to be the first step of PAH formation, benzene and toluene were chosen as seed molecules for simulations. These molecules were among the most abundant single ring aromatic species based on experimentally observed mass spectra for the acetylene/oxygen flame. These seeds were considered to begin growth at a distance from the fuel outlet (DFFO) of 5.5 mm, which approximately locates the maximum rate of production of H radicals and was considered to be the beginning of the main chemical reaction zone, favourable to PAH growth. At this distance, based on the experimental mass spectra, the concentration of toluene is estimated to be approximately half that of benzene. This 2:1 ratio was used to compute the mass distribution. Important PAH species were also grouped using SPRINT coordinates, described in Chapter IV. Synthesis of experimental and simulated observations elucidated the chemical composition of prominent masses in this range and demonstrated that peaks in mass spectra generally consist of a mixture of PAH isomers. Importantly, both experiment and simulation a variety of chemical species that extends beyond the traditional classification of PAH species based on thermodynamic stability. The SNAPS PAH growth mechanism used for these simulations was the "reduced" case mechanism described in Chapter V, in order to further test the uncertainty regarding 5-membered ring migration rates.

6.2 Results and Discussion

6.2.1 Comparison with Experimental Mass Distributions

Figure 6.2 shows a comparison between experimental and simulated mass distributions at DFFO = 5.75 mm (simulation time of 1.85 ms). The latter was computed using a weighted average of 2000 each of benzene-seed and toluene-seed trajectories.

The computed distribution displays higher frequency of low molecular weight masses. This discrepancy can be ascribed to the fact that these species may not coagulate as easily and are preferentially lost in the sampling system. Nevertheless, the simulation results reproduce the trend of the measured spectra at this distance. Peaks associated with an even number of carbons (e.g. masses of approximately 202, 226, 252) can be traced to benzene-seed trajectories, while those associated with odd carbon number (e.g. masses of approximately 214, 232, 264), can be traced to toluene-seed trajectories. This result suggests the importance of methyl-substituted PAHs. Although the current growth mechanism includes methyl addition, it is limited by available chemical rates in literature. The current prevalence of odd numbered carbons, therefore, may indicate that additional exploration is needed for PAH reaction pathways involving methyl radicals.

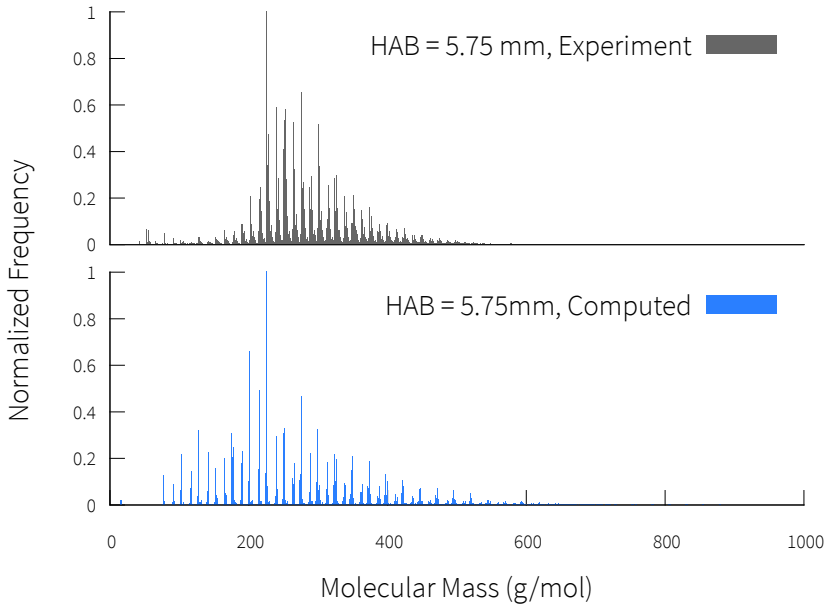

Figure 6.2: Comparison of ensemble-averaged mass distributions computed by SNAPS (2000 trajectories) compared with experimentally measured values in the counterflow acetylene/oxygen flame at a distance of 5.75 mm (simulation time of 1.85 ms) from the fuel outlet.

Importantly, the results of this simulation elucidate the limitations of the current

methodology for simulating the counterflow configuration. Specifically, simulations agree well with mass distributions at 5.75 mm DFFO, ostensibly because up to this point in the flame, the axial component of the flow velocity is fast enough, relative to the radial component, such that the trajectory of a growing particle can be well described as following the center streamline. However, as the flow approaches the stagnation plane, the axial velocity slows in magnitude while the radial component grows. Under these conditions, it is far less likely that a particle would be growing along the center streamline and as a result, the simulations do not agree well with experimental mass distributions at these distances. For example, Figure 6.3 shows an example mass distribution computed for a DFFO of 6 mm, which is vastly different from the experimental mass spectra for this distance.

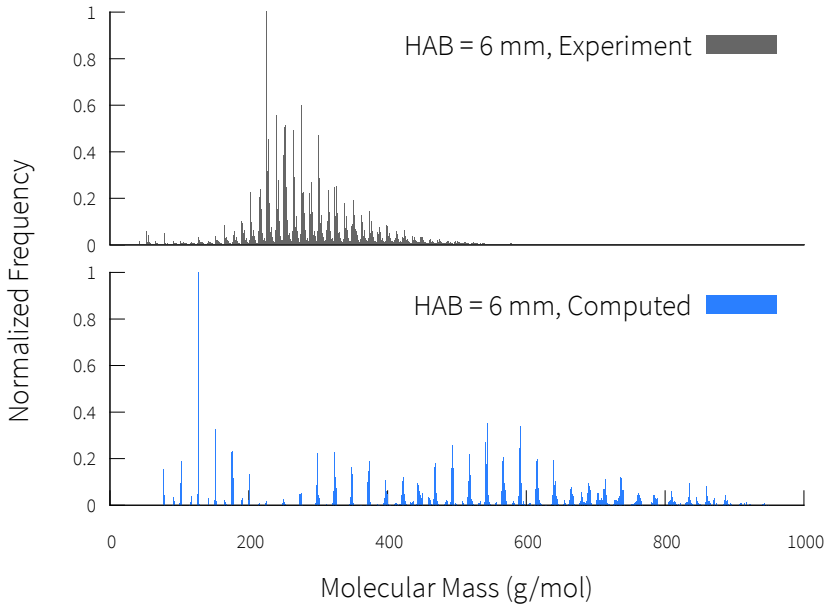

Figure 6.3: Comparison of ensemble-averaged mass distributions computed by SNAPS (96 trajectories) compared with experimentally measured values in the counterflow acetylene/oxygen flame at a distance of 6 mm (simulation time of 3.8 ms) from the fuel outlet.

The distribution exhibits sigificantly higher PAH masses than the experimental measurement. This result can be ascribed to the fact that, in the current simulation

methodology, the axial velocity of the particle decreases as it approaches the flame, thus spending longer amounts of time in regions of increasing temperature and radical concentrations, leading to greater particle growth. This result highlights a limitation of the streamline assumption, as many particles would be expected to flow away from the center streamline instead of continuing to grow to large masses. Future work will need to involve development of a method to couple SNAPS with more complex combustion environments, in order to widen the scope of potential investigations. For example, an "escape" event could be added to particle growth trajectories under the current methodology, to account for flow away from the center streamline. Such an adjustment may improve predictions of particle mass distributions. Nevertheless, the good agreement between experiment and simulations for a DFFO of 5.75 mm still provides useful insight within current model limitations. In particular, the good agreement corroborates the validity of the "reduced" case PAH mechanism.

6.2.2 PAH Structures and Reaction Pathways

SNAPS simulations provided molecular structures associated with mass distribution peaks. Figure 6.4 shows the most commonly observed structures for carbon numbers between 12 and 18. These structures account for the cluster of masses associated with peaks that differ by hydrogen content. These hydrogens were neglected to focus specifically on carbon structure, as some hydrogen addition or abstraction is expected within the sampling line. In experiments, Skeen et al. compare photoionization efficiency (PIE) curves of known species to those measured on sampled PAH mass to conjecture about the types of PAH species associated with a given peak [58]. Aiding this approach, the simulations allow the evaluation of the plausibility of such conjecture and elucidate molecular detail about peaks in mass spectra.

For example, experiments show a peak around 154 amu, which has been hypothesized to be a mixture of PAH species with 12 carbons. Based on analysis of PIE curves,

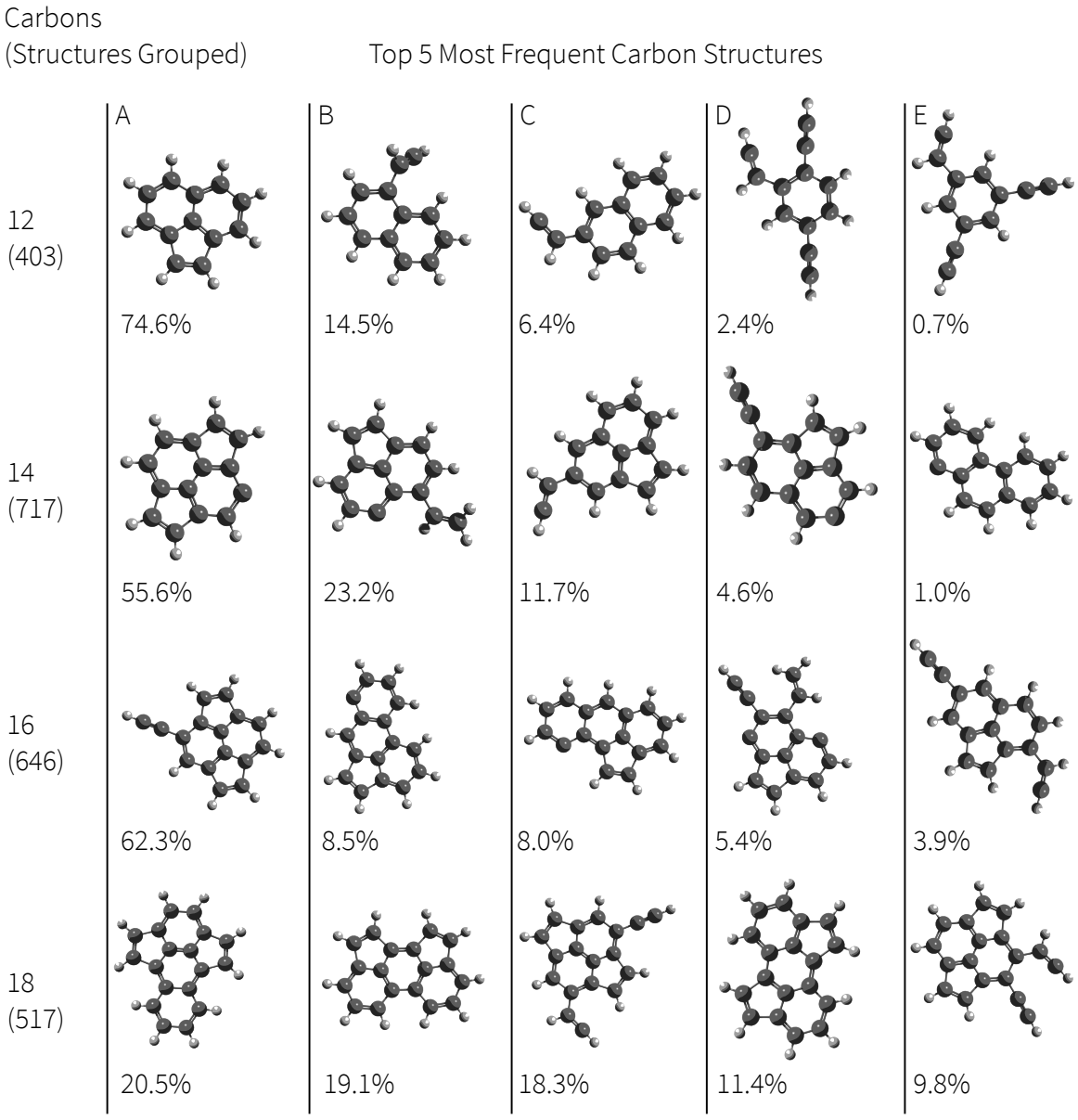

Figure 6.4: Top 5 most frequent carbon structures observed at 5.75 mm from the fuel outlet (simulation time of 1.85 ms) in 20000 simulations for varying number of carbons. The value "Structures Grouped", shown in parenthesis on the left below the number of carbons in each row, represents the quantity of trajectories with structures matching the specified number of carbons at this distance.

experiments proposed species that important PAH species could include biphenyl, 1-vinylnaphthalene, or acenaphthene, which are illustrated in Figure 6.5. Comparing with simulation results for C12, the most common isomer was an acenaphthylene structure, followed by a 1-vinylnapthalene radical structure. Although acenaphthylene has as mass of 152 amu, reactions such as the hydrogenation of the double bond in the 5-membered ring, in the flame or sampling line, can lead to acenaphthene, which has a mass of 154 amu. These simulation results therefore corroborate experimental observations and the existence of these species in flames.

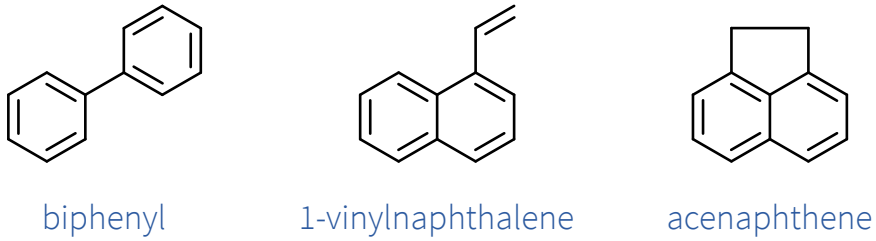

Figure 6.5: Proposed species with mass 154 amu based on experimental analysis with photoionization efficiency curves.

Importantly, the simulation results further show deviation from the common PAH stabilomer table. In particular, species with 16 carbons are commonly assumed to be pyrene; however, pyrene was observed with a frequency of only 0.5%. Instead, the simulation results show a much wider variety of potential PAH species. In particular, the structures again show the importance of 5-membered rings, which are prevalent throughout the classified structures. The most commonly observed C16 structure (C16 column A) contains two 5-membered rings and was also identified as a stabilomer by Stein and Fahr [65]. Moreover, the acetylene addition reaction was the most common addition reaction, accounting for 19.0% of all reactions, and is reflected in separating the most commonly observed structures from C12 to C18. These simulation results demonstrate the importance of the existing HACA growth mechanism, but also suggest avenues for future exploration, namely reactions involving 5-membered rings. Altogether, the results of the counterflow diffusion show a signifi-

cant amount of similarity to the previous benzene and ethylene laminar flames. This similarity across fuels, as well as flame conditions further corroborates the importance of acetylene and the HACA mechanism in soot precursor formation.

6.3 Summary

In a counterflow acetylene/oxygen flame, mass distributions computed from SNAPS simulations reproduced experimentally measured mass spectra at relatively short distances from the fuel outlet. Additionally, simulations were again able to provide valuable molecular detail of the compositions of PAHs associated with peaks in mass spectra, augmenting experimental observation and corroborating conjecture based on measurements. Simulations once again demonstrated the importance of acetylene and the HACA mechanism as important components of soot precursor growth. Importantly, difficulty in modeling PAH growth closer to the stagnation plane points to a need for future work improving coupling between SNAPS and flame simulation. Altogether, these results demonstrate the value of the SNAPS methodology in investigating PAH growth, as well as the wealth of areas still available to explore.

CHAPTER VII

Conclusions and Future Work

Towards elucidating the inception of carbonaceous nanoparticles and soot formation, this work has investigated the composition, morphology, and growth of polycyclic aromatic hydrocarbon (PAH) in combustion using a stochastic simulation approach. The developed Stochastic Nanoparticle Simulator (SNAPS) software represents a novel approach to explore the complex reaction networks involved in the chemical growth of particles. The extensibility of the code in particular enables the investigation of not just CNPs, but many other potential growth systems as well. Combined with a concurrently devised chemical reaction mechanism for polycyclic aromatic hydrocarbon (PAH) growth, the SNAPS algorithm was verified against equivalent deterministic simulations and a methodology was devised to simulate PAH growth in premixed laminar flames.

This methodology was applied to successfully simulate PAH growth in benzene/air, ethylene/oxygen, and acetylene/oxygen flames. The simulation results were corroborated by comparison with experimental measurements and revealed molecular-level detail concerning the growth of PAH. For a premixed laminar benzene flame, simulations agreed well with species concentration ratios within an order of magnitude, and reproduced major peaks in mass distributions. These results supported the credibility of simulations produced by the SNAPS software and the PAH chemical mechanism.

In addition, important insights about PAH growth were gleaned from simulations. The time evolution of average particle mass showed that PAHs do not grow infinitely via chemical reactions, instead only experiencing significant growth in regions with high temperatures and radical concentration. In addition, graph theory in the form of SPRINT coordinates was applied to particle ensembles in order to group and determine the most frequently produced molecular structures in simulations. This procedure allowed the identification of the important PAH structures for given peaks in mass distributions. Simulated PAHs exhibited significant presence of 5-membered rings, which contrasted substantially from conventional theory of the most important PAHs, namely pericondensed 6-membered ringed species. Analysis of major reaction pathways showed the importance of acetylene addition, reversible reactions, and molecular rearrangement, reflected in observed PAH structures that are not connected via a direct growth pathway.

Further investigation of a premixed ethylene/oxygen flame involved probing the importance of 5-membered rings and associated reactions in the growth of PAHs, especially in contrast with conventional views of the major PAHs in combustion. The concept of pericondensed 6-membered rings is pervasive throughout models for soot formation, especially in chemical mechanisms for growth through species such as pyrene and coronene, as well as in concepts of particle nucleation involving the physical agglomeration of such species. Simulation results shows the influence of the gas phase concentration of acetylene, as well as the unimolecular ring closure of attached acetyl chains forming 5-membered rings, which was kinetically favourable compared with the formation of 6-membered rings. Comparison of experimental and computed mass distributions showed the best agreement using a mechanism involving 5-membered rings. Importantly, a mechanism created to mimic conventional PAH growth through pericondensed 6-membered ring species was unable to accurately model the experimental data. Moreover, examination of important reaction pathways

and species showed that pericondensed 6-membered rings do form, but are more likely to form through the transformation or migration of 5-membered rings, rather than directly through sequential addition of acetylene.

In simulations of a counter-flow apparatus, SNAPS successfully reproduced experimental mass spectra at relatively short distances from the fuel outlet in an acetylene/oxygen flame. Again, simulations were able to provide valuable molecular detail of the compositions of PAHs associated with peaks in mass spectra, augmenting experimental observation and corroborating conjecture based on measurements. Importantly, difficulty in modeling PAH growth closer to the stagnation plane of the counterflow plane points to a need for future work improving coupling between SNAPS and flame simulation.

Comparing simulation results across all flames studied revealed common themes characterizing the chemical growth of PAHs in combustion. Species are primarily formed within the main chemical reaction zone of flames, characterized by high temperature and gas phase concentrations of radicals and carbon containing species for mass growth. Of the potential soot precursor species contributing to mass growth, acetylene was dominant by a significant margin, owing to its much larger concentration within the chemical growth regions of the flame. This phenomenon was observed in all flames studied, despite the difference in fuel. Although PAHs were observed to grow through the relatively simple HACA mechanism, even this small set of reactions lead to a wide variety of species. This diversity will have a substantial impact on models for physical aggregation, which depends heavily on the chemical composition and morphology of interacting PAHs. Models for the physical interaction of PAHs and their dimerization tendencies will need to account for this variety. Nevertheless, the observed similarity of growth across different flames will facilitate the development of such a model, which will benefit the study of particle nucleation.

The methodology and results of this work form a strong framework for future

exploration in many areas, including further development of the SNAPS software, expansion and refinement of the PAH chemical growth mechanism, and the extension of the SNAPS methodology to the simulation of physical interactions and particle aggregates. For example, while simulations were successful in reproducing some experimental quantities, they also revealed areas which will greatly benefit from continued development. Coupling between flame simulation, or environmental parameters, and SNAPS simulations is an important area to improve simulation of more complex flame environments, such as the counterflow environment simulated in Chapter VI. In particular, a better understanding of particle growth trajectories and environmental parameters such as temperature and gas phase species concentrations would greatly improve the applicability of SNAPS.

In addition, the software could be developed to address environmental and growth factors that are currently problematic for the SNAPS methodology. These factors include environments with low temperature and/or radicals, leading to low reaction rates and long timesteps that do not properly capture the changing flame environment, as discussed in Chapter III. Another issue is the highly reversible reactions involved in PAH growth, which lead to significant computational inefficiency. There are documented theoretical techniques in the area of stochastic chemical kinetics [81] that could be adapted and applied to ameliorate these issues. For example, the "weighted" stochastic simulation algorithm [134, 135] contains a methodology to simulate the probability that a very rare reaction will occur within a given time interval. This technique will help to mitigate simulation issues with low-reactivity environments. Similarly, "tau-leaping" methods [136, 137] exploit the fact that sequential transition events can be modeled using a Poisson distribution, such that multiple reactions could be selected within a given time interval. These methods will aid in simulating highly reversible reactions. In a scenario where multiple corresponding forward and reverse reactions are selected within a given time interval, SNAPS sim-

ulations could make modifications only for the last reaction, saving computational time spent on energy minimization and rejection routines. Finally, the "slow-scale" stochastic simulation algorithm [138] has been developed to simulate systems that contain both "fast" and "slow" reaction channels, where the "slow" reaction channels have more of an impact on the behaviour of the system. In the context of particle growth, "fast" reaction channels would be highly reversible reactions that do not necessarily increase particle mass, while "slow" channels would be addition reactions that depend on the collision with another particle. The "slow-scale" algorithm contains an approximate method to preferentially simulate the "slow" reaction channels in order to increase computational efficiency. Adaptation of this methodology to SNAPS is another avenue to improve performance.

Beyond improvement of the SNAPS software, further development of growth mechanisms, both chemical and physical, will greatly improve the description of PAH growth and soot formation. The results of this work strongly show the importance of 5-membered ring species and pathways, which will be an important area of exploration moving forward. In addition to chemical pathways, physical aggregation is another important growth mechanism that will require exploration. A strong model for the physical interactions between PAH, accounting for the variety of structures demonstrated in this work, will be a novel and important contribution. Moreover, such a model will enable the further extension of SNAPSs to model particle aggregates. The object-oriented structure of the SNAPS code will facilitate incorporation into an expanded code that simulates the chemical growth of invididual molecules, as well as their aggregation and subsequent combined chemical and physical growth. Beyond the formation of soot, such software represents the long term goal of SNAPS, to simulate nanoparticle growth processes, from gas phase precursors through inception and beyond.

Altogether, the work completed in this investigation provides novel and impactful

insight into the chemical growth of PAHs, important precursors in CNP inception and soot formation. In addition to illuminating the complex PAH growth process, this work provides a strong foundation that will drive future investigations towards a comprehensive atomistic description of particle inception and soot formation. Importantly, SNAPS simulations provide a level of detail that is typically not accessible by experimental techniques, and therefore provides an important tool for augmenting and interpreting experiments. Such capability will unequivocally have a profound impact in engineering of novel combustion technologies, particularly in toxicological assessment, emission control of carbonaceous nanoparticles and soot, as well as in flame synthesis of nanomaterials.

APPENDIX

APPENDIX A

Social Permutation Invariant Coordinates (SPRINT) for Molecular Structure Classification

Social permutation invariant topological coordinates (SPRINT) [130] are a useful application of spectral graph theory to the classification of atomic structures for molecular simulation. These coordinates are quantitative descriptors of molecular structure, and contain information about the short and long range topology of a molecule. The quantitative nature of SPRINT coordinates greatly facilitates differentiation and grouping of molecular structures produced in SNAPS simulations. Much of the following description has been adapted from a more detailed one by Pietrucci and Andreoni [130].

A molecule can be considered as a graph, where atoms and bonds correspond to nodes and edges, respectively. Such a graph has a contact matrix A, where each element ij in the matrix represents a pair of atoms. $a_{ij} = 1$ if i and j are connected by a bond, and is 0 otherwise. All elements a_{ii} for an atom connected to itself are likewise 0. The Perron-Frobenius theorem holds for A, which is symmetric, non-negative, and irreducible as it represents a connected graph (i.e. a molecule), where all nodes are connected through a path. Two important quantities of A are its largest modulus eigenvalue λ^{max}, which is real, positive, and nondegenerate and the

corresponding eigenvector $\vec{\nu}^{max}$, which has all nonzero components with equal sign. For SPRINT coordinates, the positive sign convention is utilized. For N atoms, SPRINT coordinates are defined as follows:

$$S_i = \sqrt{N}\lambda^{max}\nu_i^{max,sorted}; \qquad i = 1, 2, \ldots, N$$

where $\nu_i^{max,sorted}$ is the ith element of the eigenvector $\vec{\nu}^{max}$ sorted from smallest to largest value. This sorting operation makes the set $\{S_i\}$ invariant with respect to $N!$ permutations of labels given to N identical atoms. Thus, any given structure will have the same SPRINT coordinates regardless of how its atoms are indexed.

A general function for the elements of the contact matrix A is convenient for computer simulations. For this purpose, a_{ij} can be defined as a smooth, differentiable function of interatomic distance between two atoms r_{ij} as follows:

$$a_{ij} = \frac{1 - (r_{ij}/r_0)^n}{1 - (r_{ij}/r_0)^m}$$

where r_0, n, and m must be chosen, based on typical bond lengths of the system of interest, to clearly dilineate between bonded and non-bonded atoms. In the current work, values for these parameters were chosen as: $r_0 = 2.5$, $n = 6$, and $m = 24$. These values were successful in producing SPRINT coordinates that differentiated distinct molecular PAH structures.

BIBLIOGRAPHY

BIBLIOGRAPHY

[1] Friedlander SK, Pui DYH. Emerging Issues in Nanoparticle Aerosol Science and Technology. *Journal of Nanoparticle Research*. 2004;6(2):313–320.

[2] Kammler HK, Mädler L, Pratsinis SE. Flame Synthesis of Nanoparticles. *Chemical Engineering & Technology*. 2001;24(6):583–596.

[3] Kay A, Grätzel M. Low cost photovoltaic modules based on dye sensitized nanocrystalline titanium dioxide and carbon powder. *Solar Energy Materials and Solar Cells*. 1996;44(1):99–117.

[4] Soots (IARC Summary & Evaluation, Volume 35). 1985.

[5] Carbon Black (IARC Summary & Evaluation, Volume 65). 1996.

[6] Nel A, Xia T, Mädler L, Li N. Toxic Potential of Materials at the Nanolevel. *Science*. 2006;311(5761):622–627.

[7] Nel AE, Mädler L, Velegol D, Xia T, Hoek EMV, Somasundaran P, Klaessig F, Castranova V, Thompson M. Understanding biophysicochemical interactions at the nano–bio interface. *Nature Materials*. 2009;8(7):543–557.

[8] Fubini B, Ghiazza M, Fenoglio I. Physico-chemical features of engineered nanoparticles relevant to their toxicity. *Nanotoxicology*. 2010;4(4):347–363.

[9] Chang R, Violi A. Insights into the Effect of Combustion-Generated Carbon Nanoparticles on Biological Membranes: A Computer Simulation Study. *The Journal of Physical Chemistry B*. 2006;110(10):5073–5083.

[10] Fiedler SL, Violi A. Simulation of Nanoparticle Permeation through a Lipid Membrane. *Biophysical Journal*. 2010;99(1):144–152.

[11] Choe S, Chang R, Jeon J, Violi A. Molecular Dynamics Simulation Study of a Pulmonary Surfactant Film Interacting with a Carbonaceous Nanoparticle. *Biophysical Journal*. 2008;95(9):4102–4114.

[12] Elvati P, Violi A. Free Energy Calculation of Permeant–Membrane Interactions Using Molecular Dynamics Simulations. In: *Nanotoxicity*, edited by Reineke J, no. 926 in Methods in Molecular Biology, pp. 189–202. Humana Press. 2012;.

[13] Abdul-Khalek IS, Kittelson DB, Graskow BR, Wei Q, Bear F. Diesel Exhaust Particle Size: Measurement Issues and Trends. *Tech. Rep. 980525*, SAE International, Warrendale, PA. 1998.

[14] Wang H. Formation of nascent soot and other condensed-phase materials in flames. *Proceedings of the Combustion Institute*. 2011;33(1):41–67.

[15] Laine RM, Marchal JC, Sun HP, Pan XQ. Nano-α-Al2O3 by liquid-feed flame spray pyrolysis. *Nature Materials*. 2006;5(9):710–712.

[16] Izvekov S, Violi A. A Coarse-Grained Molecular Dynamics Study of Carbon Nanoparticle Aggregation. *Journal of Chemical Theory and Computation*. 2006; 2(3):504–512.

[17] Frenklach M. Reaction mechanism of soot formation in flames. *Physical Chemistry Chemical Physics*. 2002;4(11):2028–2037.

[18] Singh J, Patterson RI, Kraft M, Wang H. Numerical simulation and sensitivity analysis of detailed soot particle size distribution in laminar premixed ethylene flames. *Combustion and Flame*. 2006;145(1–2):117–127.

[19] Alfè M, Apicella B, Barbella R, Rouzaud JN, Tregrossi A, Ciajolo A. Structure–property relationship in nanostructures of young and mature soot in premixed flames. *Proceedings of the Combustion Institute*. 2009;32(1):697–704.

[20] D'Anna A. Combustion-formed nanoparticles. *Proceedings of the Combustion Institute*. 2009;32(1):593–613.

[21] Sirignano M, Collina A, Commodo M, Minutolo P, D'Anna A. Detection of aromatic hydrocarbons and incipient particles in an opposed-flow flame of ethylene by spectral and time-resolved laser induced emission spectroscopy. *Combustion and Flame*. 2012;159(4):1663–1669.

[22] Richter H, Howard J. Formation of polycyclic aromatic hydrocarbons and their growth to soot—a review of chemical reaction pathways. *Progress in Energy and Combustion Science*. 2000;26(4–6):565–608.

[23] Jäger C, Mutschke H, Henning T, Huisken F. From PAHs to Solid Carbon. *European Astronomical Society Publications Series*. 2011;46:293–304.

[24] Mansurov ZA. Soot Formation in Combustion Processes (Review). *Combustion, Explosion and Shock Waves*. 2005;41(6):727–744.

[25] Mansurov ZA. Formation of soot from polycyclic aromatic hydrocarbons as well as fullerenes and carbon nanotubes in the combustion of hydrocarbon. *Journal of Engineering Physics and Thermophysics*. 2011;84(1):125–159.

[26] Karataş AE, Gülder ÖL. Soot formation in high pressure laminar diffusion flames. *Progress in Energy and Combustion Science*. 2012;38(6):818–845.

[27] Xi J, Zhong BJ. Soot in Diesel Combustion Systems. *Chemical Engineering & Technology*. 2006;29(6):665–673.

[28] Wersborg B, Howard J, Williams G. Physical mechanisms in carbon formation in flames. *Symposium (International) on Combustion*. 1973;14(1):929–940.

[29] Dobbins R, Fletcher R, Lu W. Laser microprobe analysis of soot precursor particles and carbonaceous soot. *Combustion and Flame*. 1995;100(1–2):301–309.

[30] Dobbins R, Fletcher R, Chang HC. The evolution of soot precursor particles in a diffusion flame. *Combustion and Flame*. 1998;115(3):285–298.

[31] D'Alessio A, D'Anna A, D'Orsi A, Minutolo P, Barbella R, Ciajolo A. Precursor formation and soot inception in premixed ethylene flames. *Symposium (International) on Combustion*. 1992;24(1):973–980.

[32] Sgro L, De Filippo A, Lanzuolo G, D'Alessio A. Characterization of nanoparticles of organic carbon (NOC) produced in rich premixed flames by differential mobility analysis. *Proceedings of the Combustion Institute*. 2007;31(1):631–638.

[33] Siegmann K, Sattler K, Siegmann H. Clustering at high temperatures: carbon formation in combustion. *Journal of Electron Spectroscopy and Related Phenomena*. 2002;126(1–3):191–202.

[34] Zhao B, Yang Z, Wang J, Johnston MV, Wang H. Analysis of Soot Nanoparticles in a Laminar Premixed Ethylene Flame by Scanning Mobility Particle Sizer. *Aerosol Science and Technology*. 2003;37(8):611–620.

[35] Zhao B, Uchikawa K, Wang H. A comparative study of nanoparticles in premixed flames by scanning mobility particle sizer, small angle neutron scattering, and transmission electron microscopy. *Proceedings of the Combustion Institute*. 2007;31(1):851–860.

[36] Zhao B, Yang Z, Li Z, Johnston MV, Wang H. Particle size distribution function of incipient soot in laminar premixed ethylene flames: effect of flame temperature. *Proceedings of the Combustion Institute*. 2005;30(1):1441–1448.

[37] Zhao B, Yang Z, Johnston MV, Wang H, Wexler AS, Balthasar M, Kraft M. Measurement and numerical simulation of soot particle size distribution functions in a laminar premixed ethylene-oxygen-argon flame. *Combustion and Flame*. 2003;133(1–2):173–188.

[38] Grotheer HH, Pokorny H, Barth KL, Thierley M, Aigner M. Mass spectrometry up to 1 million mass units for the simultaneous detection of primary soot and of soot precursors (nanoparticles) in flames. *Chemosphere*. 2004;57(10):1335–1342.

[39] Grotheer HH, Pokorny H, Happold J, Baquet TG, Thierley M, Aigner M, Baumstark-Khan C, CEHellweg, Arenz A. On Combustion Generated Nanoparticles and their Biological Effects. Part I:Measurement of Nanoparticles and their Detection in and Behind Flames. *Current Nanoscience*. 2007;3(3):199–205.

[40] Grotheer HH, Wolf K, Hoffmann K. Photoionization mass spectrometry for the investigation of combustion generated nascent nanoparticles and their relation to laser induced incandescence. *Applied Physics B*. 2011;104(2):367–383.

[41] Zhang QL, O'Brien SC, Heath JR, Liu Y, Curl RF, Kroto HW, Smalley RE. Reactivity of large carbon clusters: spheroidal carbon shells and their possible relevance to the formation and morphology of soot. *The Journal of Physical Chemistry*. 1986;90(4):525–528.

[42] Kroto H. Space, Stars, C60, and Soot. *Science*. 1988;242(4882):1139–1145. PMID: 17799730.

[43] Gerhardt P, Löffler S, Homann K. Polyhedral carbon ions in hydrocarbon flames. *Chemical Physics Letters*. 1987;137(4):306–310.

[44] Maricq MM. An examination of soot composition in premixed hydrocarbon flames via laser ablation particle mass spectrometry. *Journal of Aerosol Science*. 2009;40(10):844–857.

[45] Homann KH. Fullerenes and Soot Formation— New Pathways to Large Particles in Flames. *Angewandte Chemie International Edition*. 1998; 37(18):2434–2451.

[46] Frenklach M, Wang H. Detailed modeling of soot particle nucleation and growth. *Symposium (International) on Combustion*. 1991;23(1):1559–1566.

[47] Herdman JD, Miller JH. Intermolecular Potential Calculations for Polynuclear Aromatic Hydrocarbon Clusters. *The Journal of Physical Chemistry A*. 2008; 112(28):6249–6256.

[48] Schuetz CA, Frenklach M. Nucleation of soot: Molecular dynamics simulations of pyrene dimerization. *Proceedings of the Combustion Institute*. 2002; 29(2):2307–2314.

[49] Miller JH. Aromatic excimers: evidence for polynuclear aromatic hydrocarbon condensation in flames. *Proceedings of the Combustion Institute*. 2005; 30(1):1381–1388.

[50] Miller JH. The kinetics of polynuclear aromatic hydrocarbon agglomeration in flames. *Symposium (International) on Combustion*. 1991;23(1):91–98.

[51] Sabbah H, Biennier L, Klippenstein SJ, Sims IR, Rowe BR. Exploring the Role of PAHs in the Formation of Soot: Pyrene Dimerization. *The Journal of Physical Chemistry Letters*. 2010;1(19):2962–2967.

[52] Chung SH, Violi A. Peri-condensed aromatics with aliphatic chains as key intermediates for the nucleation of aromatic hydrocarbons. *Proceedings of the Combustion Institute*. 2011;33(1):693–700.

[53] Elvati P, Violi A. Thermodynamics of poly-aromatic hydrocarbon clustering and the effects of substituted aliphatic chains. *Proceedings of the Combustion Institute*. 2013;34(1):1837–1843.

[54] Totton TS, Misquitta AJ, Kraft M. A quantitative study of the clustering of polycyclic aromatic hydrocarbons at high temperatures. *Physical Chemistry Chemical Physics*. 2012;14(12):4081–4094.

[55] Houston Miller J, Smyth KC, Mallard WG. Calculations of the dimerization of aromatic hydrocarbons: Implications for soot formation. *Symposium (International) on Combustion*. 1985;20(1):1139–1147.

[56] Chung SH, Violi A. Nucleation of fullerenes as a model for examining the formation of soot. *The Journal of Chemical Physics*. 2010;132(17):174502–174502–9.

[57] Öktem B, Tolocka MP, Zhao B, Wang H, Johnston MV. Chemical species associated with the early stage of soot growth in a laminar premixed ethylene–oxygen–argon flame. *Combustion and Flame*. 2005;142(4):364–373.

[58] Skeen SA, Michelsen HA, Wilson KR, Popolan DM, Violi A, Hansen N. Near-threshold photoionization mass spectra of combustion-generated high-molecular-weight soot precursors. *Journal of Aerosol Science*. 2013;58:86–102.

[59] D'Alessio A, D'Anna A, Gambi G, Minutolo P. The spectroscopic characterisation of UV absorbing nanoparticles in fuel rich soot forming flames. *Journal of Aerosol Science*. 1998;29(4):397–409.

[60] D'Anna A, Commodo M, Sirignano M, Minutolo P, Pagliara R. Particle formation in opposed-flow diffusion flames of ethylene: An experimental and numerical study. *Proceedings of the Combustion Institute*. 2009;32(1):793–801.

[61] Minutolo P, Gambi G, D'Alessio A. Properties of carbonaceous nanoparticles in flat premixed C2H4/air flames with C/O ranging from 0.4 to soot appearance limit. *Symposium (International) on Combustion*. 1998;27(1):1461–1469.

[62] D'Anna A, Violi A. A kinetic model for the formation of aromatic hydrocarbons in premixed laminar flames. *Symposium (International) on Combustion*. 1998; 27(1):425–433.

[63] Bruno A, Ossler F, de Lisio C, Minutolo P, Spinelli N, D'Alessio A. Detection of fluorescent nanoparticles in flame with femtosecond laser-induced fluorescence anisotropy. *Optics Express*. 2008;16(8):5623–5632.

[64] Reilly P, Gieray R, Whitten W, Ramsey J. Direct observation of the evolution of the soot carbonization process in an acetylene diffusion flame via real-time aerosol mass spectrometry. *Combustion and Flame*. 2000;122(1–2):90–104.

[65] Stein SE, Fahr A. High-temperature stabilities of hydrocarbons. *The Journal of Physical Chemistry*. 1985;89(17):3714–3725.

[66] Weilmünster P, Keller A, Homann KH. Large molecules, radicals, ions, and small soot particles in fuel-rich hydrocarbon flames: Part I: positive ions of polycyclic aromatic hydrocarbons(PAH) in low-pressure premixed flames of acetylene and oxygen. *Combustion and Flame*. 1999;116(1–2):62–83.

[67] Keller A, Kovacs R, Homann KH. Large molecules, ions, radicals and small soot particles in fuel-rich hydrocarbon flames. Part IV. Large polycyclic aromatic hydrocarbons and their radicals in a fuel-rich benzene–oxygen flame. *Physical Chemistry Chemical Physics*. 2000;2(8):1667–1675.

[68] Fialkov A, Dennebaum J, Homann KH. Large molecules, ions, radicals, and small soot particles in fuel-rich hydrocarbon flames part V: Positive ions of polycyclic aromatic hydrocarbons (PAH) in low-pressure premixed flames of benzene and oxygen. *Combustion and Flame*. 2001;125(1–2):763–777.

[69] Fialkov A, Homann KH. Large molecules, ions, radicals, and small soot particles in fuel-rich hydrocarbon flames: Part VI: positive ions of aliphatic and aromatic hydrocarbons in a low-pressure premixed flame of n-butane and oxygen. *Combustion and Flame*. 2001;127(3):2076–2090.

[70] Griesheimer J, Homann KH. Large molecules, radicals ions, and small soot particles in fuel-rich hydrocarbon flames: Part II. Aromatic radicals and intermediate PAHs in a premixed low-pressure naphthalene/oxygen/argon flame. *Symposium (International) on Combustion*. 1998;27(2):1753–1759.

[71] Miller JH, Herdman JD, Green CD, Webster EM. Experimental and computational determinations of optical band gaps for PAH and soot in a N2-diluted, ethylene/air non-premixed flame. *Proceedings of the Combustion Institute*. 2013; 34(2):3669–3675.

[72] Tregrossi A, Ciajolo A, Barbella R. The combustion of benzene in rich premixed flames at atmospheric pressure. *Combustion and Flame*. 1999;117(3):553–561.

[73] Cain JP, Camacho J, Phares DJ, Wang H, Laskin A. Evidence of aliphatics in nascent soot particles in premixed ethylene flames. *Proceedings of the Combustion Institute*. 2011;33(1):533–540.

[74] Cain JP, Gassman PL, Wang H, Laskin A. Micro-FTIR study of soot chemical composition—evidence of aliphatic hydrocarbons on nascent soot surfaces. *Physical Chemistry Chemical Physics*. 2010;12(20):5206–5218.

[75] Russo C, Alfè M, Rouzaud JN, Stanzione F, Tregrossi A, Ciajolo A. Probing structures of soot formed in premixed flames of methane, ethylene and benzene. *Proceedings of the Combustion Institute*. 2013;34(1).

[76] Frenklach M, Clary DW, Gardiner Jr WC, Stein SE. Detailed kinetic modeling of soot formation in shock-tube pyrolysis of acetylene. *Symposium (International) on Combustion*. 1985;20(1):887–901.

[77] Miller JA, Melius CF. Kinetic and thermodynamic issues in the formation of aromatic compounds in flames of aliphatic fuels. *Combustion and Flame*. 1992; 91(1):21–39.

[78] Apicella B, Carpentieri A, Alfè M, Barbella R, Tregrossi A, Pucci P, Ciajolo A. Mass spectrometric analysis of large PAH in a fuel-rich ethylene flame. *Proceedings of the Combustion Institute*. 2007;31(1):547–553.

[79] Shukla B, Koshi M. A highly efficient growth mechanism of polycyclic aromatic hydrocarbons. *Physical Chemistry Chemical Physics*. 2010;12(10):2427–2437.

[80] Shukla B, Koshi M. A novel route for PAH growth in HACA based mechanisms. *Combustion and Flame*. 2012;.

[81] Gillespie DT, Hellander A, Petzold LR. Perspective: Stochastic algorithms for chemical kinetics. *The Journal of Chemical Physics*. 2013;138(17):170901–170901–14.

[82] CHEMKIN 10112, Reaction Design: San Diego. 2011.

[83] Appel J, Bockhorn H, Frenklach M. Kinetic modeling of soot formation with detailed chemistry and physics: laminar premixed flames of C2 hydrocarbons. *Combustion and Flame*. 2000;121(1–2):122–136.

[84] Blanquart G, Pepiot-Desjardins P, Pitsch H. Chemical mechanism for high temperature combustion of engine relevant fuels with emphasis on soot precursors. *Combustion and Flame*. 2009;156(3):588–607.

[85] Marchal C, Delfau JL, Vovelle C, Moréac G, Mounaïm-Rousselle C, Mauss F. Modelling of aromatics and soot formation from large fuel molecules. *Proceedings of the Combustion Institute*. 2009;32(1):753–759.

[86] Raj A, Prada IDC, Amer AA, Chung SH. A reaction mechanism for gasoline surrogate fuels for large polycyclic aromatic hydrocarbons. *Combustion and Flame*. 2012;159(2):500–515.

[87] Wang H, Frenklach M. A detailed kinetic modeling study of aromatics formation in laminar premixed acetylene and ethylene flames. *Combustion and Flame*. 1997;110(1–2):173–221.

[88] Wang Y, Raj A, Chung SH. A PAH growth mechanism and synergistic effect on PAH formation in counterflow diffusion flames. *Combustion and Flame*. 2013; 160(9):1667–1676.

[89] Sirignano M, Kent J, D'Anna A. Modeling Formation and Oxidation of Soot in Nonpremixed Flames. *Energy & Fuels*. 2013;27(4):2303–2315.

[90] McQuarrie DA. Stochastic Approach to Chemical Kinetics. *Journal of Applied Probability*. 1967;4(3):413–478. ArticleType: research-article / Full publication date: Dec., 1967 / Copyright © 1967 Applied Probability Trust.

[91] Frenklach M. On surface growth mechanism of soot particles. *Symposium (International) on Combustion*. 1996;26(2):2285–2293.

[92] Frenklach M, Schuetz CA, Ping J. Migration mechanism of aromatic-edge growth. *Proceedings of the Combustion Institute*. 2005;30(1):1389–1396.

[93] Whitesides R, Frenklach M. Detailed Kinetic Monte Carlo Simulations of Graphene-Edge Growth. *The Journal of Physical Chemistry A*. 2010; 114(2):689–703.

[94] Celnik M, Raj A, West R, Patterson R, Kraft M. Aromatic site description of soot particles. *Combustion and Flame*. 2008;155(1–2):161–180.

[95] Raj A, Celnik M, Shirley R, Sander M, Patterson R, West R, Kraft M. A statistical approach to develop a detailed soot growth model using PAH characteristics. *Combustion and Flame*. 2009;156(4):896–913.

[96] Raj A, Sander M, Janardhanan V, Kraft M. A study on the coagulation of polycyclic aromatic hydrocarbon clusters to determine their collision efficiency. *Combustion and Flame*. 2010;157(3):523–534.

[97] Sander M, Patterson RI, Braumann A, Raj A, Kraft M. Developing the PAH-PP soot particle model using process informatics and uncertainty propagation. *Proceedings of the Combustion Institute*. 2011;33(1):675–683.

[98] Chen D, Zainuddin Z, Yapp E, Akroyd J, Mosbach S, Kraft M. A fully coupled simulation of PAH and soot growth with a population balance model. *Proceedings of the Combustion Institute*. 2013;34(1):1827–1835.

[99] Violi A, Venkatnathan A. Combustion-generated nanoparticles produced in a benzene flame: A multiscale approach. *The Journal of Chemical Physics*. 2006; 125(5):054302–054302–8.

[100] Violi A, Kubota A, Truong T, Pitz W, Westbrook C, Sarofim A. A fully integrated kinetic monte carlo/molecular dynamics approach for the simulation of soot precursor growth. *Proceedings of the Combustion Institute*. 2002; 29(2):2343–2349.

[101] Violi A, Sarofim AF, Voth GA. Kinetic Monte Carlo - Molecular Dynamics Approach to Model Soot Inception. *Combustion Science and Technology*. 2004; 176(5-6):991–1005.

[102] Violi A. Modeling of soot particle inception in aromatic and aliphatic premixed flames. *Combustion and Flame*. 2004;139(4):279–287.

[103] Violi A, Voth GA. A Multi-scale Computational Approach for Nanoparticle Growth in Combustion Environments. In: *High Performance Computing and Communications*, edited by Yang LT, Rana OF, Martino BD, Dongarra J, no. 3726 in Lecture Notes in Computer Science, pp. 938–947. Springer Berlin Heidelberg. 2005;.

[104] Chung SH, Violi A. Insights on the nanoparticle formation process in counterflow diffusion flames. *Carbon*. 2007;45(12):2400–2410.

[105] D'Anna A, Sirignano M, Kent J. A model of particle nucleation in premixed ethylene flames. *Combustion and Flame*. 2010;157(11):2106–2115.

[106] Voter AF. Introduction to the Kinetic Monte Carlo Method. In: *Radiation Effects in Solids*, edited by Sickafus KE, Kotomin EA, Uberuaga BP, no. 235 in NATO Science Series, pp. 1–23. Springer Netherlands. 2007;.

[107] Bortz A, Kalos M, Lebowitz J. A new algorithm for Monte Carlo simulation of Ising spin systems. *Journal of Computational Physics*. 1975;17(1):10–18.

[108] Gillespie DT. A general method for numerically simulating the stochastic time evolution of coupled chemical reactions. *Journal of Computational Physics*. 1976;22(4):403–434.

[109] Gillespie DT. Exact stochastic simulation of coupled chemical reactions. *The Journal of Physical Chemistry*. 1977;81(25):2340–2361.

[110] O'Boyle NM, Banck M, James CA, Morley C, Vandermeersch T, Hutchison GR. Open Babel: An open chemical toolbox. *Journal of Cheminformatics*. 2011;3(1):33. PMID: 21982300.

[111] O'Boyle NM, Morley C, Hutchison GR. Pybel: a Python wrapper for the OpenBabel cheminformatics toolkit. *Chemistry Central Journal*. 2008;2(1):5.

[112] Daylight Theory: SMARTS - A Language for Describing Molecular Patterns. 2013.

[113] Fletcher R, Reeves CM. Function minimization by conjugate gradients. *The Computer Journal*. 1964;7(2):149–154.

[114] Bixon M, Lifson S. Potential functions and conformations in cycloalkanes. *Tetrahedron*. 1967;23(2):769–784.

[115] Levitt M, Lifson S. Refinement of protein conformations using a macromolecular energy minimization procedure. *Journal of Molecular Biology*. 1969;46(2):269–279.

[116] Press WH. *Numerical recipes: the art of scientific computing*. xx, 702 p. Cambridge ; New York, N.Y.: Cambridge University Press. 1989.

[117] Stuart SJ, Tutein AB, Harrison JA. A reactive potential for hydrocarbons with intermolecular interactions. *The Journal of Chemical Physics*. 2000; 112(14):6472.

[118] Ni B, Lee KH, Sinnott SB. REBO potential for hydrocarbon-oxygen interactions. *Journal of physicsCondensed matter*. 2004;16(41):7261. Journal Article.

[119] Halgren TA. Merck molecular force field. I. Basis, form, scope, parameterization, and performance of MMFF94. *Journal of Computational Chemistry*. 1996;17(5-6):490–519.

[120] Halgren TA. MMFF VI. MMFF94s option for energy minimization studies. *Journal of Computational Chemistry*. 1999;20(7):720–729.

[121] Wang H, Frenklach M. Calculations of Rate Coefficients for the Chemically Activated Reactions of Acetylene with Vinylic and Aromatic Radicals. *The Journal of Physical Chemistry*. 1994;98(44):11465–11489.

[122] Bittner J, Howard J. Composition profiles and reaction mechanisms in a near-sooting premixed benzene/oxygen/argon flame. *Symposium (International) on Combustion*. 1981;18(1):1105–1116.

[123] Kislov VV, Islamova NI, Kolker AM, Lin SH, Mebel AM. Hydrogen Abstraction Acetylene Addition and Diels-Alder Mechanisms of PAH Formation: A Detailed Study Using First Principles Calculations. *J Chem Theory Comput*. 2005;1(5):908–924.

[124] Violi A. Cyclodehydrogenation Reactions to Cyclopentafused Polycyclic Aromatic Hydrocarbons. *The Journal of Physical Chemistry A*. 2005;109(34):7781–7787.

[125] Richter H, Granata S, Green WH, Howard JB. Detailed modeling of PAH and soot formation in a laminar premixed benzene/oxygen/argon low-pressure flame. *Proceedings of the Combustion Institute*. 2005;30(1):1397–1405.

[126] Abid AD, Heinz N, Tolmachoff ED, Phares DJ, Campbell CS, Wang H. On evolution of particle size distribution functions of incipient soot in premixed ethylene–oxygen–argon flames. *Combustion and Flame*. 2008;154(4):775–788.

[127] Abid A, Tolmachoff E, Phares D, Wang H, Liu Y, Laskin A. Size distribution and morphology of nascent soot in premixed ethylene flames with and without benzene doping. *Proceedings of the Combustion Institute*. 2009;32(1):681–688.

[128] Mebel AM, Lin MC, Chakraborty D, Park J, Lin SH, Lee YT. Ab initio molecular orbital/Rice–Ramsperger–Kassel–Marcus theory study of multichannel rate constants for the unimolecular decomposition of benzene and the H+C6H5 reaction over the ground electronic state. *The Journal of Chemical Physics*. 2001; 114(19):8421–8435.

[129] Lai JYW, Elvati P, Violi A. Stochastic Atomistic Simulation of Polycyclic Aromatic Hydrocarbon Growth in Combustion. *Physical Chemistry Chemical Physics*. 2014;.

[130] Pietrucci F, Andreoni W. Graph Theory Meets Ab Initio Molecular Dynamics: Atomic Structures and Transformations at the Nanoscale. *Physical Review Letters*. 2011;107(8):085504.

[131] Smith GP, Golden DM, Frenklach M, Moriarty NW, Eiteneer B, Goldenberg M, Bowman CT, Hanson RK, Song S, Gardiner Jr WC, Lissiansk VVi, Qin Z. GRI-Mech 3.0. 2000. Web Page.

[132] Kislov VV, Sadovnikov AI, Mebel AM. Formation Mechanism of Polycyclic Aromatic Hydrocarbons beyond the Second Aromatic Ring. *The Journal of Physical Chemistry A*. 2013;117(23):4794–4816.

[133] Kang K, Hwang J, Chung S, Lee W. Soot zone structure and sooting limit in diffusion flames: Comparison of counterflow and co-flow flames. *Combustion and Flame*. 1997;109(1–2):266–281.

[134] Kuwahara H, Mura I. An efficient and exact stochastic simulation method to analyze rare events in biochemical systems. *The Journal of Chemical Physics*. 2008;129(16):165101.

[135] Gillespie DT, Roh M, Petzold LR. Refining the weighted stochastic simulation algorithm. *The Journal of Chemical Physics*. 2009;130(17):174103.

[136] Gillespie DT. Approximate accelerated stochastic simulation of chemically reacting systems. *The Journal of Chemical Physics*. 2001;115(4):1716–1733.

[137] Cao Y, Gillespie DT, Petzold LR. Efficient step size selection for the tau-leaping simulation method. *The Journal of Chemical Physics*. 2006;124(4):044109–044109–11.

[138] Cao Y, Gillespie DT, Petzold LR. The slow-scale stochastic simulation algorithm. *The Journal of Chemical Physics*. 2004;122(1):014116.